# Harvesting Electrical Energy from a Stationary Bike: An Experimental Approach

A thesis presented in partial fulfillment of the requirements for the degree of

**Master of Engineering**

in

**Electronics and Computer Systems Engineering**

By

**Sanjay Samuel David**

**Supervised by Professor Subhas Mukhopadhyay**

SCHOOL OF ENGINEERING AND ADVANCED TECHNOLOGY

MASSEY UNIVERSITY

PALMERSTON NORTH

NEW ZEALAND

JANUARY 2014

## Abstract

*In any gym there are people on treadmills, stationary bikes, elliptical or rowing machines producing power in order to burn calories. The power being produced is dissipated primarily as heat. Human energy, if captured and used as an alternative to fossil fuel could supply a gym with clean sustainable energy that would be good for the environment and save the gym money. The process of capturing, converting and storing this energy is known as Energy Harvesting (EH).*

*This project examines the use of a stationary bike to harvest energy with the use of magnets and an electromagnet. The aim was to create a device that would not require modifications to be made to a standard stationary bike, thus making it affordable and easy to use. A prototype of a stationary bike was designed using SolidWorks and experiments conducted to test the feasibility of this method of EH, results were positive. A typical stationery bike was acquired, experiments were conducted to determine the ideal set up for optimum EH and modifications were made as required. Based on the findings of these experiments the final set-up of the stationary bike incorporated an electromagnet made with high permeability, magnets were attached to a flywheel of a stationary bike with their poles alternating to enhance production of flux, suitable number of magnets were determined and the air gap in the circuit was adjusted to control reluctance. After the set-up was complete the bike was ridden and power output recorded, the findings showed that while energy was harvested the quantity was not significant. Therefore this method of EH is not efficient on a stand-alone machine; however with further research and in conjunction with other forms of EH it could be used. This project was successful in creating a method of EH from a stationary bike using magnets and an electromagnet, without modifying the bike; it is a step in research, in the journey towards capturing and converting wasted energy.*

.

# Acknowledgements

First of all I would like to thank God for giving me this opportunity. I would like to acknowledge my supervisor, Professor Subhas Mukhopadhyay, for his continuous support, encouragement, patience, valuable advice, technical help and supervision of my project without which I would not have been able to achieve completion; thank you sir.

I would also like to acknowledge Ken Mercer, Colin Plaw, Bruce Collins, Anthony Wade and Asif Iqbal Zia for their assistance with technical matters and their valuable input and advice that improved my experimental work. I would also like to thank Ian Thomas for helping with the building of the prototype model at the workshop and for teaching me the function of various equipment. I would like to thank Morio Fukuoka for sharing his extensive knowledge regarding designing and producing a number of parts for the project and also for teaching the use of the CNC machine. I would also like to thank my fellow students at Massey University for their help and support.

I would like to thank my parents for their unconditional love and support. Thank you for always believing in me and for the sacrifices you made in giving me this opportunity. I thank my brother and sisters for always being available to help in any way possible. Special thanks to Sneha Selvaraj for her input into the project and assistance with proof reading. I would also like to thank all my friends and extended family for your love, support and prayers without which I would not have been able to accomplish this.

Last but not least I would like to acknowledge baby Nadia my little niece who added laughter to my study breaks.

# Contents

# List of Figures

# List of Tables

# Chapter 1. INTRODUCTION

## 1.1. Introduction

Energy is everywhere in the environment surrounding us and is available in many forms. Capturing this energy and converting it to electrical energy has been the subject of many research investigations. This process is known as Energy Harvesting (EH). Recent advancement in technology has made it possible for many real life applications to be powered by EH.

To meet the worlds increasing energy needs, many companies around the world are investing in the research and development of environmentally sustainable technologies. This research has progressed in the fields of solar, wind and nuclear energy. However, there exists a large untapped source of dissipated energy that has potential to help solve this energy problem.

Every day, gym goers produce lots of energy just by doing their daily workout on exercise equipment. The power generated by the equipment is dissipated primarily as heat. This energy, if used as an alternate to fossil fuels could supply clean sustainable energy. This would be good for the environment and also save gyms money at the same time. However, this energy is produced in mechanical form rather than electrical form, but slight modifications to the exercise equipment would allow the energy being produced to be converted to electrical energy which can be harvested, and stored for a later time.

The main objective of this project is to design an EH system to harvest the energy being generated by stationary bikes using magnets and an electromagnet. The goal is to design a system that could be added on as an attachment to any stationary bike with a flywheel. Below is an outline of the process undertaken for this project.

Chapter two is a literature review conducted to examine existing research on EH, Green gyms and rotational energy harvesting. The literature review revealed a gap in research in the use of magnets to assist in EH from a stationary bike. This project addresses the gap by experimenting EH with the use of magnets first on a prototype and then on a stationary bike.

A prototype was made to replicate a stationary bike. The details of the design of the prototype and the experiments conducted are outlined in chapter three. The model for the prototype was designed using Solidworks (CAD software). The prototype was used to help identify the factors that needed to be considered when building an energy harvester for a stationary bike. The results showed that this method of EH would be feasible on a stationary bike.

Chapter four is an outline of the methodology used for the setup of a stationary bike for EH and chapter five lists the experiments conducted using tables, graphs and equations. This chapter also includes an analysis of the experiment results.

Experiments conducted investigated the effects of the following factors on the power generated: the material of the electromagnet, the pole orientation of the magnets, the number of magnets placed on the flywheel of the bike, the strength of the magnets used and the air gap present in the magnet.

The results obtained are discussed and conclusions drawn on the best setup for this method of EH. Data recorded and calculated showed that while there was energy harvested it was not significant and therefore could not be used as a stand-alone source of EH. Recommendations for further research are identified.

# Chapter 2. LITERATURE REVIEW

## 2.1. The energy problem

Fossil fuels are finite and environmentally costly. Consumption of fossil fuel is the main contributor for the rise of carbon dioxide (CO2) levels in the atmosphere, making it a significant cause for global warming [4]. This reduces agricultural production and causes social and biological difficulties [4]. The United States of America, which constitutes less than 4% of the world's population, is responsible for 22% of the CO2 produced from the consumption of fossil fuels, which is higher than any other nation, or as seen in Figure 2.1. Reducing the consumption of fossil fuels will reduce the speed of global warming [3, 4].

In recent times, the supply of energy has been one of the most pressing and debated subjects. It is widely accepted that the change in climate and greenhouse gas emissions are connected. Additionally there is a consensus that the fossil fuel reserves of the world are running low [18]. Consequently, as the electricity requirements of the world increases, it is important to look for alternate sources of energy for electricity production.

Sustainable, environmentally friendly energy can be acquired by capturing energy from ambient sources or by nuclear fission. Ambient energy is available widely and large-scale technologies are being developed to capture it efficiently. Of these, the main sources are solar, wind, wave, hydroelectric and nuclear power. On the other side of the spectrum, there are small quantities of wasted energy that would be useful if captured. Attaching a dynamo to any turning wheel can be considered as a source to produce electric power. As a few cardio-vascular machines in a gym turn a wheel it is possible that gyms can be a potential source to produce electrical power. Harvesting even a fraction of this energy can have a huge environmental and economic impact. This is where EH comes in [1, 19].

**Table 1. *Fossil and solar energy use in the United States and world, in kilowatt-hours and quads.***

| | United States | | World | |
|---|---|---|---|---|
| Form of energy | kWh x $10^9$ | Quads | kWh x $10^9$ | Quads |
| Petroleum | 10,973.1 | 37.71[a] | 43,271.7 | 148.70[b] |
| Natural gas | 6431.1 | 22.10[a] | 24,414.9 | 83.90[b] |
| Coal | 6314.7 | 21.70[a] | 27,295.8 | 93.80[b] |
| Nuclear power | 2249.4 | 07.73[a] | 6984.0 | 24.00[b] |
| Biomass | 1047.6 | 03.60[a] | 8439.0 | 29.00 |
| Hydroelectric power | 989.4 | 03.40[a] | 7740.6 | 26.60[b] |
| Geothermal | 93.1 | 00.32[b] | 291.0 | 01.00 |
| Biofuels (ethanol) | 26.2 | 00.09[c] | 52.4 | 00.18 |
| Wind energy | 11.6 | 00.04 | 232.8 | 00.80 |
| Solar thermal | 11.6 | 00.04 | 11.6 | 00.04 |
| Photovoltaics | 11.6 | 00.04 | 11.6 | 00.04 |
| Total consumption | 28,159.4 | 96.77 | 118,745.4 | 408.06 |

*Note:* A quad is a unit of energy equal to 1 quadrillion British thermal units.
a. Adapted from USBC (2001).
b. Adapted from DOE/EIA (2001).
c. Adapted from Pimentel (2001).

**Figure 2.1:** Fossil Fuel consumption of the world

## 2.2. Energy Harvesting

In recent times many universities and companies have invested time and money into research and development of EH. This is in response to the growing need to have clean sustainable energy and also due to the fact that the world is running low on the fossil fuels which provide power for our everyday activities.

### 2.2.1. What is Energy Harvesting?

The term EH, is also known as energy scavenging or power harvesting [2]; is the process of capturing small quantities of energy from any number of naturally-occurring energy sources, which would otherwise be dissipated or lost (e.g. as sound, light, heat, movement or vibration); collecting them and storing them for later use [5, 6]. Park (2009) is of the opinion that EH is made up of 3 key components namely: energy conversion, harvesting and conditioning circuit and energy storage.

Bickerstaffe (2011) argues that the common definition of EH as the process of converting ambient energy into electrical energy is too narrow. He suggests the term should be defined as "the collection and storage of ambient energy for on-demand, off-grid use". This is because the common definition of EH considers only the transducer technology for energy conversion, and assumes that the energy must be converted into electricity. Whereas his definition takes a broader view, where the transducer is one component of a complete system that provides power for applications where other sources of energy are unavailable or unsuitable. [8]

EH, includes electrodynamics, thermovoltics, piezoelectrics and photovoltaics, among other options, which are presently being implemented in a wide range of applications [7]. Harrop & Das, (2012) are of the opinion that this technology has now got to a tipping point, as more efficient energy gathering, storage and low power electronics are now readily available, affordable, reliable and last longer. for many number of applications to be feasible [7].

EH devices effectively and efficiently capture, collect, store, condition and manage this energy and provide it in a form which can be used to achieve many helpful tasks (see Figure 2.1) [5, 15].

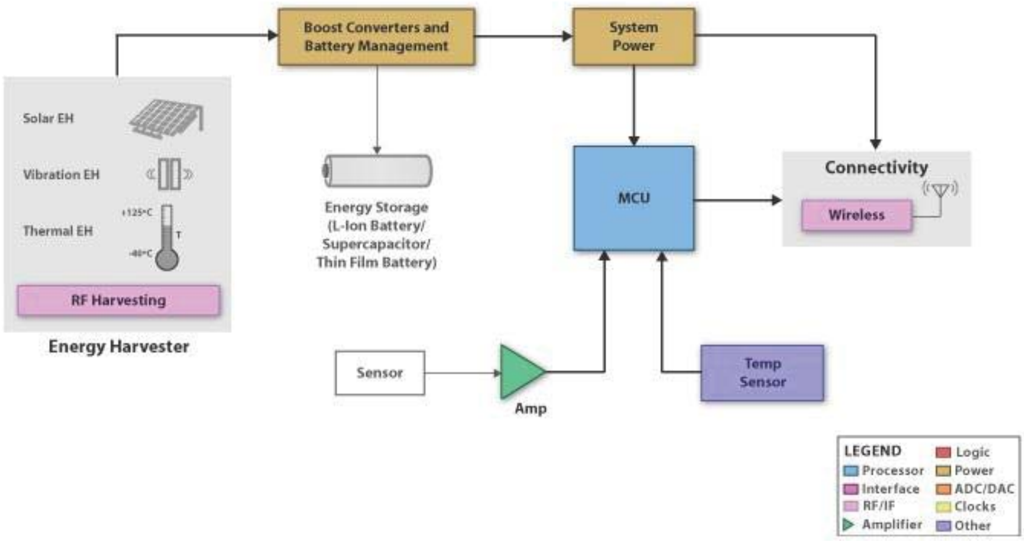


**Figure 2.2:** Process of Energy Harvesting

### 2.2.2. Why Energy Harvesting?

The process of harvesting abundant energy from the environment to power small devices or assist larger devices – has secured a sure foot-hold in building and industrial markets, powering wireless sensors to improve efficiency, reduce costs and increase automation [10].

Wireless sensor networks are allowing technology to be used in a wide range of applications. Ultra-low-power wireless powering solutions cover a broad range of products, such as batteries, power management of ICs, sensor and control systems, mesh networks, radio frequency identification devices and microelectro-mechanical systems. Although many of these applications are stationary, almost every wireless sensor network utilizes some form of battery back-up—both primary and secondary [11].

Developments in technology have increased the efficiency of devices which capture minute amounts of energy from the surroundings and transform it into electrical energy. In addition, advance developments in microprocessor technology have increased the power efficiency, essentially reducing the amount of power consumption. In combination, these advances have created interest in the engineering community to develop more applications that utilize EH for power [5].

EH is positioning itself as an alternative to batteries, and it could result in becoming a "supplement" to batteries. Maintaining batteries and replacing them is often said to be the biggest motivation to use EH [12]. In addition, EH can be used as an alternative energy source to enhance the reliability of a system, supplement a primary power source and prevent power interruptions [5].

EH is a reliable and attractive alternate for wall plugs and expensive batteries for remote applications as it can provide inexhaustible energy from natural energy sources wherever the system is deployed. If designed and installed properly this makes the system maintenance free and is able to provide free energy for the lifetime of the application [9, 5, 8, 11]. Self-powered wireless sensors do not require a lot of wiring and are easy to install. Maintenance of EH systems are low as energy harvesters allow for devices to function unattended which eliminates the need for service visits to replace batteries. This reduces installation and maintenance costs run by energy harvesters [13].

EH is also driven by the desire to address the issue of global warming and climate change [11]. Dependency on battery power is reduced or completely eliminated when a system is powered by an energy harvesting device which helps reduce the negative impact batteries have on the environment [13].

### 2.2.3. Sources of Energy Harvesting

A huge variety of sources are available for EH. This includes solar power, thermoelectricity, ocean waves, physical motions (either active/passive human power) and piezoelectricity. Yildiz, states that "no single power source is sufficient for all applications", and that the selection of energy sources must be considered according to the application characteristics [2].

An advantage of EH is that it is virtually unlimited and is essentially free if the energy is captured at or near the system location [5]. Table 2.1 and Figure 2.3 give a compiled list of the various sources for EH [2, 5, 9, 11].

| | |
|---|---|
| Mechanical Energy | from sources such as vibration, mechanical stress and strain |
| Thermal Energy | waste energy from furnaces, heaters, and friction sources |
| Light Energy | captured from sunlight or room light via photo sensors, photo diodes, or solar panels |
| Electromagnetic Energy | from inductors, coils and transformers |
| Natural Energy | from the environment such as wind, water flow, ocean currents, and solar |
| Human Body | a combination of mechanical and thermal energy naturally generated from bio-organisms or through actions such as walking and sitting |
| Other Energy | from chemical and biological sources |

**Table 2.1:** Sources of Energy Harvesting

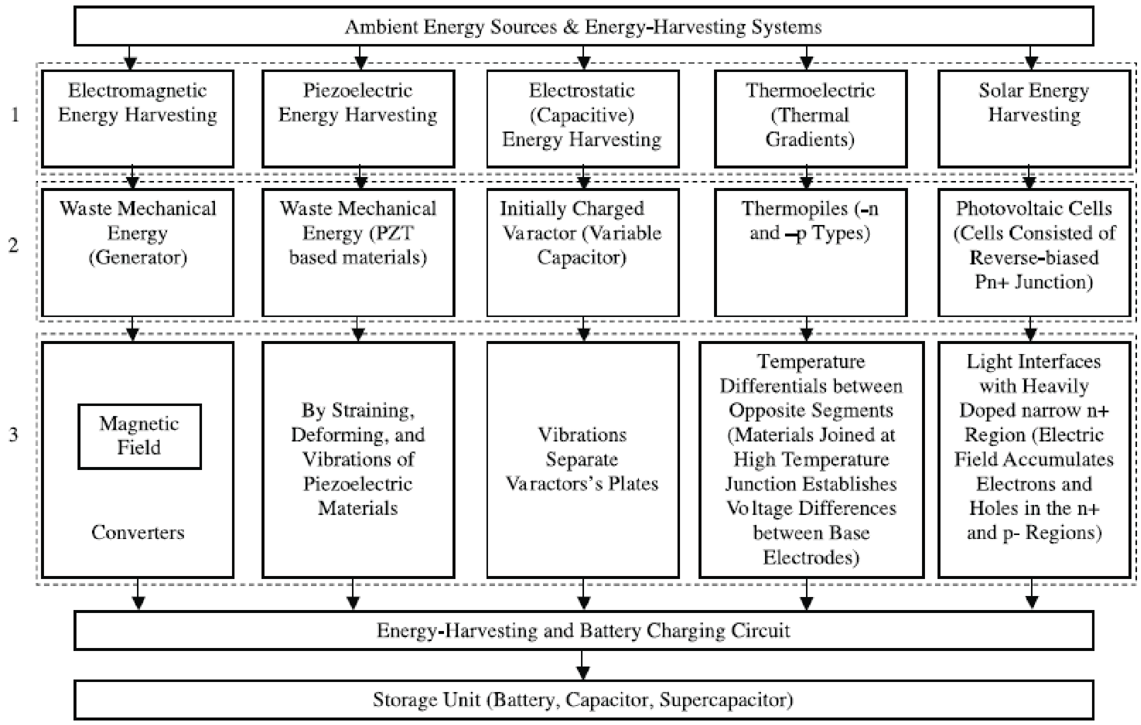


**Figure 2.3:** Ambient Energy Systems

### 2.2.4. Applications of Energy Harvesting

Advancements in technology have made it possible to power many real life applications using EH. The use of Wireless sensor network systems benefit from EH as systems such as ZigBee can be powered by EH. For example, when a wireless node is installed at a remote location where a battery or wall plug is either unavailable or unreliable, EH can supply the necessary power. Another example is that EH can make a remote control node to be a self-powered electronic system. In other instances, the overall reliability and efficiency can be enhanced where multiple energy sources are used [5]. This project examines the application of EH in the context of a gym.

## 2.3. Green Gym

Gyms take a lot of energy to power televisions, air conditioning, vending machines, lighting and other equipment. Implementing energy harvesters where the energy harvested is used to power devices in the gym will help reduce the power costs of a gym.

In almost every gym there are people performing controlled and repetitive movements. As people exercise the energy created by motion is lost. Channelizing this kinetic energy into energy that can be harvested and used is the idea/concept of a Green Gym.

A green gym is a gym dedicated to reduce their power consumption by using various EH techniques to generate power to meet their energy needs. This has not reached the point where the whole gym is powered by alternate energy but has drastically reduced the amount of energy these gyms would consume.

Currently there are a growing number of gyms all over the world implementing EH units on to their machines to reduce their power bills and also to produce clean sustainable energy. This is being done by installing energy harvesting units mostly on to stationary bikes from which power is generated as the bike is pedalled.

### 2.3.1. Who's doing it and how are they doing it?

The general idea of attaching a generator to exercise equipment has been around for many decades. The concept of harvesting energy from an exercise machine was introduced by a Hong Kong gym called California Fitness who fitted 18 exercise machines which were used to charge a battery and power fluorescent lights [15]. Since then, there have been three establishments in the United States that have been working to commercialize this technology, each taking a slightly different approach than the other as explained below [16].

In 2007, Hudson Harr, a graduate of the University of Florida collected used elliptical machines and electrical parts [17]. He found that the machines already had DC generators inside, which powered the monitoring console on the machine [16, 17]. Harr noticed that the power generated by the generator was dissipated across a bank of resistors. Getting rid of these resistors meant that Harr could harvest the energy which was otherwise dissipated. Harr's strategy was to wire each elliptical machine to a central unit containing an inverter which converts the DC power generated to AC, see Figure 2.4. The inverter in turn connects the AC power to the building's electrical system and can ultimately feed the grid [16]. This strategy gave birth to ReRev, the first commercial company who retrofitted exercise machines with a module which harvested energy.
Since then Harr's company, ReRev, has installed systems at many colleges, including Drexel University, James Madison University, Oregon State University, Texas State University, and the University of Florida [16].

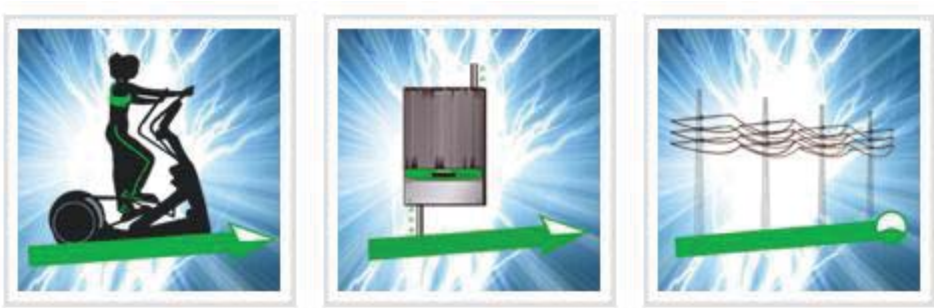

**Figure 2.4:** ReRev's strategy to generate power

At around the same time another company, The Green Revolution, started by Jay Whelan and Mark Sternberg, decided to use EH but on exercise bikes instead of elliptical machines like ReRev. They began by propping the back wheel of an ordinary bike on a triangular frame, next they connected the back wheel to a car alternator and boosted the generated power, this in turn raised the resistance of motion [16, 17].

Their idea was to design and build completely new exercise bikes with generators connected to them. However gym owners did not want to buy all new equipment. Therefore the Green

Revolution team decided to design a module which could be fitted onto bikes that gyms already had. This module could be directly attached to the bikes, where the generated electricity was fed to two 12V batteries wired in series. This is shown in Figure 2.5. When the bike was pedalled, the batteries got charged, and when the battery is fully charged, the inverter converted the 24V DC power into 110V AC and sent the power to the grid [16].


**Figure 2.5:** Energy Harvesting Modules built by The Green Revolution

While the team at Green Revolution decided against making custom machines, Mike Tagget an entrepreneur, decided to design his own custom machines. He began marketing his strategy at trade shows by attracting visitors to his booth where he would generate electricity with the machines he designed. Demonstrations at such events led to the idea which Taggett later unveiled as the Human Dynamo, a custom designed stationary bike [16].

In addition to the usual pedal, Taggett, included hand cranks at the top of the machine which provided riders an upper body workout and so helped generate more electricity. Taggett's design is shown in Figure 2.6. The Human Dynamo was designed where the sprockets of the bike were chained together, which made the hand and leg cranks to both spin at the same speed to turn the flywheel on the bike [16].


**Figure 2.6:** The Human Dynamo

To reduce the costs involved Taggett made a system in which several machines could be connected together to drive a single generator. This configuration was coined by him and his team as the Team Dynamo, shown in Figure 2.7. With this configuration a total of up to 10 machines could be connected to one big generator and one electronic package. This cuts down expense and maintenance costs as there was only one big generator and one electronic package instead of one each for each machine [16].

**Figure 2.7:** The Team Dynamo

## 2.4. Example of a regular gym

As the search for alternative sources of energy continues, David Pickup (2010) conducted research to examine the possibility and economics of a human powered gym. He studied the probability of an untapped potential power plant present within each of us.
Pickup first considered the amount of power consumed in a gym and then estimated the power that could be generated by that particular gym.

### 2.4.1. Power Consumption of the gym

Pickup studied the power consumption of Addlestone Leisure center (ALC), a gym based in Surrey, United Kingdom. He was provided with accurate and current data and based on his past experiences of visiting several gyms over the years, he determined that the ALC gym was a typical setup [20].

First, he considered the air conditioning of the gym. An estimate of the power consumed by a standard air conditioning unit is 600W [21]. In most gyms there is usually more than one air conditioning units making it one of the main power users in a gym. The ALC gym had three such units, which gave a total power estimate for air conditioning to be 1800W.

Next he considered the power consumed by the lights and music played in the gym. The ALC gym used ten 20W fluorescent tubes, which meant that ALC was using an estimate of 200W for their lighting. The power consumed from the music systems present in ALC was 50W [22].

Televisions are a common and popular addition in most gyms. A typical large T.V uses around 100W [23]. Every gym usually has multiple televisions around the gym; ALC had a total of five T.Vs. This gave a total of 500W of power consumed by T.Vs at ALC.

A lot of gadgets get used at gyms these days. Most people take their own personal gadgets, such as ipods and phones into the gym with them. For the convenience of gym goers most gyms these days provide slots in the gyms where people can charge their electronic devices as they exercise. Powering these devices does not require a lot of power and is usually around 5W [24]. It is important to note that this is not the total power consumed by the gym; rather it is the amount of power consumed by each individual machine.

Table 2.2 shows the collected values of the power usage for ALC gym. The total communal power consumption of the gym is estimated to be 2550W, and the individual power consumption is estimated to be 5W. This total value is not complete, as the power consumed by the reception equipment, such as phones and computer were not included. Also the power consumed by the equipment present in the changing rooms, such as showers and hairdryers were not included. This is an estimate of the power consumed in the gym workout area, which is where the power would be generated.

| Device | Total Power Estimate |
|---|---|
| Air Conditioning | 1800W |
| Lights | 200W |
| Televisions | 500W |
| Music System | 50W |
| **Total** | **2550W** |

**Table 2.2:** Communal power consumption at ALC gym

### 2.4.2. Power Generation

An estimate of the power generated by one exercise machine was made. A stationary bike was chosen because of its simplicity and the availability of information. Estimates of the total power generated by a human on a stationary bike was found to be 50W [25], 75-100W [26] and 60-120W [22]. The value of 80W was taken, as most people working out at a gym would not be working out at high levels for extended periods of time. Since gym machines are not 100% efficient, not all of the generated power could be used as electricity. The efficiency of a stationary bike is around 70% [22]. So the power generated which can be used is approximately 56W.

In ALC there were 14 stationary bikes which could be used to generate power. In terms of generating electricity, elliptical and stationary bikes were considered to be equivalent, while treadmills, rowing machines and weight machines were ignored. As stated above it is possible to generate about 56W from each of these machines, so these 14 machines could generate 784W. This showed that the machines, in the ALC gym, were capable of generating about 32% of the total communal power consumption of the gym.

Based on that, Pickup (2010) concluded that a gym cannot be powered just by the power generated by the machines. However this could reduce costs quite significantly for the gym as they would be able to generate up to 32% of their energy need in the gym area. Not only would it reduce their monthly power bill but it will also reduce a gyms carbon footprint, as the energy generated by EH is clean, sustainable and has no negative impacts on the environment.

## 2.5. Electromagnetic Energy Harvesting

Nineteenth century scientists such as Hans Oersted, Joseph Henry, Michael Faraday, James Maxwell, and Heinrich Hertz pioneered the early work in electromagnetism. The famous Maxwell equations describe the interplay between magnetic and electric fields. One of these equations, Faraday's law of induction, describes how a time varying magnetic field will induce an electric field. Thus a permanent magnet moving relative to a conductive coil of wire will induce an electric potential (i.e. a voltage) across the terminals of the coil. Faraday was the first to develop an electric generator based on this principle [27]. Today electrical generators have widespread use in power generation systems such as fossil fuels, nuclear power, hydroelectric power and wind turbines. This section will focus on an overview of induction energy harvesters, i.e. electromagnetic generators that produce power from ambient energy. Arnold [28] and Mitcheson [29, 30] provide comprehensive reviews of some electromagnetic energy harvesting techniques.

Inductive energy harvesters can be categorized by how they achieve a relative velocity between the coil and the magnet. Linear harvesters feature the magnet moving along a straight line relative to the coil. Rotational harvesters use magnets mounted on a spinning rotor with stationary coils mounted around the rotor. Pendulum harvesters feature the magnet on a pendulum moving relative to a stationary coil. Beam-based harvesters attach either a magnet or a coil to an elastic beam. This project uses rotational EH.

### 2.5.1. Rotational Energy Harvesters

Several researchers have studied rotational energy harvesters. Typically these harvesters require a mechanism to convert the linear motion of a vibrating structure into a rotational motion to drive the device. Rotational energy harvesters are not limited in displacement like linear harvesters, and this allows for larger power densities. However rotational generators typically operate at higher frequencies than linear generators [28]. An early electromagnetic energy harvester is the Seiko Kinetic self-powered wristwatch, first introduced at the 1986 Basel Fair [39]. The motion of the wearer turned an eccentric mass on the rotor of a small electric generator. There was no need for the user to wind the mainspring of the watch or replace a battery.

Yeatman [40] studied the maximum power density of rotating and gyroscopic energy harvesters. His work concluded that rotational devices can achieve higher power densities than linear energy harvesters, but they require low parasitic damping. Furthermore if a torsion spring is used to connect the rotating mass to a rigid frame, then the spring must have a large angular range. Trimble *et al.* [41] examined a simple generator consisting of a rotating mass suspended by a torsion spring. Magnets attached to the rotating mass moved relative to coils mounted on the rigid housing. The 80 cm3 prototype device was able to produce over 200 mW at a resonance frequency of 16 Hz and an angular acceleration of 150 rad/s2.

The above has been a summary of existing literature on EH. However the literature review did not bring up the use of magnets in a stationary bike for EH. This project aims to add to research literature by exploring the use of magnets and an electromagnet to harvest energy through experimenting first with a prototype for feasibility and then on a stationary bike.

# Chapter 3. THE PROTOTYPE

## 3.1. Introduction

This project is based on the idea of using electromagnetic EH on stationary bikes to generate electricity. As experimenting on an actual stationary bike would require a lot of man power, initial experiments were done on a small scale prototype model of the proposed idea to harvest energy. From experiments conducted it was found that the most efficient way of producing electricity, on a stationary bike, is by continuously turning a flywheel at various speeds through an electromagnetic energy harvester [19].

Most stationary bikes and cross-trainers have large flywheels which spin when the machine is used, making them the most effective machines to generate electricity. Human-powered gyms based in Hong Kong [52] and Portland, Oregon [53] reflects this.

To create a prototype model which has the key functionalities of a stationary bike, a small disc made out of mild steel was used. This disc imitated the flywheel present in a stationary bike. Varied number of neodymium magnets were placed on different locations of the disk. A DC motor was used to spin the disc through a U shaped electromagnetic core. Experiments were conducted by changing pole orientation of the magnets, the number of magnets and the placements of magnets on the disk to check what would give the best/highest output. The outputs were rectified, boosted and analyzed across various loads.

## 3.2. Stationary bike

To design a model which depicts a stationary bike, it was imperative to study the basic characteristics of a stationary bike. A stationary bike by design is basically a modified bicycle. It is designed for high intensity training which regular bikes cannot handle. Built from strong materials, mostly steel frames, these bikes are able to withstand a lot of pressure. The pedals are commonly connected to a gear which is fixed and constant resistance is provided by the flywheel mechanism. The flywheels usually varies in weight; the heavier it is the greater the momentum. [47]

Figure 3.1 depicts a common stationary bike found in gyms across the world. The stationary bike is very similar to a bicycle. The only difference is that it does not move when pedaled and hence the term stationary. As the bike is pedalled the flywheel, located in the front, spins and builds momentum. It is designed to feel a lot like riding a regular bicycle. All stationary bikes have a knob present on the bike with which the rider can increase or decrease the resistance while pedalling [47].


**Figure 3.1:** Stationary Bike

## 3.3. Design of a prototype

To develop a prototype that imitated the functionality of a stationary bike, the main aspects of a stationary bike had to be transferred on to the prototype model. Since the flywheel was needed to produce and harvest energy, it was vital that the prototype model had a flywheel/disc and a means to spin the flywheel.

The project aims to come up with a technique where gyms would not have to buy new machines to harvest the energy generated by the machines, but rather attach a module to the existing machines. As most stationary bikes have large flywheels in the front, as seen in Figure 3.1, attaching a harvester in the front under the flywheel seemed logical.

Based on experiments conducted it was found that an efficient way to harvest energy from a stationary bike was to use the rotation of the flywheel and pass it through an electromagnet core. To implement this, neodymium magnets had to be placed on the disc and passed through a U shaped electromagnet. As the disc was spun, the magnets placed on the disc passed through the core of the electromagnet. The electromagnet had to be designed in a way that the flux generated by the magnets would pass through the core to produce power.

The prototype was designed using Solidworks, a CAD software. Figure 3.2 shows the first design of the prototype. It consisted of a U shaped electromagnet, a disc and a motor to spin the disc through the core.

Figure 3.3 gives a different view of the design and points out where the magnets were to be placed on the disc.

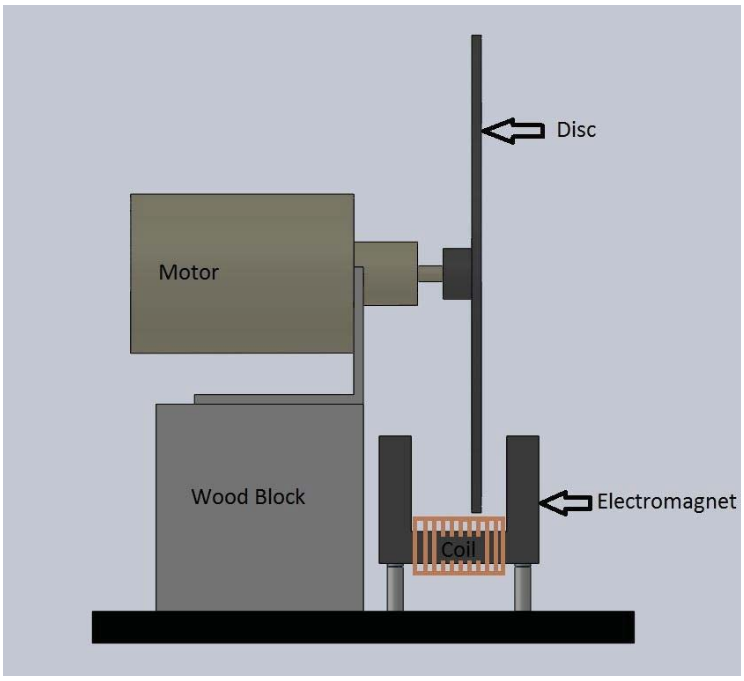


**Figure 3.2:** First design of prototype in CAD software

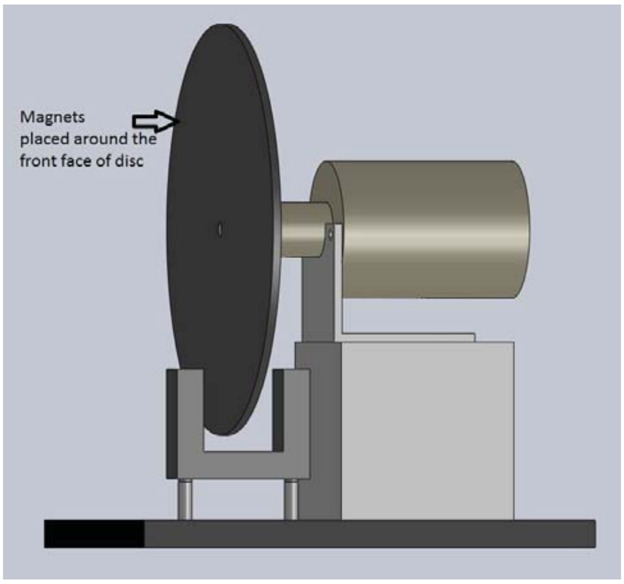


**Figure 3.3:** Side angle view of the prototype

A U shaped electromagnet with a gap of 30mm between the two ends was initially designed. However, this meant that there would be a huge air gap resulting in a lot of losses, hence the design had to be modified. Magnetic flux is reluctant to travel through air; it is easier for it to travel through iron [54]. From this it can be concluded that air has a high reluctance, and iron has a low reluctance. Therefore, in order to reduce the losses, a new design was made in which the air gap was reduced. Figure 3.4 shows the new and final design of the prototype.

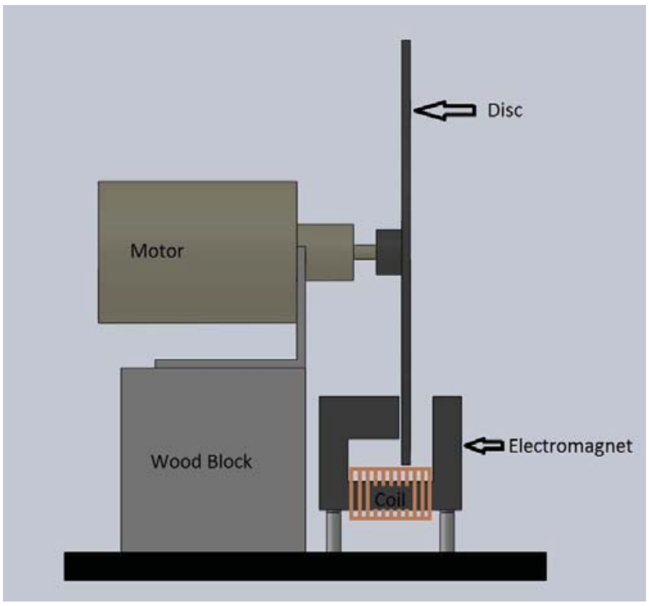


**Figure 3.4:** Final Design of Prototype model

## 3.4. Flywheel

To replicate the properties of a flywheel from a stationary bike for the prototype model a disc of 150mm, 3mm thick, was made out of mild steel. Figure 3.5 shows the CAD drawing of the disc.

Mild steel was chosen because it is the most common form of steel. The price was relatively low, but still provided the material properties that were acceptable for many applications. Mild steel was used though there were materials with better permeability due to availability and cost.

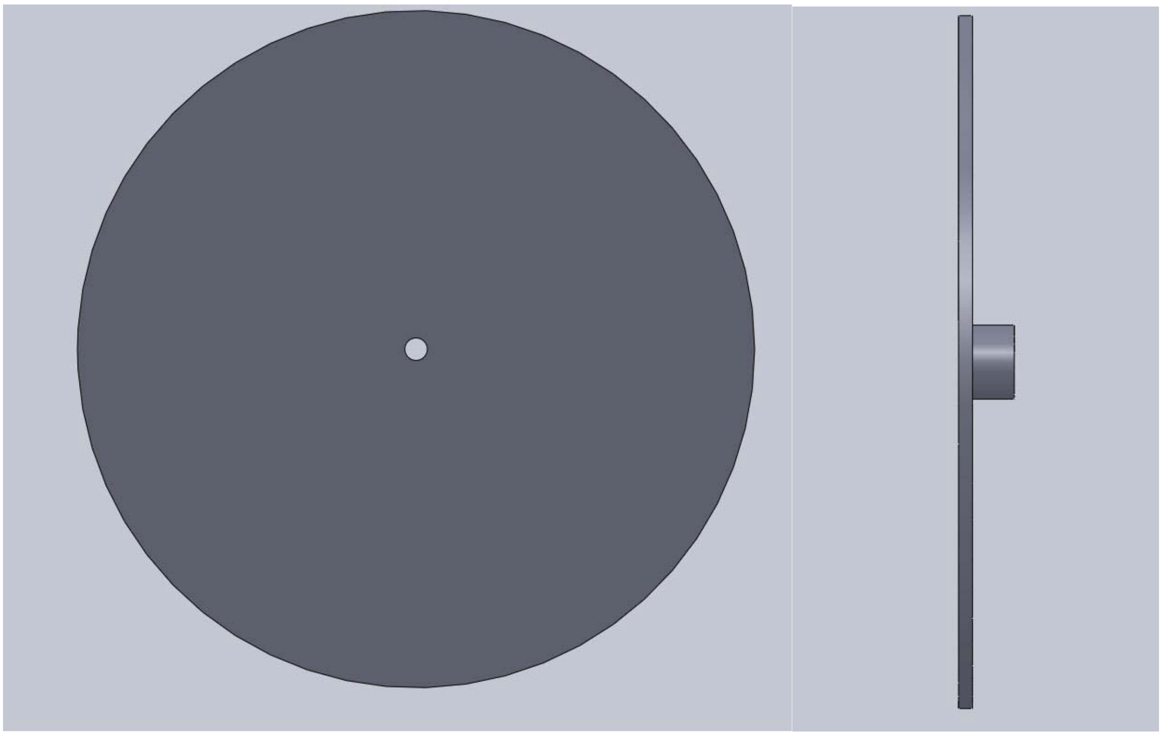

**Figure 3.5:** CAD design of the Flywheel for the prototype model

## 3.5. Electromagnet

The most important piece in EH is the device or module which captures and converts ambient energy into electrical energy. For this setup, the energy harvester is an electromagnet made out of iron core. The initial design of the electromagnet was a U shaped electromagnet made out of mild steel. Mild steel was chosen because of its cost, availability and good permeability properties.

Figure 3.6 shows the CAD design on the left and the mild steel electromagnet on the right. This was machined out of 15mm thick block of mild steel. The center of the core was wound with 0.5mm gauge enamel covered copper wire. It consisted of 250 turns and wound layer upon layer. Later, this was mounted in such a way that the flywheel was approximately 1mm above the coil.

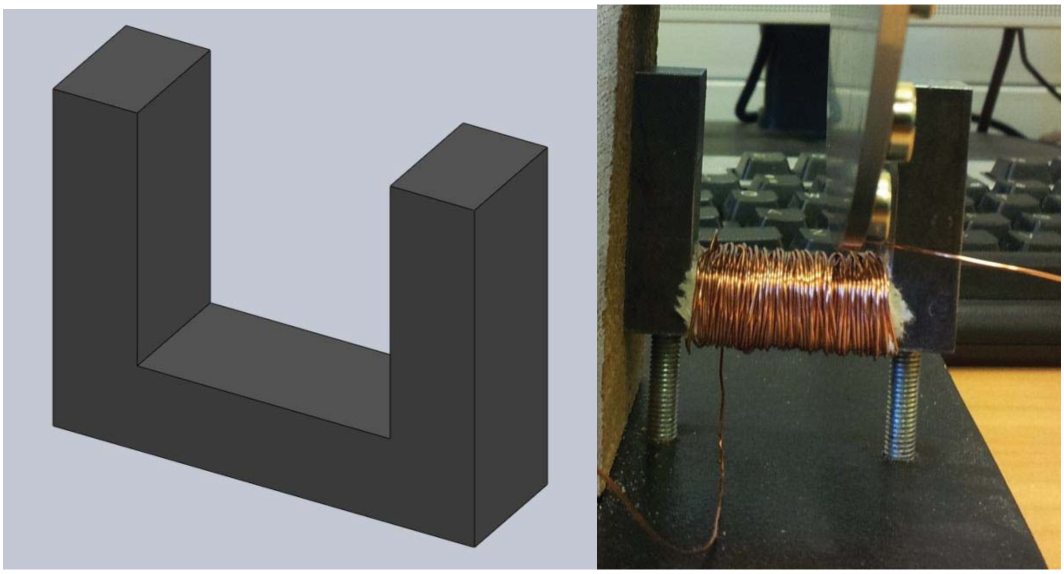

**Figure 3.6:** 3D Model and Initial Design of the Electromagnet

As discussed earlier this design was later changed as having a U shaped electromagnet with a large air gap in the middle meant that there would be huge losses of power. A new electromagnet was designed to reduce the air gap.

Figure 3.7 shows the 3D model of the modified design of the electromagnet on the left. Changing the design from a U shaped electromagnet to the design, as shown in figure 3.7, helped reduce the reluctance. This enabled a more complete circuit for the magnetic flux to travel as the air gap was very small.

The windings on the modified electromagnet remained the same as the U shaped electromagnet. It consisted of 250 turns of 0.5mm gauge enamel covered copper wire, wound layer upon layer from side to side. Figure 3.7 shows the electromagnet after it was wound with the coil on the right.

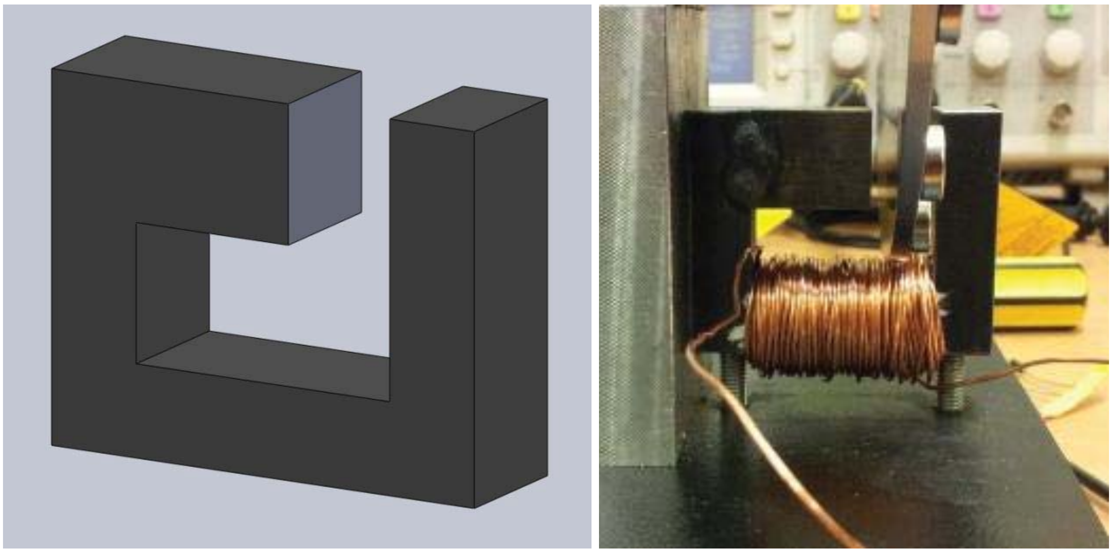

**Figure 3.7:** 3D Model and Final Design of the Electromagnet

## 3.6. Motor

In an actual stationary bike the flywheel spins when the bike is pedalled. For the prototype a 12V high power DC motor was used to spin the flywheel. Figure 3.8 shows the motor used to spin the flywheel. This motor was connected to a voltage generator and the speed of the disc was controlled by varying the voltage on the voltage generator.

 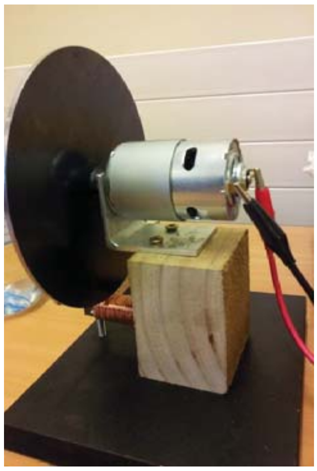

**Figure 3.8:** 12V DC Motor

## 3.7. Magnets

Materials containing neodymium are frequently used in green energy devices such as wind turbines and hybrid because of their strong permanent magnetism. 'Neodymium magnets' are commonly an alloy of neodymium, iron and boron that forms a tetragonal crystal structure with the molecular formula $Nd_2Fe_{14}B$ [48]. This alloy has numerous appealing properties, such as a Curie temperature of 585 K (suggesting that this material will retain its ferromagnetism at high temperatures) and has a high energy product of 440 kJ/m$^3$, which is almost ten times that of ceramic ferrite magnets [49].

Although there are many uses for neodymium in the electronics industry, it is evident that its worth in renewable energy devices is increasingly relevant as the implementation of these technologies increases [51]. Based on these properties and benefits, neodymium magnets were chosen for this project.

Magnets come in all types of shapes, sizes, and magnetization direction. For the purpose of this project, a Neodymium disc magnet of a 10mm diameter and 3mm thickness was used as shown in Figure 3.9. For this magnet the magnetization direction had to be axial, as the poles needed to be on the flat side of the magnets. Table 3.1 is the specification of the magnet.

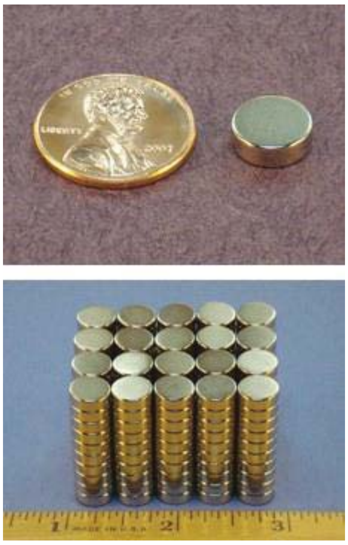

**Figure 3.9:** 10mm Disc Magnet

| | |
|---|---|
| Type | Disc |
| Dimensions | 10mm dia x 3mm thick |
| Magnetization Direction | Axial |
| Material | NdFeB, Grade N42 |
| Plating | NiCuNi |
| Max Op Temperature | 176ºF (80ºC) |
| Br Max | 13,200 Gauss |
| BH Max | 42 MGOe |

**Table 3.1:** Magnet Specifications

Figure 3.10 is a graph of a pull force test conducted on this particular magnet. The test shows the maximum force needed to pull this magnet free from a flat steel plate. This was found to be about 4.41 lbs.

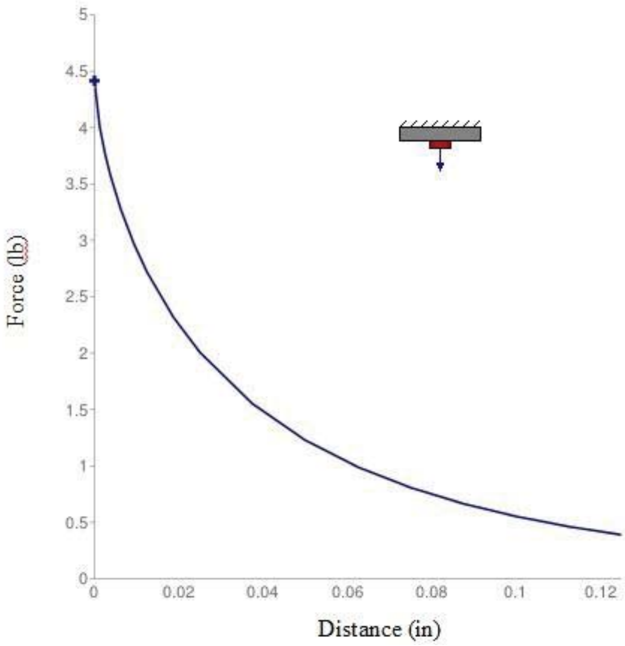


**Figure 3.10:** Pull Force of Magnet

Figures 3.11 shows the magnetic field visual of the magnet in free space and Figure 3.12 gives the BH characteristics of the magnet.

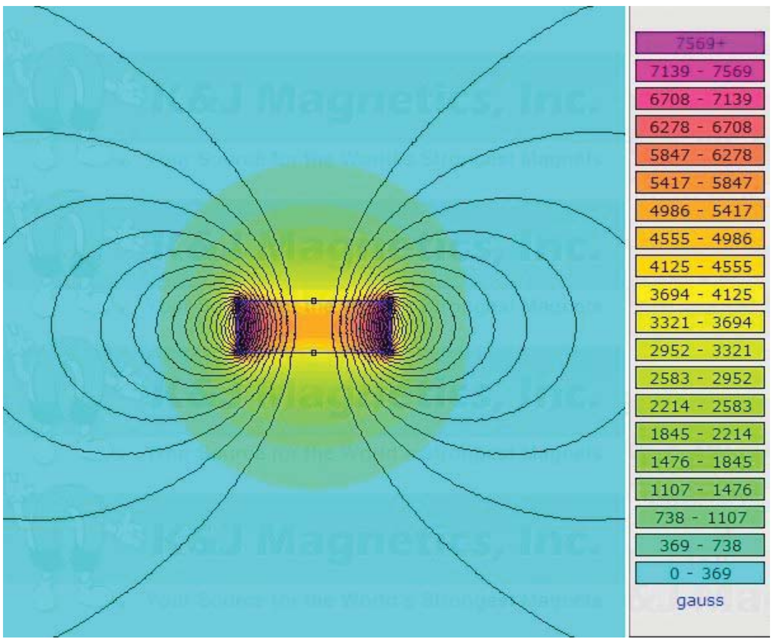


**Figure 3.11:** Magnetic Field of D62 Magnet

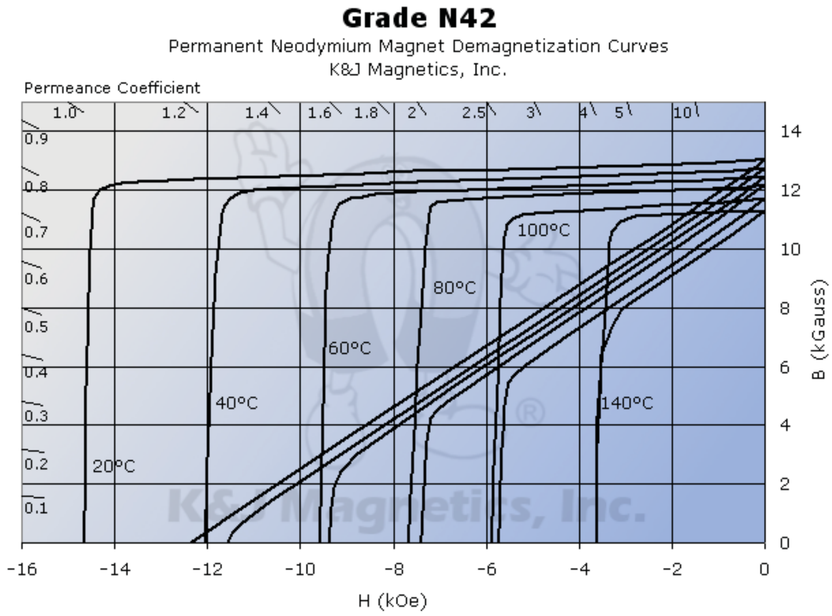


**Figure 3.12:** BH characteristics of the magnet

## 3.8. Experiments

The main goal of the prototype model was to find the most suitable setup for a stationary bike to get the best possible output from the harvester. The following factors needed to be considered to note the effect on the output of placing the magnets on a flywheel and rotating them through the electromagnet.

a) The number of magnets on the disc
b) The placement of the magnets on the disc
c) Pole orientation of the magnets

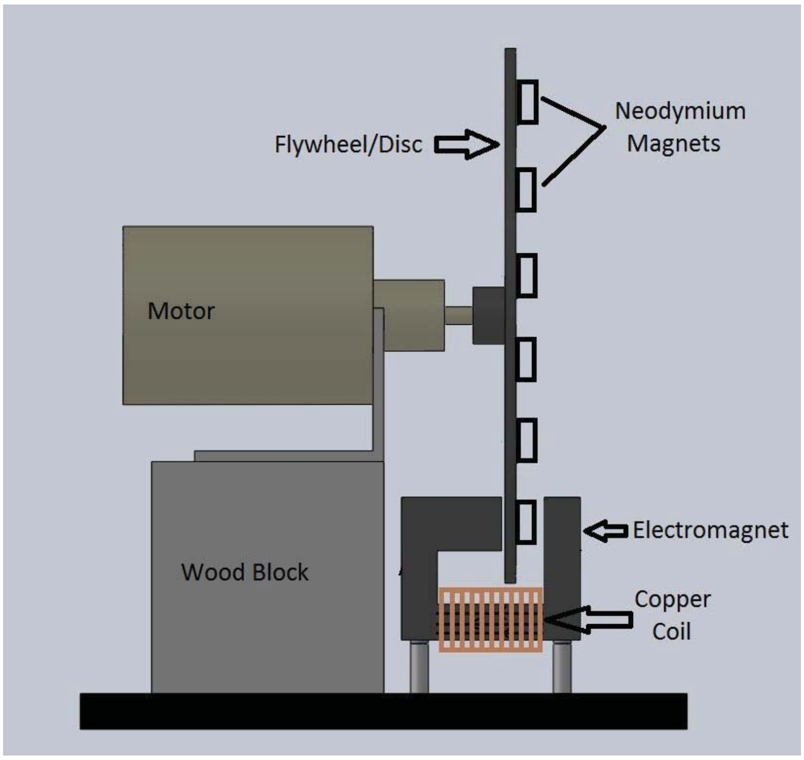


**Figure 3.13:** 3D model of the Prototype

Experiments were conducted with these factors in mind to find the setup that would give the best possible output. The prototype was setup as seen in Figure 3.13.

Figure 3.14 shows the prototype in action. The disc was connected to the motor which was powered by a voltage generator. The speed of the motor and the disc was controlled by varying the voltage on the voltage generator. Multiple magnets were placed on the disc and spun through the electromagnet. The output of the electromagnet was connected to an oscilloscope and the waveforms were captured.

**Figure 3.14:** Prototype Model running

The waveforms were used to analyse and note the effects the three factors listed above had on the output of the electromagnet. Once the best setup was found the output of the electromagnet was rectified and boosted. This was done in order to note the amount of power this kind of a setup could generate. Figure 3.15 shows the steps taken to note the amount of power that could be generated by this set up.


**Figure 3.15:** Process diagram of the experiment

### 3.8.1. Pole orientation of the magnets

Before checking the effects of the number of magnets and the placement of magnets, it was imperative to check the pole orientation that would best suit this setup. As seen in figure 3.16

the magnetic flux goes from the North pole to the South pole. Based on this characteristic, it was assumed that having all magnets with the same pole orientation would be ideal. This meant that all the magnets on the disc had the same pole face touching the disc.

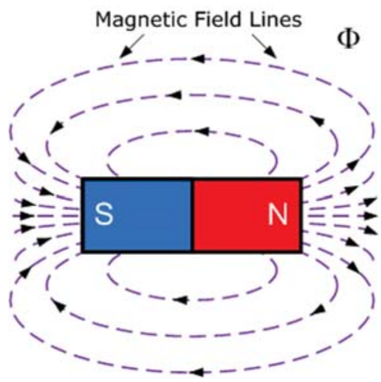


**Figure 3.16:** Magnet displaying magnetic field lines

Figure 3.17 gives a visual of this. As the flux would go from north to south, it was assumed that having the magnets as displayed in Figure 3.16 would mean that the magnetic field lines would pass through the electromagnet such that it passes through the core and the coil in the electromagnet.

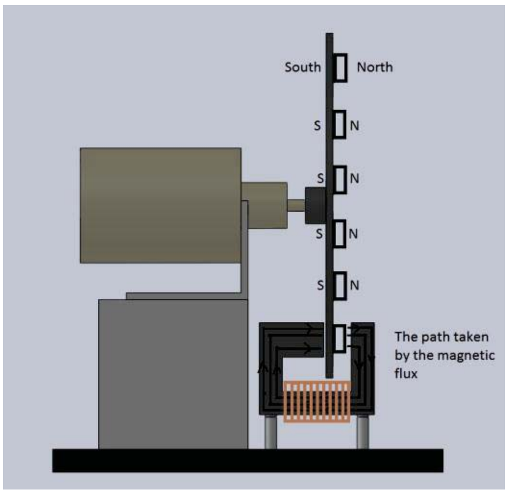


**Figure 3.17:** Prototype with all the magnets facing same poles.

An experiment was done with a setup as shown in Figure 3.17. The output from the coil was connected to an oscilloscope from which waveforms were captured. The experiment was repeated with the changed pole orientation of the magnets, so that the magnets alternated poles. This is shown in Figure 3.18.

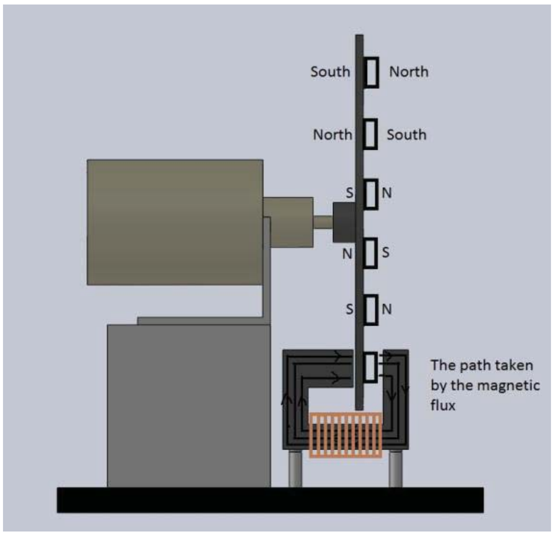


**Figure 3. 18: Magnets with alternating poles**

Both experiments were run exactly the same way. The disc was spun at the same speed of 200RPM. The only difference was the pole orientation of the magnets. Waveforms from both experiments were captured and analysed as shown in Figure 3.19.

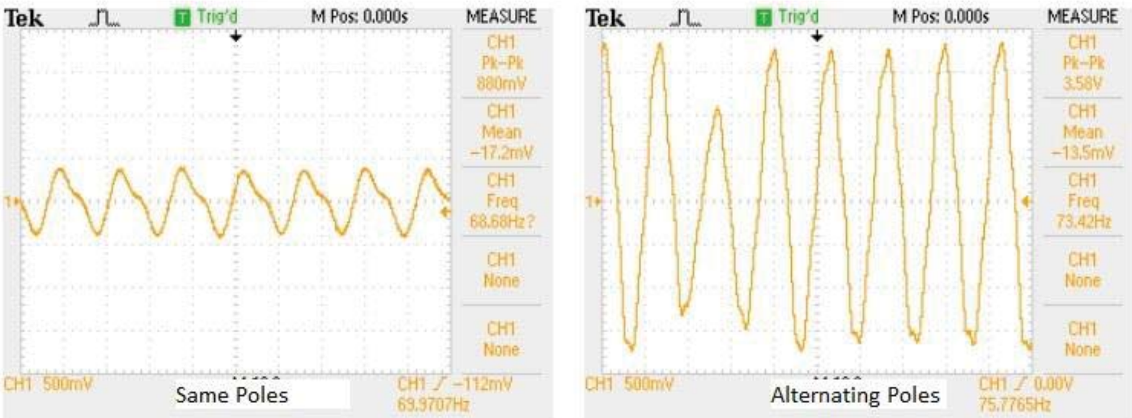


**Figure 3.19:** Magnets with same poles and alternating poles at 200RPM

The peak-peak voltage of the captured waveforms was used to note the strength of the signal coming from the electromagnet. Figure 3.19 shows, on the left, that when the disc was spun at 200RPM, the peak-peak voltage coming from the coil was 880mV. However, when the disc was spun at 200RPM with magnets having alternating poles, the peak-peak voltage of the coil was 3.58V as seen in Figure 3.19, on the right. Comparing these two waveforms it was evident that alternating the poles on the magnets would produce a much higher output.

When all the magnets were placed having the same poles in one direction, the only change was that the magnetic field was varying in strength. As a magnet approaches the coil, the magnetic strength increases and as the magnet passes the strength decreases. This continued to happen as each magnet passed through. As a result, only a small amount of Electro Magnetic Flux (EMF) was being generated. But when the magnets were placed where the poles alternate, not only did the magnetic strength change but also the direction of the magnetic field changed and hence created more flux.

### 3.8.2. Number of magnets

After deciding that having alternating poles gave a higher output, tests were run to note the effect the number of magnets on the disc, would have on the output. The magnets were placed with equal distance between each magnet. To be precise a drawing matching the size of the disc was done in Solidworks, which marked out the placement of the magnets. Figure 3.20 shows how the magnets were placed on the disc.

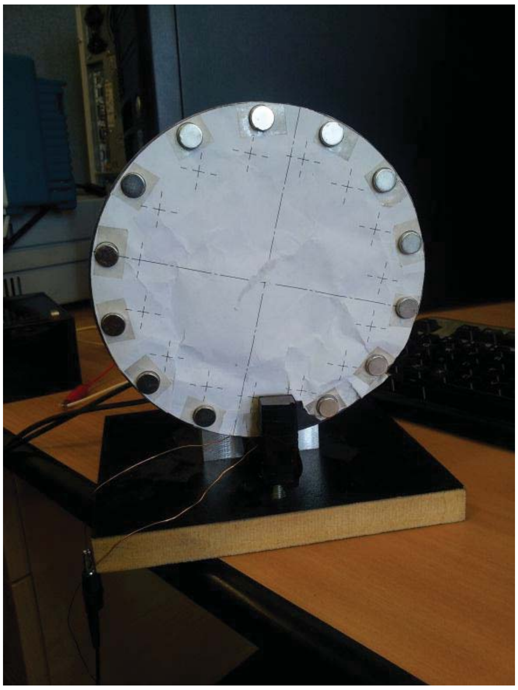

**Figure 3.20:** Placement of magnets on the disc

Four experiments were conducted and each test had different number of magnets on the disc. Spinning the disc at various speeds, experiments tested the effect on the output when the disc had 8, 10, 12 and 14 magnets. The outputs from the coil were connected to an oscilloscope and waveforms were captured. Table 3.2 shows the peak-peak output voltages at various speeds for the four tests conducted.

| Speed (RPM) | 8 Magnets (Pk-Pk V) | 10 Magnets (Pk-Pk V) | 12 Magnets (Pk-Pk V) | 14 Magnets (Pk-Pk V) |
|---|---|---|---|---|
| 74 | 0.48 | 0.76 | 0.96 | 0.36 |
| 95 | 0.88 | 0.96 | 1.04 | 0.44 |
| 123 | 1.16 | 1.2 | 1.64 | 0.52 |
| 148 | 1.48 | 1.58 | 1.8 | 0.56 |
| 176 | 1.64 | 1.88 | 2.08 | 0.64 |
| 212 | 1.96 | 2.08 | 2.32 | 0.68 |

**Table 3.2:** Peak-peak voltage with 8, 10, 12 and 14 magnets

With the data acquired from the tests conducted, it was noted that having more magnets did not necessarily mean better outputs. The output increased when the magnets were increased from 8 to 10 magnets and 10 to 12 magnets. However, increasing the number of magnets from 12 to 14 made the output drop drastically. Figure 3.21 shows the relationship of the number of magnets with respect to the speed of the disc. This showed that for this setup having 12 magnets with alternating poles gave the highest output.

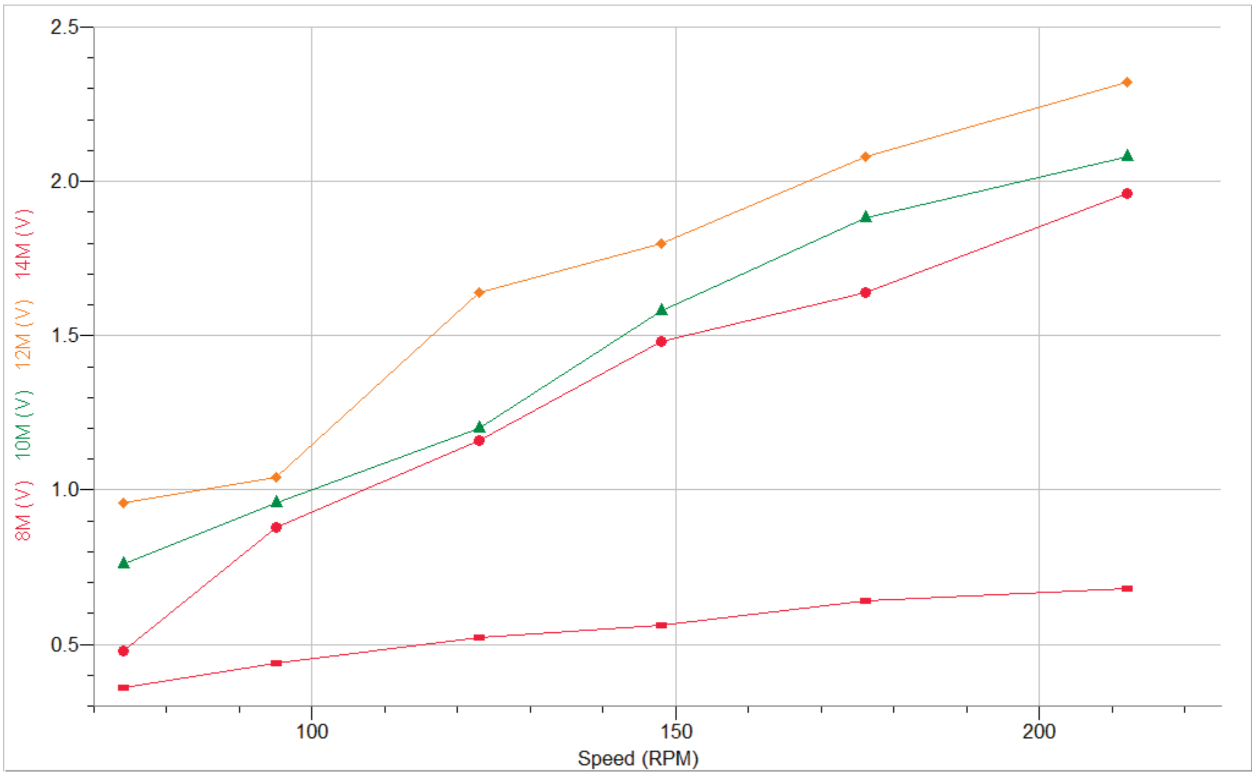


**Figure 3.21:** Relationship between number of magnets and the speed

With the data acquired from the experiment it was noted that the higher the number of magnets the higher the change in the magnetic field strength and direction. This created more flux, which in turn generated more EMF. However, there was a limitation to this concept as having too many magnets very close to each other produced very little flux. As the number of magnets were increased the space between the magnets was reduced. Since the magnets were placed on the disc where they alternate poles, having the magnets too close to each other would cause the output to decrease since, the magnetic field lines of a magnet would go from a magnet into the magnet opposite to it instead of cutting the coil.

Figure 3.22 are the waveforms captured when the disc was spun at 212RPM with 8, 10, 12, and 14 magnets. The waveforms clearly showed that having 12 magnets with alternating poles would give the best output.

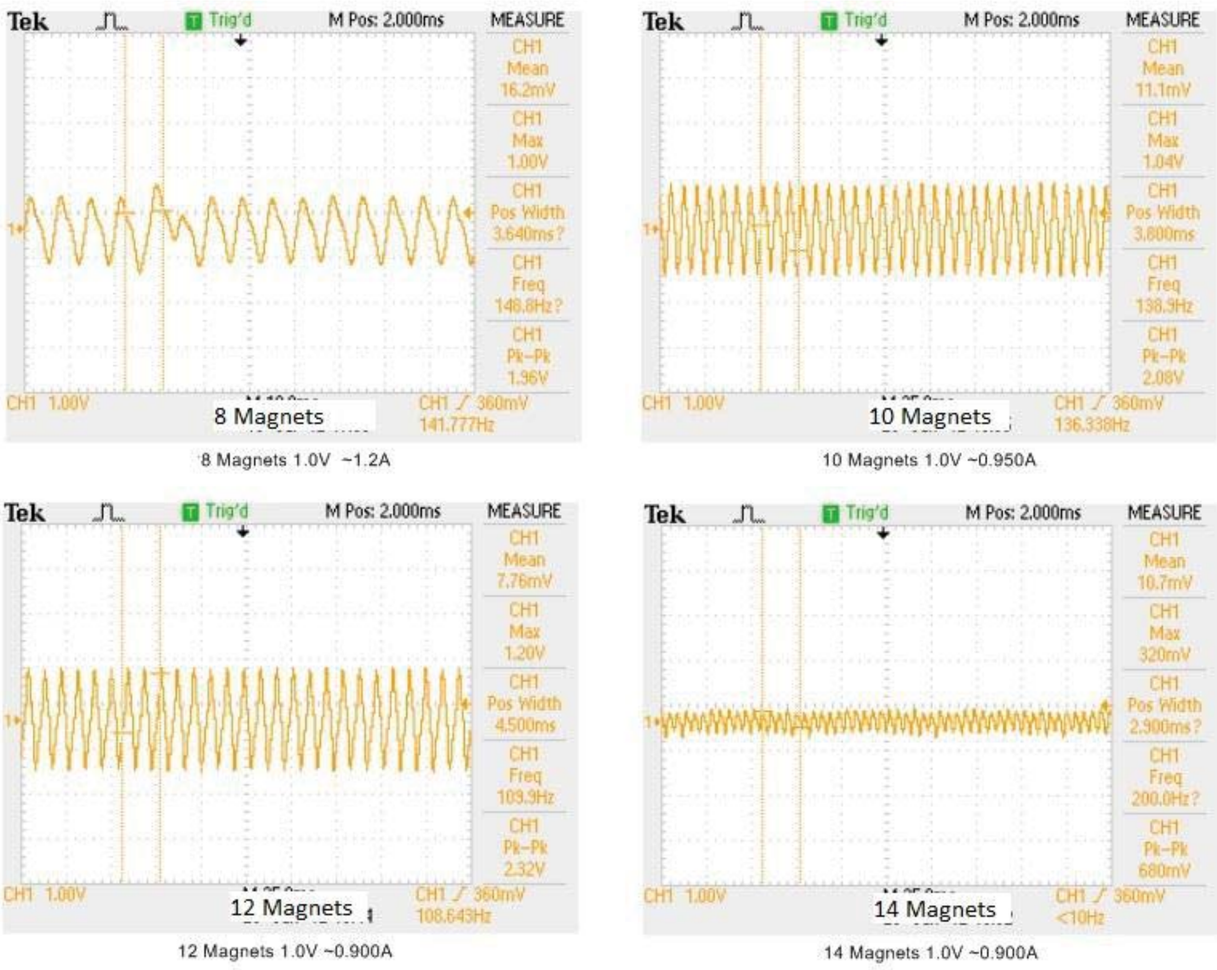


**Figure 3.22:** Waveforms of the outputs with 8, 10, 12 & 14 magnets at a speed of 212RPM

### 3.8.3. Placement of magnets

Once the number of magnets was decided, experiments were conducted to see if having the magnets on different parts of the disc affected the output. The magnets were placed on two parts of the disc, close to the edge of the disc and in line with the electromagnet. Figure 3.23

shows the magnets placed in line with the electromagnet, (on the left), and the magnets placed to the edge of the disc (on the right).

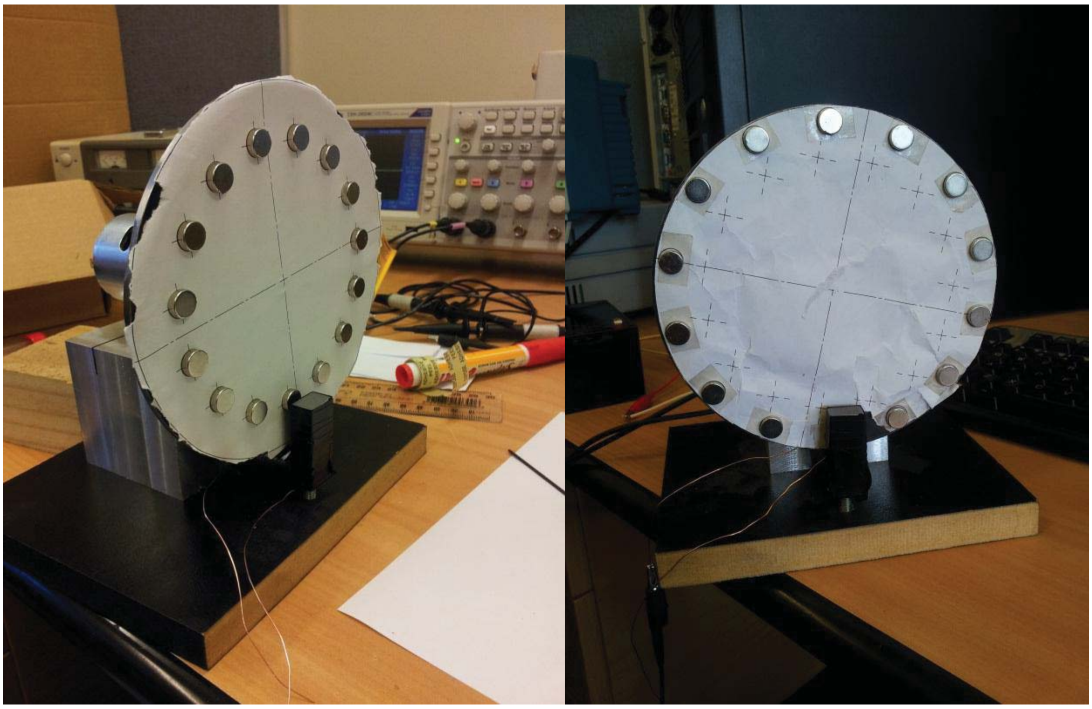

**Figure 3. 23:** Magnets in line with the electromagnet and to the edge of disc

Having the magnet to the edge of the disc, meant that there was an air gap of 4mm between the disc and the edge of the electromagnet. Placing the magnets in line with the electromagnet reduced this air gap from 4mm to 1mm as the thickness of the magnet was 3mm. Further, having the magnets in line with the electromagnet made a closed loop making it easier for the flux to pass through. Figure 3.24 shows a 3D model setup of what this looked like.

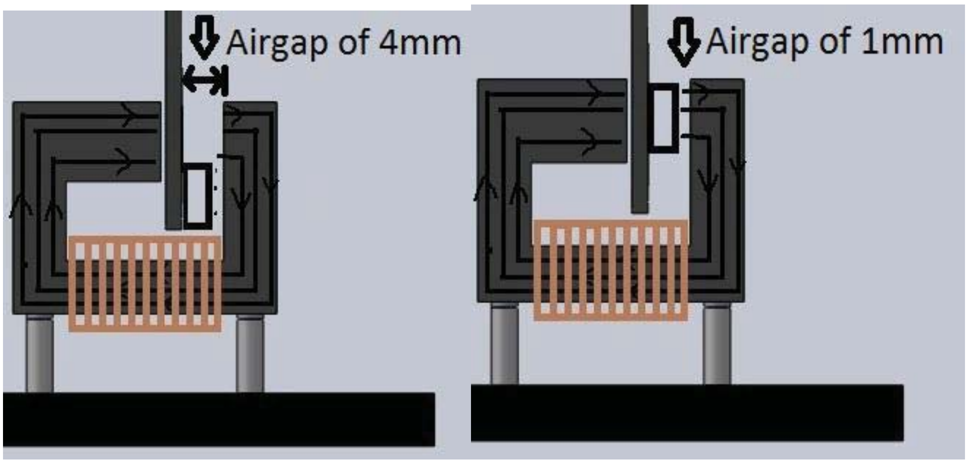


**Figure 3.24:** Magnet to the edge of disc and Magnet in line with the electromagnet

Experiments were run at various speeds with 12 magnets on the disc. The results of these experiments are shown in Table 3.3.

| **Speed (RPM)** | **12 Magnets (Pk-Pk V)** | **12 Magnets to the edge (Pk-Pk V)** |
|---|---|---|
| 74 | 0.96 | 1.12 |
| 95 | 1.04 | 1.48 |
| 123 | 1.64 | 1.8 |
| 148 | 1.8 | 2.13 |
| 176 | 2.08 | 2.44 |
| 212 | 2.32 | 2.8 |

**Table 3.3:** Peak-Peak voltages of magnets to the edge and in line with the electromagnet

Results showed that both closeness of the magnet to the coil and minimal air gap would give the best output. In this setup one had to be chosen over the other because of the way the electromagnet is designed. Reducing the air gap meant having the magnet away from the coil. Not having the magnet close to the coil meant having a lower output. Since this experiment was looking for what would give the higher output, having magnets to the edge was chosen over having the magnets in line with the electromagnet. Figure 3.26 shows the peak-peak output voltage with respect to the speed of the disc and figure 3.25 shows the waveforms captured when magnets were placed in line with the electromagnet and when magnets were placed to the edge of the electromagnet.

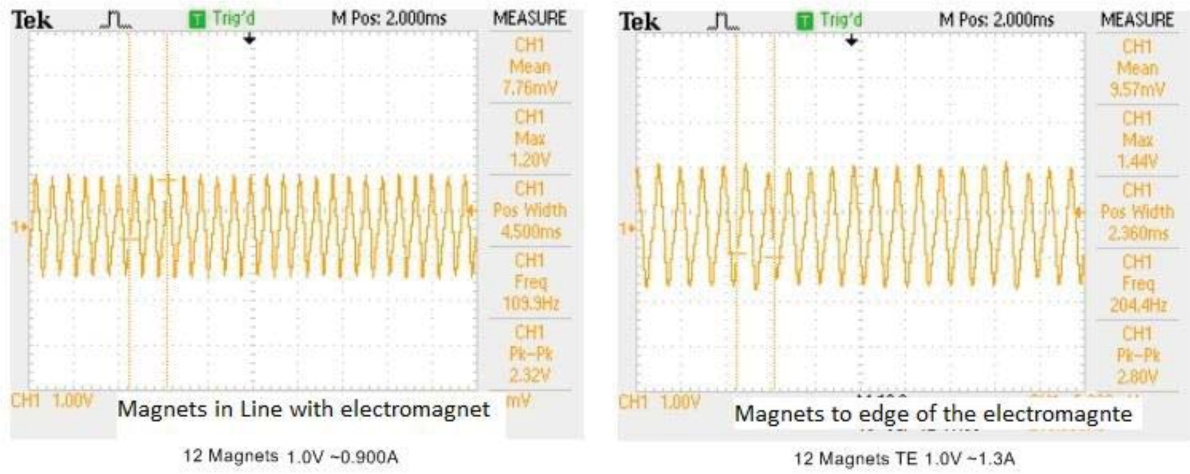


**Figure 3.25:** Waveforms for magnet placed in line with Electromagnet to the edge of disc

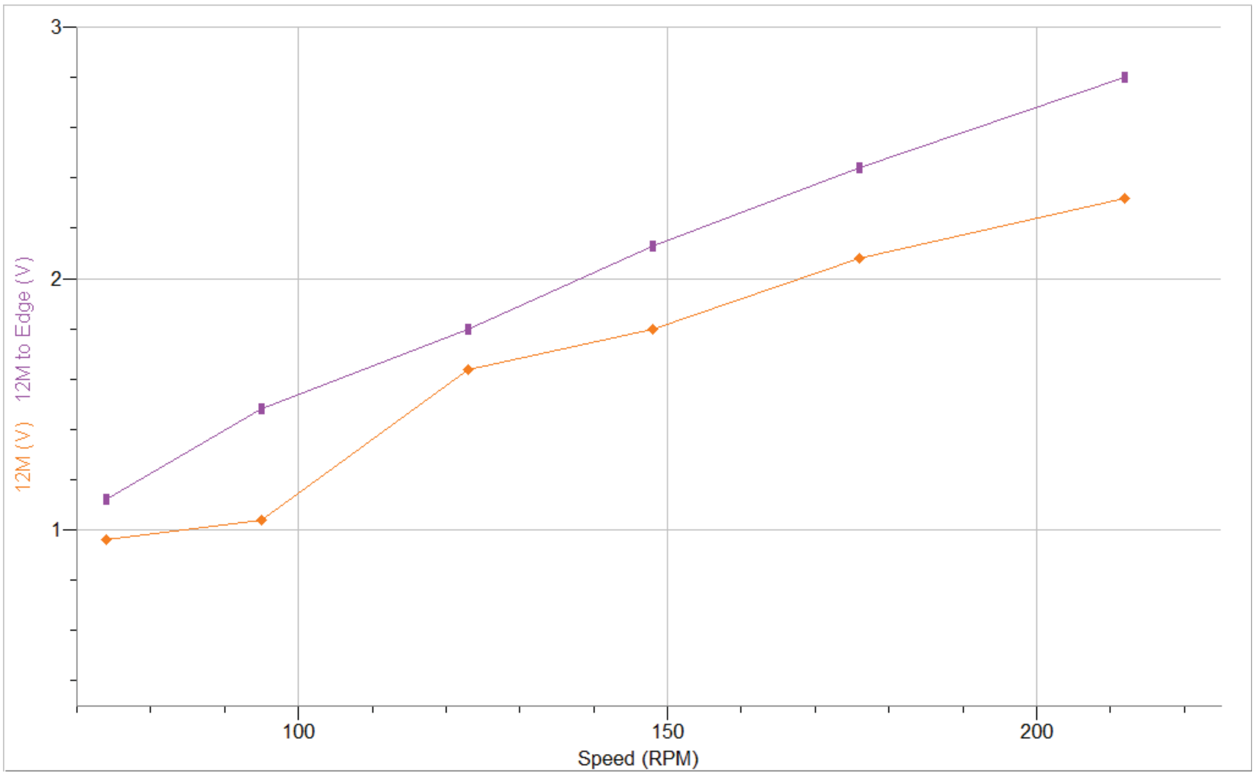


**Figure 3.26:** Relationship between magnet placement and speed

## 3.9. Electronic Circuits

The output from the electromagnet is an AC signal. This signal had to be rectified before being connected to a boost converter. A simple rectification circuit was made with the use of four Schotky diodes. Once the signal was rectified, it then needed to be boosted and put across a load to investigate the amount of power this kind of setup could generate.

The first circuit designed was a simple rectification circuit consisting of 4 schotkky diodes. This was used to convert the AC signal coming from the electromagnet into a DC signal. A few tests were done to note the output of the rectification circuit. It was found that the DC signal coming out of the rectification circuit ranged from 500mV to 1.5V depending on the speed of the flywheel disc.

A boost converter was required as the rectified DC signal was low. Using one of the application diagrams suggested in the LTC3105 datasheet [56] a converter design was made to meet the needs of this experiment. A converter was designed to boost the voltage coming into the converter to 4.1V.

### 3.9.1. Boost Converter

Implementation of low-power electronics is critical to minimize the circuit loss in EH. Significant research efforts have been dedicated to improve the circuit efficiency [9]. For the majority of the time the power generated by energy harvesters is quite low. Hence, it is important to have circuits which can boost the voltage generated by the harvester. Also as the signal coming into the boost converter would be low, a boost converter with low start-up voltages had to be designed. Various converter topologies were researched and the LTC3105 integrated step-up circuit by Linear Technology was chosen.

The LTC3105 stands out mainly because it was specifically designed for applications which require low start-up voltage. The LTC3105 is able to operate from high impedance sources like solar cells, has maximum power point control, low power input, burst mode to adjust peak switching current and has a low start-up voltage of 250mV [56]. All these features made the LTC3105 as the ideal power converter for this project.

Figure 3.27 is an application diagram taken from the datasheet of the LTC3105 (see appendix A). This is almost identical to the circuit utilized in this project, except for the component values. Figure 3.28 shows the internal block diagram of this chip.

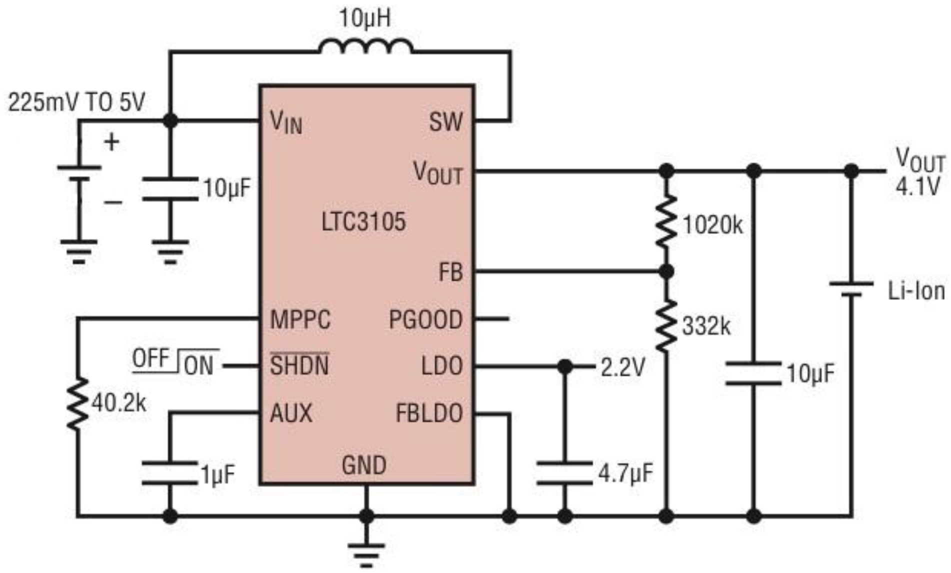


**Figure 3.27:** Step-up Circuit from data sheet

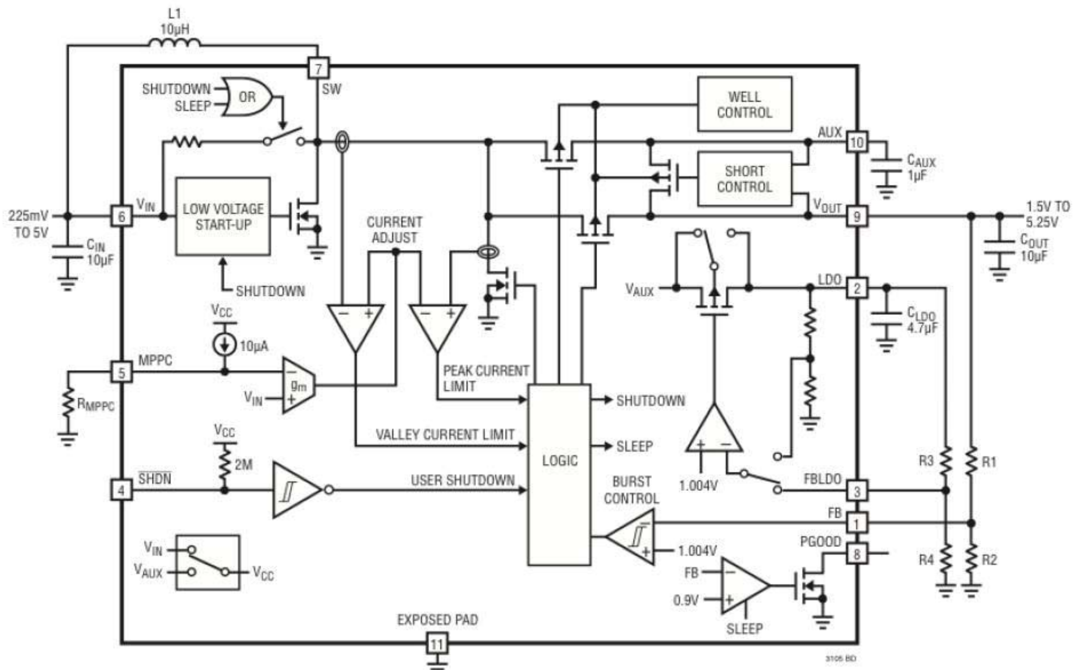


**Figure 3.28:** Internal Block Diagram of LTC3105

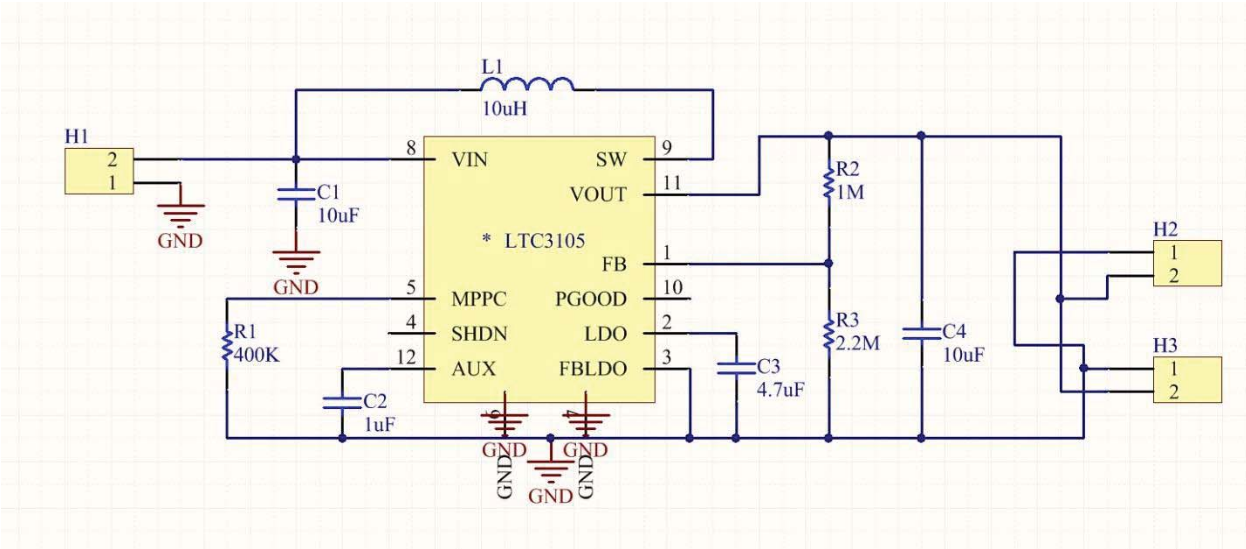


**Figure 3.29:** Boost Converter Schematic

Figure 3.29 shows the circuit schematic that was drawn in Altium Designer, an electronics design software. The LTC3105 begins by charging the $C_{AUX}$ and keeps charging it till it reaches 1.4V. At this time the maximum power point control (MPPC) is not yet enabled. When $V_{AUX}$ reaches to 1.4V the LDO output is regulated by the converter. Once this is done the output is turned ON and the converter begins to operate and boost the voltage to 4.1V. Figure 3.30 shows the waveforms of this process.

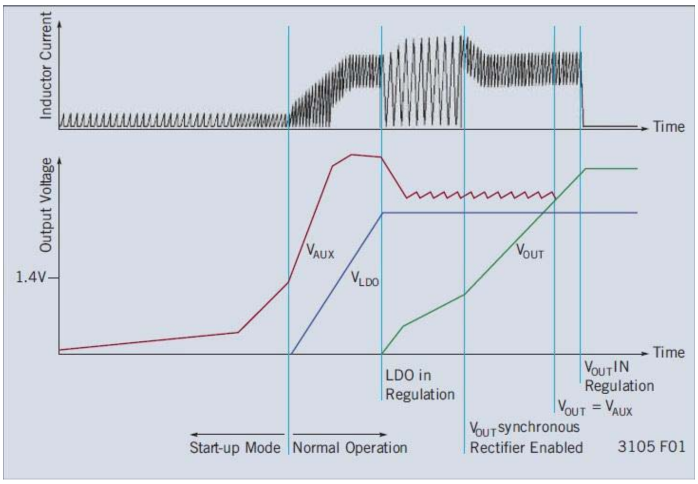


**Figure 3.30:** Waveform for LTC3105 at start-up mode and normal operation mode

As the energy coming in from the harvester varies depending on the person pedalling the bike, it is necessary to have a control in place, to make sure that the circuit is not dropping below or going higher than the threshold value. This is where the MPPC is useful as it allows the user to set the desired input voltage operating point for a given power source. This is done via the resistor connected to the MPPC pin, allowing the IC to make sure it operates the input at this fixed voltage. When $V_{IN}$ is greater than the set MPPC voltage the inductor current is increased until $V_{IN}$ is pulled down, and when $V_{IN}$ is lesser than the set MPPC voltage the inductor current is reduced until $V_{IN}$ rises to the MPPC set point. This is important for this experiment as the voltage coming in $V_{IN}$ keeps fluctuating so having MPPC helps keep the input to the converter constant [56].

Figure 3.31 shows the PCB design before it was printed on to a circuit board and Figure 3.32 shows the PCB with all the components mounted onto the board.

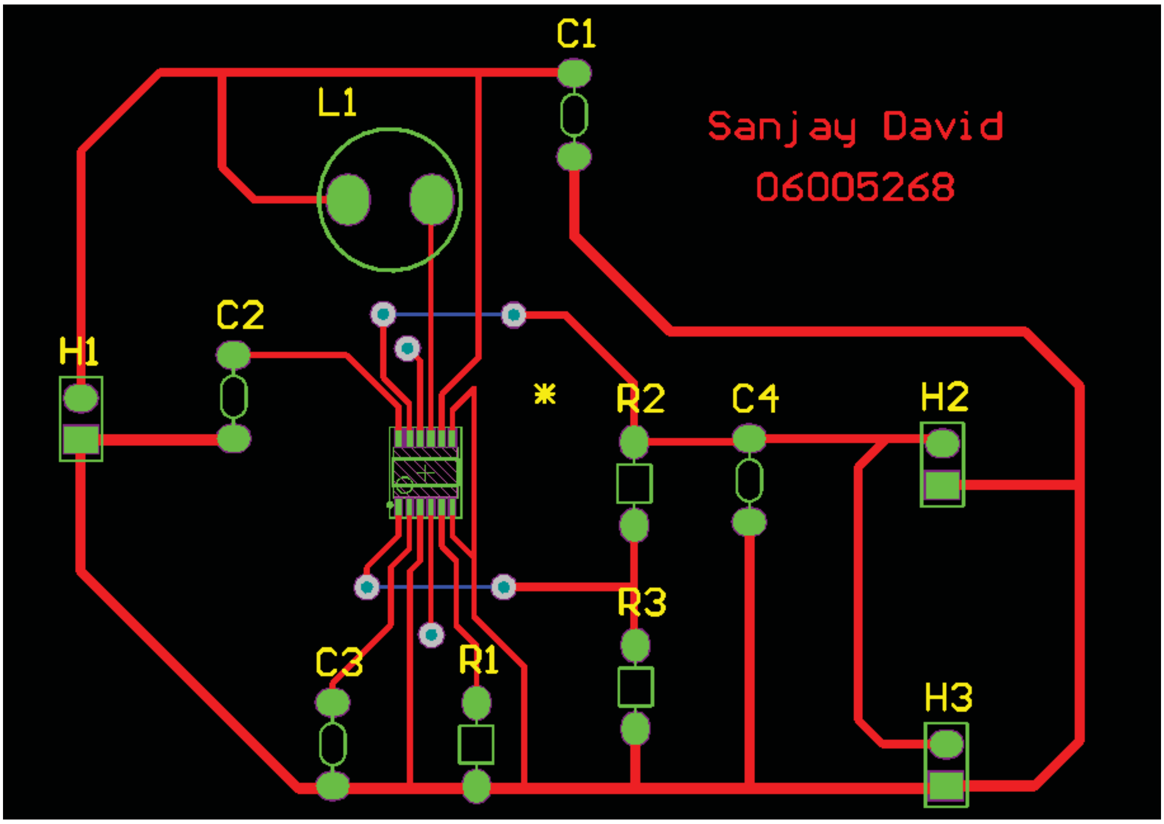


**Figure 3.31:** Printed Circuit Board design in Altium

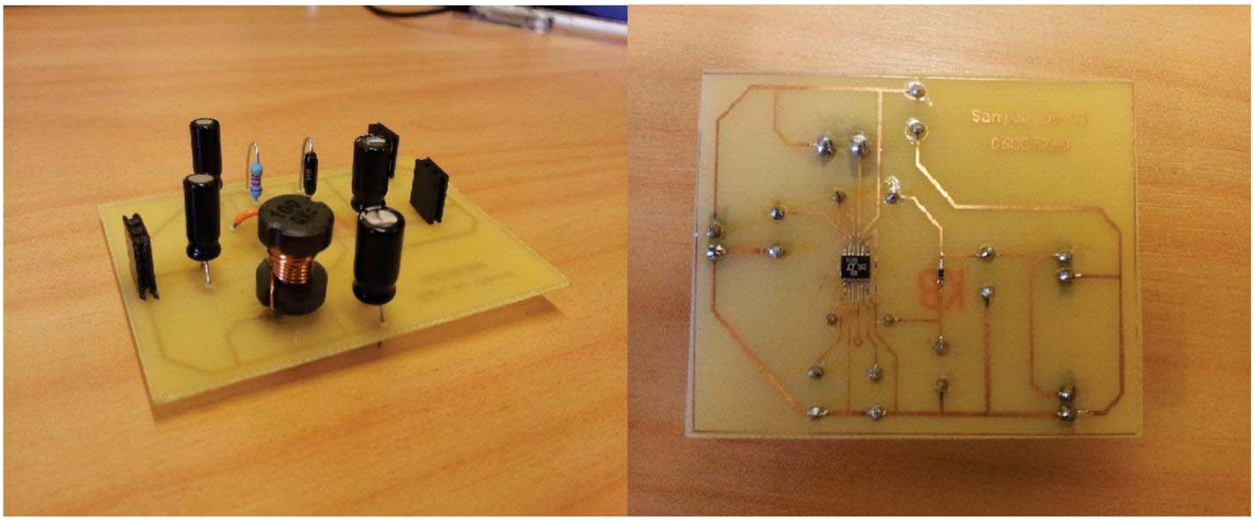

**Figure 3.32:** Boost Converter with parts mounted on board

### 3.9.2. Power Calculations

The experiments that were discussed showed that for this setup, using 12 magnets with alternating poles placed to the edge of the disc would provide the best output. The following experiments were done with the model setup in that manner. Figure 3.33 shows the steps that were taken for these experiments.

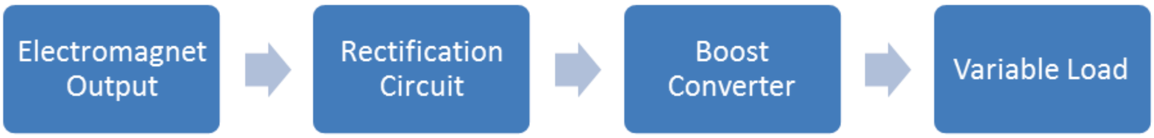


**Figure 3.33:** Process block diagram for power calculations

The AC signal generated by the electromagnet was rectified and boosted, using the converter discussed earlier in this chapter. Figure 3.34 shows the setup for the power calculations made.

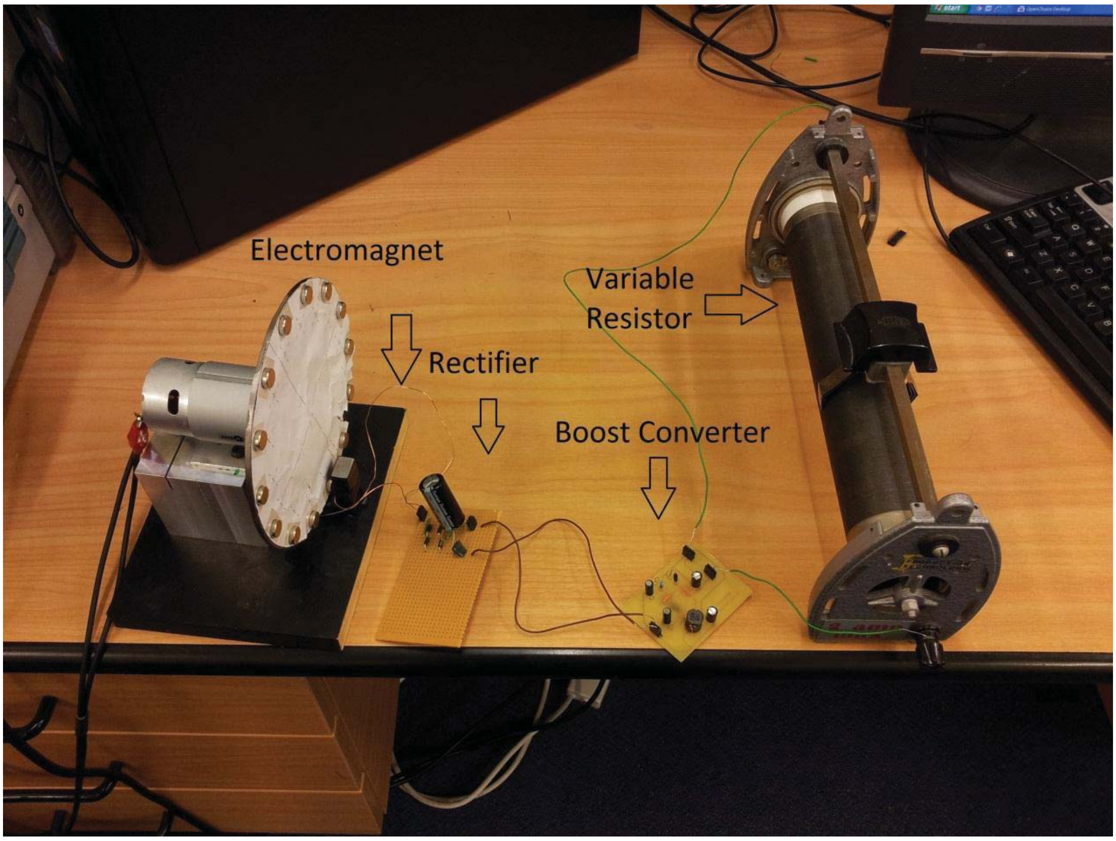


**Figure 3.34:** Setup to calculate power

Before the load was connected to the boost converter a few tests were done to check if the boost converter was operational. Table 3.4 shows the output from the rectification circuit and the output from the boost converter at different speeds.

| 12M AP Rectified & Boosted | | |
|---|---|---|
| **Speed (RPM** | **Rectified (V)** | **Boosted (V)** |
| 74 | 0.0788 | 4.18 |
| 95 | 0.721 | 4.19 |
| 123 | 0.936 | 4.18 |
| 148 | 1.06 | 4.18 |
| 176 | 1.31 | 4.18 |
| 212 | 1.43 | 4.18 |

**Table 3.4:** DC outputs from Rectification and Boost Circuits

One probe of the oscilloscope was connected to the output from the rectification circuit and another probe was connected to the output from the boost converter. Figure 3.35 shows the waveforms captured. Channel 2 (the blue line) shows the output of the rectification circuit which was also the input to the boost converter. Channel 1 (the yellow line) shows the output of the boost converter. The waveform on the left was captured when the flywheel was spinning at 95RPM. The waveform on the right was captured when the flywheel was spinning at 212RPM. This showed that the boost converter was boosting the input voltage and maintaining it at 4.18V.

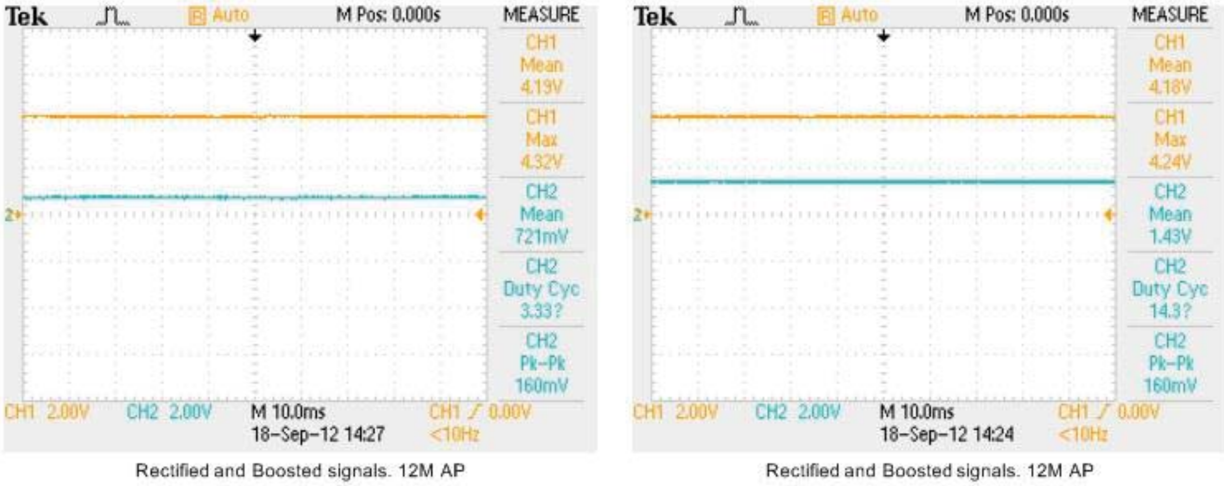


**Figure 3.35:** Waveforms of the output of rectifier and boost converter

The final step in this experiment was calculating the power output of the complete system. To calculate the output the boost converter was connected to a variable resistor. The resistor was set from a value of 10ohm to 100ohm. The flywheel was spun at four different speeds and the power was calculated. Table 3.5 shows the power values across a range of loads at different speeds.

| Load (ohm) | 74RPM (Watt) | 123RPM (Watt) | 148RPM (Watt) | 240RPM (Watt) |
|---|---|---|---|---|
| 10 | 0.0000676 | 0.0001849 | 0.00016 | 0.0021025 |
| 20 | 0.000125 | 0.0003698 | 0.0004418 | 0.00186245 |
| 30 | 0.000192533 | 0.000512533 | 0.000563333 | 0.0023763 |
| 40 | 0.00025 | 0.000648025 | 0.000765625 | 0.002544025 |
| 50 | 0.0003125 | 0.00079202 | 0.00109512 | 0.00297992 |
| 60 | 0.000416067 | 0.001170417 | 0.001392017 | 0.0036504 |
| 70 | 0.000691429 | 0.001903214 | 0.002128514 | 0.004756129 |
| 80 | 0.00091125 | 0.00190125 | 0.002194513 | 0.005040313 |
| 90 | 0.000934444 | 0.002025878 | 0.003216044 | 0.005351511 |
| 100 | 0.001225 | 0.00272484 | 0.004096 | 0.00565504 |

**Table 3. 5:** Power values at different speeds

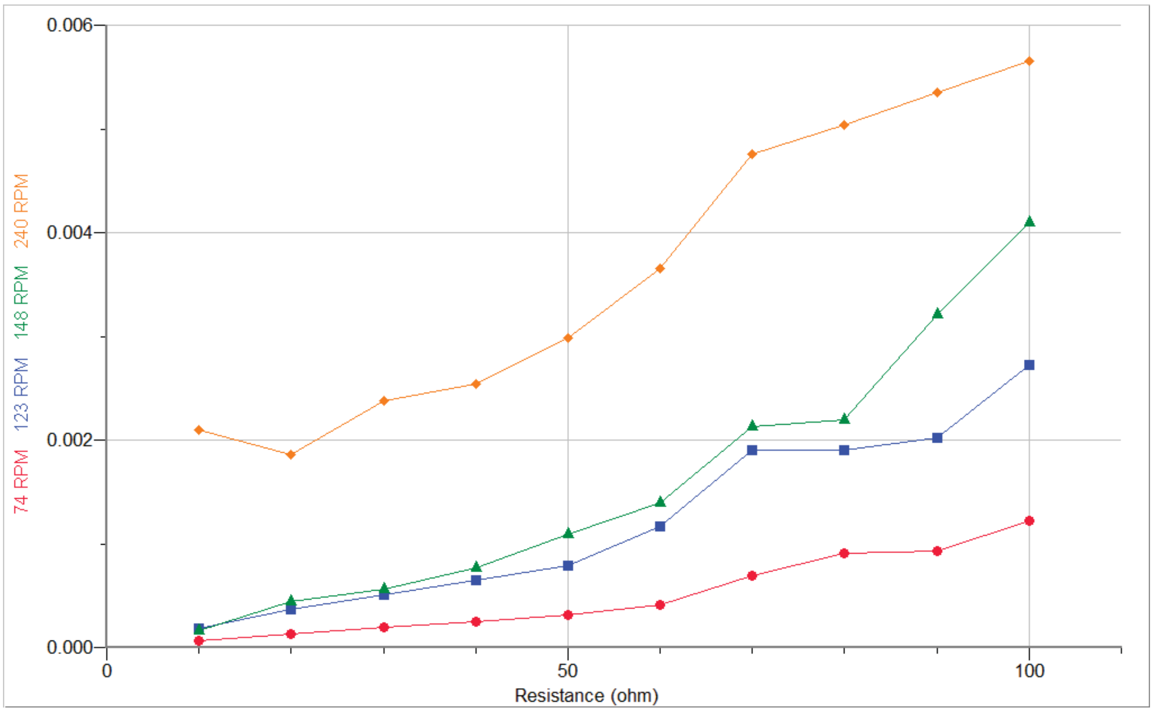


**Figure 3.36:** Power values plotted in relation to the resistance (load) and speed of the flywheel

Figure 3.36 graphs the power values across the speed and load. This shows that as the speed of the flywheel increases, the power generated by the coil increases as well.

In summary, experiments showed that having alternating poles on the flywheel would give a higher output than having magnets with the same poles. It was also found that while having more magnets produced a higher output there was a limit to the number of magnets on the disc for the desired effect. Having too many magnets meant that the magnets were too close to each other and this caused the output to drop drastically. In the case of the placement of magnets, experiments showed that having the magnets close to the coil gave the highest output. Finally, findings showed that more power was generated as the speed of the flywheel increased.

# Chapter 4. THE STATIONARY BIKE: METHODOLOGY

## 4.1. Introduction

Every machine in a gym with a flywheel can be used to harvest energy. Almost every stationary bike has a big flywheel that is visible in most bikes. This assists the objective of making an EH system which can be installed onto an exercise machine without any changes to the structure of the machine.

A common spin bike was acquired from a fitness store for the following experiments. Neodymium disc magnets of different thickness were bought. The electromagnetic core is the main part of the energy harvester for such an experiment. Mild steel and Electrical steel was used to make the electromagnet. Mounts to hold the electromagnet in place were designed and machined using a CNC machine.

## 4.2. Stationary Bike

The basic structure of a stationary bike is a modified design of a bicycle. It is designed for high intensity training which regular bikes cannot handle. These bikes are built with steel frames and are able to withstand a lot of pressure. The pedals are commonly connected to a gear which is fixed and constant resistance is provided by the flywheel mechanism. The flywheel usually varies in weight and the heavier the flywheel is the greater is the momentum. [47]

The stationary bike is designed to feel a lot like riding a regular bicycle. The only difference is that it does not move when pedalled and hence the term stationary. As the bike is pedalled the flywheel spins and builds momentum. All stationary bikes have a knob present on the bike with which the rider can increase or decrease the resistance while pedalling [47].

A Vortex Spinner bike was used for this project as seen in Figure 4.1. This stationary bike was manufactured by Elite fitness, one of the leading manufacturers of stationary bikes in

New Zealand. It comes with all the functionalities any standard stationary bike in a gym would have.

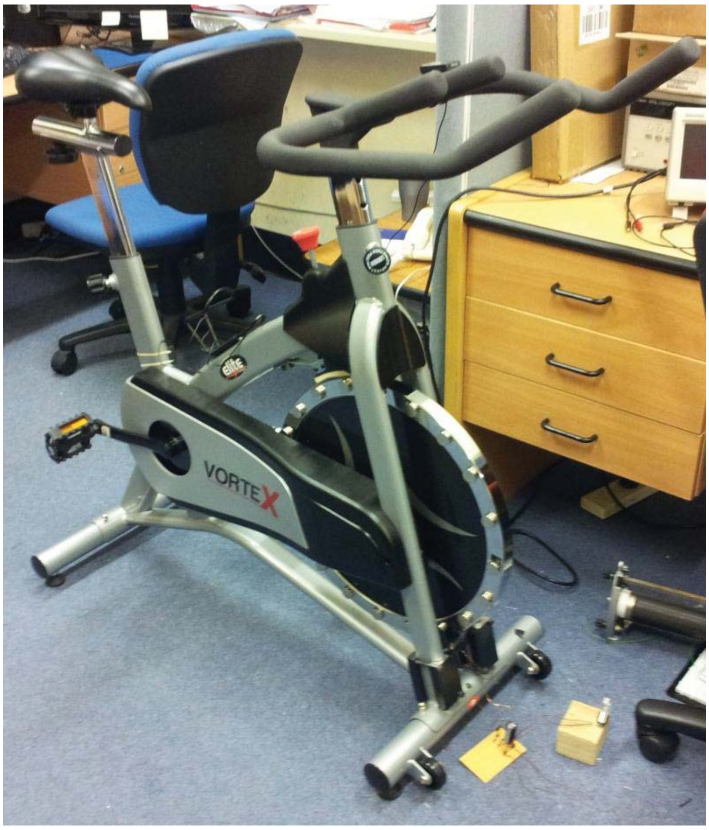


**Figure 4.1:** Vortex Spinner Bike

Stationary bikes are driven by either chains or belts. This particular model is a chain driven system. It is called a chain drive because a chain connects the flywheel of the bike to the crank [57]. Stationary bikes with chain drives are identical to the drive system of a real road bike.

### 4.2.1. Flywheel

Flywheels are designed to store and release mechanical energy. A Flywheel is disc-shaped, and true to its weight on all sides and locations of the disk. The size and weight of the flywheel is proportional to the power produced. However, there is a trade off with the amount of energy needed to get larger flywheels in motion. As a flywheel spins faster, it accumulates more energy. As it slows down, it releases that stored energy and increases the rotational momentum put out by its power source. Flywheels are made out of steel, but they can be created out of any material that can be manipulated into a wheel. Concrete, rebar, and plywood are all capable materials

A flywheel is usually located in the front of the bike, where the wheel of a bicycle would be. It is known as the heart of the exercise system. It spins and builds momentum as it is pedalled. It provides a smooth ride designed to feel a lot like biking outdoors. Resistance can be adjusted using the knob which controls the tension.

The weight of the flywheel is what makes one machine better than the other. Flywheels vary in weight and size but they usually weigh around 38lbs or 17.5 kilos [47]. The greater the weight of the flywheel, the smoother the ride. This is because the weight smoothens out the variations [57]. The stationary bike used for this project had a flywheel that weighed 18kgs as seen figure 4.2.


**Figure 4.2:** 18kg Flywheel of Vortex Spinning Bike

### 4.2.2. On-board computer

Most stationary bikes come with an on-board computer mounted in the front. It informs the rider of their speed, the distance they have travelled, the number of calories they have burned, the RPM of the bike and the time. It was quite expensive to get a stationary bike with an on-board computer; therefore a bike without this feature was bought.

A cycle computer was bought separately as this was more cost effective. It was important to know the speed of the flywheel for this project. An EONtouch 16C cycle computer was bought to display the speed of the bike. Figure 4.3 shows the main interface of the cycle computer.

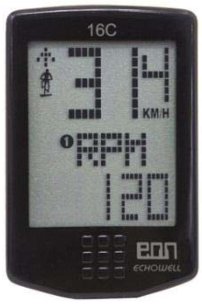


**Figure 4.3:** Cycle Computer Interface

This computer is not limited to one particular machine as it can be programmed and used on any bike. To set the computer for this project the circumference of the flywheel had to be input. This provided the speed of the bike in km/h and the RPM of the bike. The cycle computer came with a magnetic sensor and a transducer which communicated with the main computer. The magnetic sensor was placed on the flywheel and the transducer was placed parallel to the sensor. For every revolution the flywheel completed, the sensor would go past the transducer once. Since the computer knew the circumference of the flywheel, it was able to calculate the speed.

## 4.3. Electromagnet

A magnet that runs on electricity is called an electromagnet. Unlike a permanent magnet, changing the amount of electric current flowing through the electromagnet allows for its strength to be changed. Reversing the flow of electricity allows the poles of the electromagnet to be reversed [66, 2]

A magnetic field is created when electric current flows through an electromagnet. The magnetic field created by the electric current forms circles around the electric current, as shown in Figure 4.4.

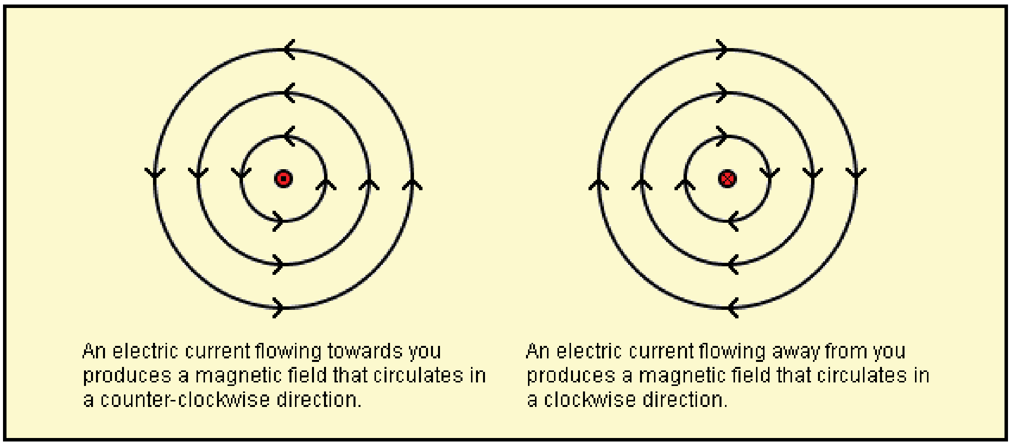


**Figure 4.4:** Magnetic field created by the flow of electric current

Two identical electromagnets were made for this project the dimensions are shown in Figure 4.5. One was made out of mild steel and the other was made out of electrical steel. The electromagnets were made out of different materials to check the effect the materials had on the output from the core. The following sections provide more detail on these two materials including a magnetic circuit analysis for both materials.

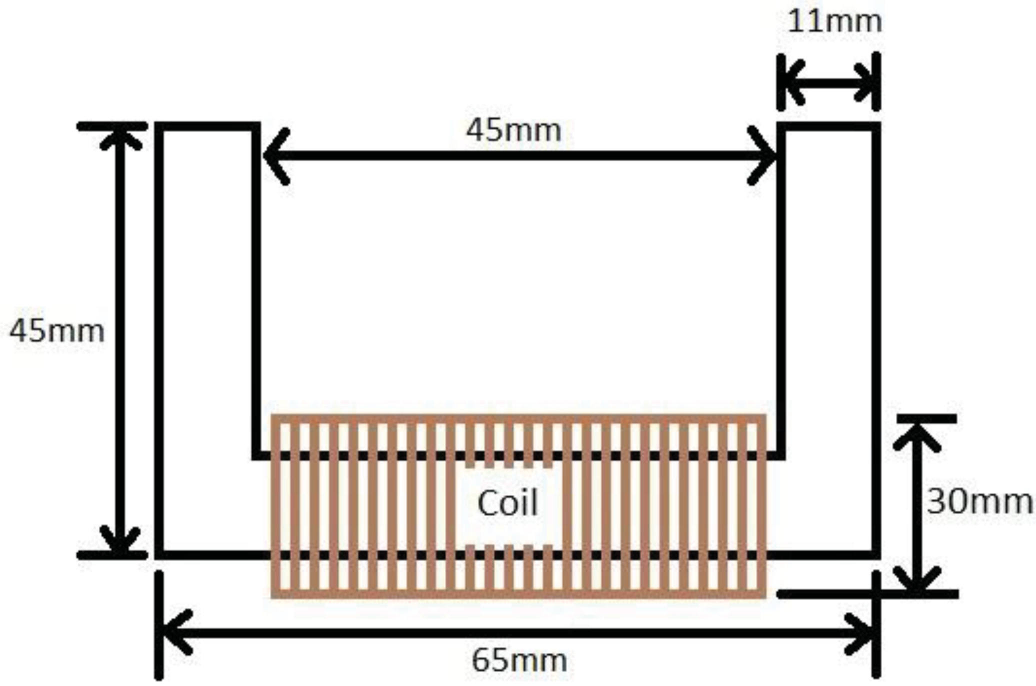


**Figure 4.5:** Dimensions of Electromagnets made for this project

### 4.3.1. Mild Steel Electromagnet

The electromagnet made of mild steel was designed in Solidworks and then machined in the workshop. The dimensions of the electromagnet was the same for both the electromagnets made. Once machined 0.5mm enamel coated copper wire was used to wire the coil. The coil was wound in the middle in layers. Each layer started from one end of the electromagnet and finished at the other end and consisted of approximately 60turns. The coil had a total of 550 turns of wire. Figure 4.6 shows the electromagnet after it was machined and the coil wound. To make sure the wound wire was held tight, black electrical tape was wrapped around the coil after every layer

**Figure 4.6:** Electromagnet made of mild steel

### 4.3.2. Electrical Steel Electromagnet

Electrical steel was used to make the second electromagnet. This steel is usually manufactured in cold rolled strips with thicknesses of 2mm or less. These strips were stacked together to form a core. A stack of these strips are usually referred to as laminations. Once stacked together these strips of steel form the laminated cores which are usually present in transformers and the stator and motor parts of electric motors [58].

Figure 4.7 shows a single sheet of the electrical steel used to make the electromagnet. Figure 4.8 shows the laminated core which consisted of 55 sheets of the U shaped electrical steel. This material was chosen as this steel is tailor made for magnetic core, mainly due to the material's high permeability and small hysteresis area [58].

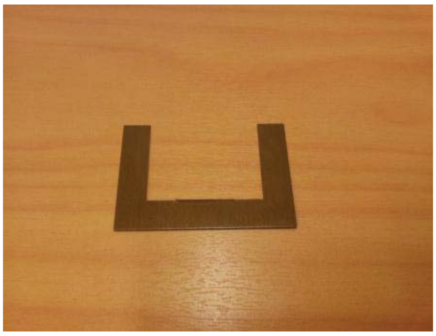

**Figure 4.7:** Single sheet of Electrical Steel

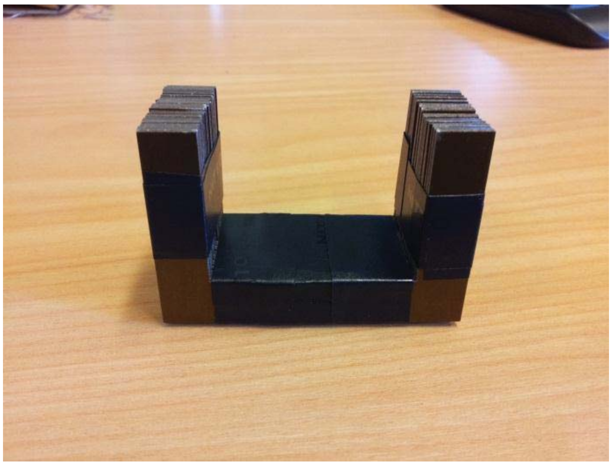

**Figure 4.8:** Laminated core of 55 sheets of Electrical Steel

After the laminated sheets were firmly stacked together they were wound with 0.5mm gauge enamel coated copper wire. The coil was wound the same way as it was done for the mild steel electromagnet. Figure 4.9 shows a particular layer of copper wire being wound around the laminated core. Electrical tape was used after each layer of winding to make sure that the wire was held tight.

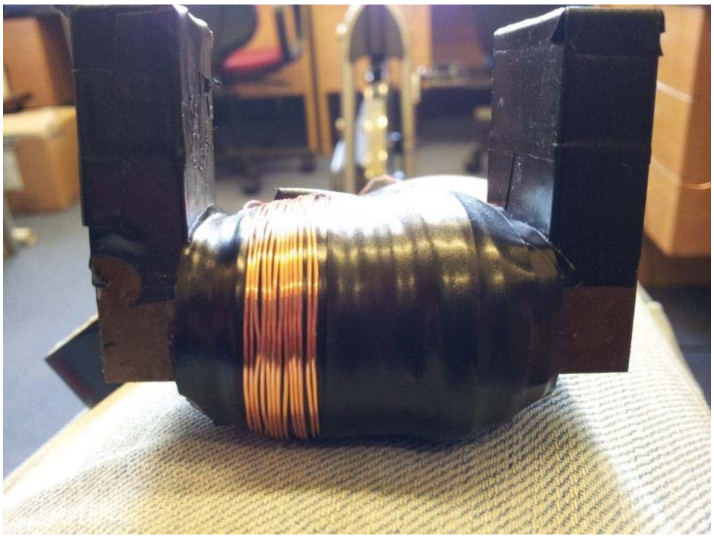

**Figure 4.9:** Electrical Steel Electromagnet

### 4.3.3. Magnetic Circuit Analysis

To analyse the magnetic circuit of the electromagnets used in this project it is important to first consider a simple magnetic circuit. Figure 4.10 is a core material consisting of current carrying coil of $N$ turns, a magnetic core length of $l_c$ and a cross sectional area $A_c$. Reluctance present in the flow of flux is given as $R$ and the permeability of the material is given by $\mu_c$.

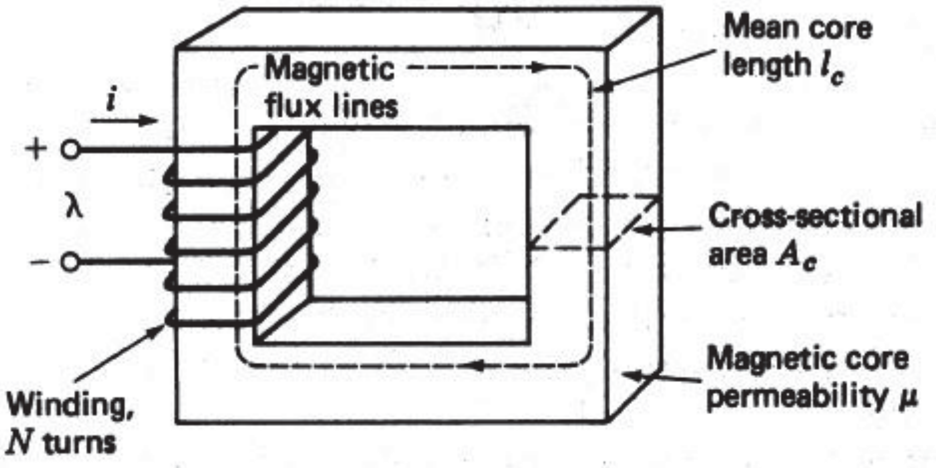


**Figure 4.10:** Simple Magnetic Circuit

By ampere's law

$$\oint_c H\, d\mathrm{l} = \oint_S J\, d\mathrm{a} \qquad \text{Equation (4.1)}$$

It can be written as

$$H_c l_c = Ni \qquad \text{Equation (4.2)}$$

Where $H_c$ is the magnetic field strength in the core, $l_c$ is the length of the core and $Ni$ the magnetomotive force. The magnetic flux through the core can be expressed as

$$\emptyset_c = B_c A_c \qquad \text{Equation (4.3)}$$

Where $\emptyset_c$ is the flux in the core, $B_c$ is the flux density of the core and $A_c$ is the cross sectional area of the core. The constitutive equation of the core material is

$$B_c = \mu H_c$$

Therefore

$$\emptyset_c = \frac{Ni}{(\frac{l_c}{\mu_c A_c})} = \frac{F}{R_c} \qquad \text{Equation (4.4)}$$

giving

$$R_c = \frac{l_c}{\mu_c A_c} \qquad \text{Equation (4.5)}$$

And

$$F = Ni \qquad \text{Equation (4.6)}$$

If the magnetic flux $\emptyset_c$ is taken as the current, the magnetomotive force $F=Ni$ as the emf of a voltage source and $R_c = {}^{l_c}/_{(\mu_c A_c)}$ (which is the magnetic reluctance), as the resistance in the circuit, an analog of Ohm's law in an electrical circuit is obtained. This is shown in figure 4.11.

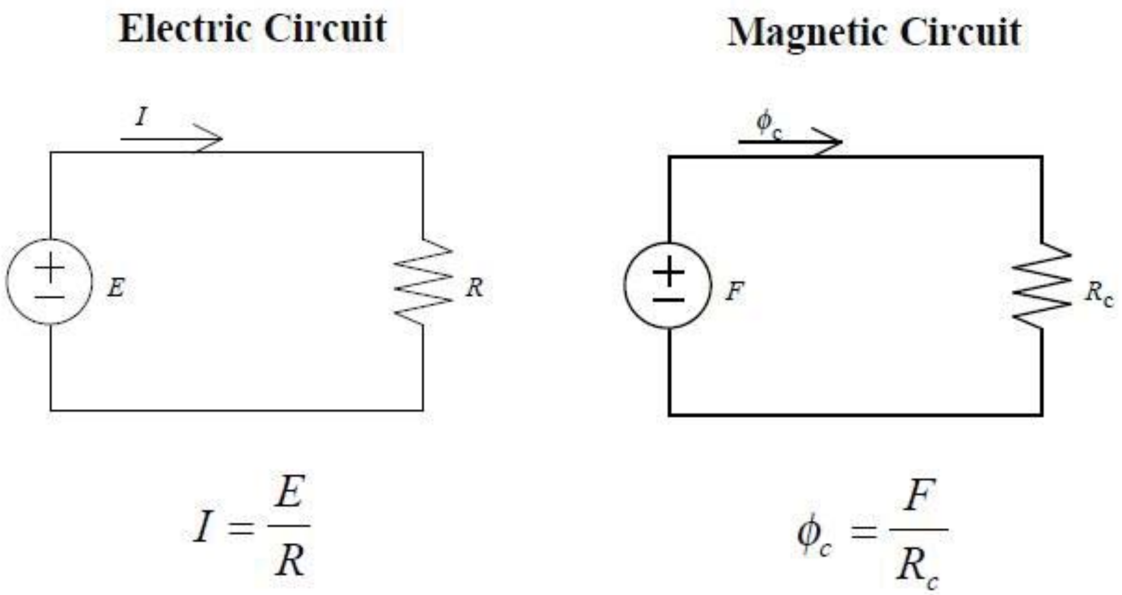


**Figure 4.11:** Electric and Magnetic Circuit

#### 4.3.3.1. Mild Steel

The magnetic circuit of the electromagnet used in this project can be analysed from the above equations. The core for this project has an air gap unlike the magnetic core above. Figure 4.12 shows the magnetic circuit for this experiment.

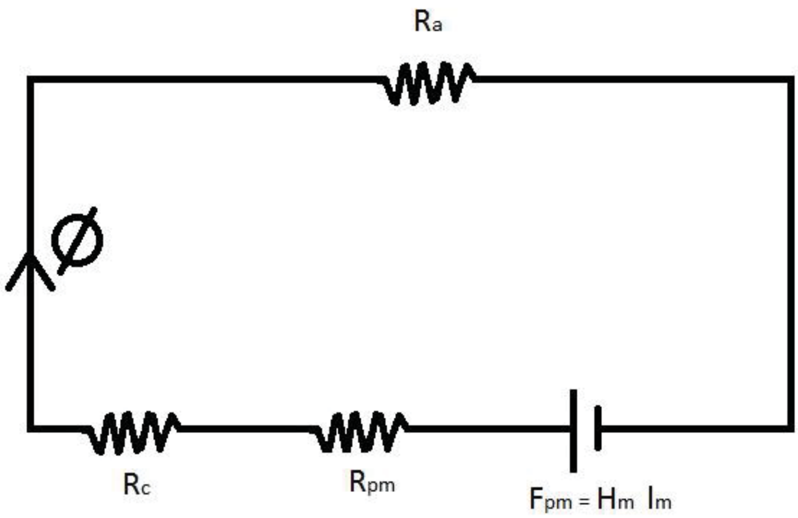


**Figure 4.12:** Magnetic circuit for this project

$R_a$ is the reluctance of air; $R_c$ is the reluctance of the core and $R_{pm}$ is the reluctance of the permanent magnet. Equation 5 was used to calculate the reluctance of this circuit.

$$R = \frac{l}{\mu_0 \mu_r * A} \qquad \text{Equation (4.7)}$$

To be able to calculate the reluctance the Length $l$, Permeability $\mu$ and Area $A$ are needed.

The length of the air gap present in this circuit is $l_a$ - 0.017m. The length of the core is $l_c$ – 0.1m and the length of the permanent magnet is $l_{pm}$ – 0.0064m

The permeability of the air is $\mu_0$ - $4\pi * 10^{-7}$, the permeability of the mild steel core is $\mu_r$ – 200 and the permeability of the permanent magnet $\mu_{pm}$ is calculated using

$$\mu_m = \frac{B_r}{\mu_0 * H_c} \qquad \text{Equation (4.8)}$$

Where $B_r$ is the flux density of the magnet and $H_c$ is the field strength of the magnet. Both these values were acquired from the B-H characteristic curve of the magnet. The magnet had a $B_r$ value of 1.3 Tesla and $H_c$ value of 1114084.6 A/m. Inserting these values into equation 4.8 provided the permeability of the magnet

$$\mu_m = \frac{1.3\ Tesla}{4\pi * 10^{-7} * 1114084.6\ {}^{A}/_{m}}$$

$$\mu_m = 0.93$$

The area of the air gap present in the circuit is $A_a$ – 0.0001$m^2$, the area of the core is $A_c$ – 0.0001$m^2$ and the area of the magnet $A_{pm}$ is calculated by

$$A_{pm} = \pi * r^2 \qquad \text{Equation (4.9)}$$

The magnet used for this project had a diameter of 0.0222m giving it a radius of 0.0111m. Inserting this into equation 4.9 gives

$$A_{pm} = \pi * 0.0111^2$$

$$A_{pm} = 0.00038\ m^2$$

Inserting the values of the length, permeability and area allows calculation of the reluctance present in the air gap, core and the permanent magnet using equation 4.7.

The reluctance of the air gap is given by

$$R_a = \frac{l_a}{\mu_o * A_a}$$

$$R_a = \frac{0.017\ m}{4\pi * 10^{-7} * 0.0001m^2}$$

$$R_a = 135281701.6 \, {}^{H}/_{m}$$

The reluctance of the core is given by

$$R_c = \frac{l_c}{\mu_o \mu_r * A_c}$$

$$R_c = \frac{0.1\ m}{4\pi * 10^{-7} * 200 * 0.0001\ m^2}$$

$$R_c = 3978873.577 \, {}^{H}/_{m}$$

The reluctance of the permanent magnet is given by

$$R_{pm} = \frac{l_{pm}}{\mu_o \mu_{pm} * A_{pm}}$$

$$R_{pm} = \frac{0.0064\ m}{4\pi * 10^{-7} * 0.93 * 0.00038\ m^2}$$

$$R_{pm} = 14411313.47 \, {}^{H}/_{m}$$

Adding the reluctance values gives

$$\Sigma R = R_a + R_c + R_{pm}$$

$$\Sigma R = 135281701.6 + 3978873.577 + 14411313.47$$

$$\Sigma R = 153671888.6 \ {}^{H}/_{m}$$

Inserting the sum total of the reluctance in the circuit into equation 4.4 gives the flux generated in the circuit to be

$$\emptyset = \frac{H_C l_m}{\Sigma R} \qquad \text{Equation (4.10)}$$

$$\emptyset = \frac{1114084.6 \, {}^{A}/_{m} * 0.0064 \ m}{153671888.6 \ {}^{H}/_{m}}$$

$$\emptyset = 0.0000464 \ weber$$

Thus giving a total flux for the magnetic circuit of the electromagnet made of mild steel.

#### 4.3.3.2. Electrical Steel

To analyse the electrical steel electromagnet the same procedure as the one used for the mild steel electromagnet is used but the permeability value for electrical steel is changed to $\mu_r$ – 5000. Changing this in the equation, the flux is calculated to be:

The reluctance of the air gap is given by

$$R_a = \frac{l_a}{\mu_o * A_a}$$

$$R_a = \frac{0.017 \ m}{4\pi * 10^{-7} * 0.0001 m^2}$$

$$R_a = 135281701.6 \, {}^{H}/_{m}$$

The reluctance of the core is given by

$$R_c = \frac{l_c}{\mu_o \mu_r * A_c}$$

$$R_c = \frac{0.1\ m}{4\pi * 10^{-7} * 5000 * 0.0001\ m^2}$$

$$R_c = 159154.9431\ {}^{H}/_{m}$$

The reluctance of the permanent magnet is given by

$$R_{pm} = \frac{l_{pm}}{\mu_o \mu_{pm} * A_{pm}}$$

$$R_{pm} = \frac{0.0064\ m}{4\pi * 10^{-7} * 0.93 * 0.00038\ m^2}$$

$$R_{pm} = 14411313.47\ {}^{H}/_{m}$$

Adding the reluctance values gives

$$\Sigma R = R_a + R_c + R_{pm}$$

$$\Sigma R = 135281701.6 + 159154.9431 + 14411313.47$$

$$\Sigma R = 149852170\ {}^{H}/_{m}$$

Inserting the sum total of reluctance in the circuit into equation 4.4 gives the flux generated in the circuit to be

$$\emptyset = \frac{H_C l_m}{\Sigma R}$$

$$\emptyset = \frac{1114084.6\,{}^{A}/_{m} * 0.0064\,m}{149852170\,{}^{H}/_{m}}$$

$$\emptyset = 0.0000476\,weber$$

Thus giving a total flux for the magnetic circuit of the electromagnet made of electrical steel.

### 4.3.4. Electromagnet Mount

The electromagnets had to be held in such a way that the flywheel would pass through the electromagnet without interfering or effecting the movement of the flywheel as seen in Figure 4.13. It was decided that having the electromagnet under the flywheel in the front of the bike would be the best way to do this, as this would not affect the functioning of the bike.

**Figure 4.13:** Location for Electromagnet

The space under the flywheel is limited and because of the way the electromagnets are a mount had to be designed to hold the electromagnets in place. Figure 4.14 gives the front view and the dimensions of this area.

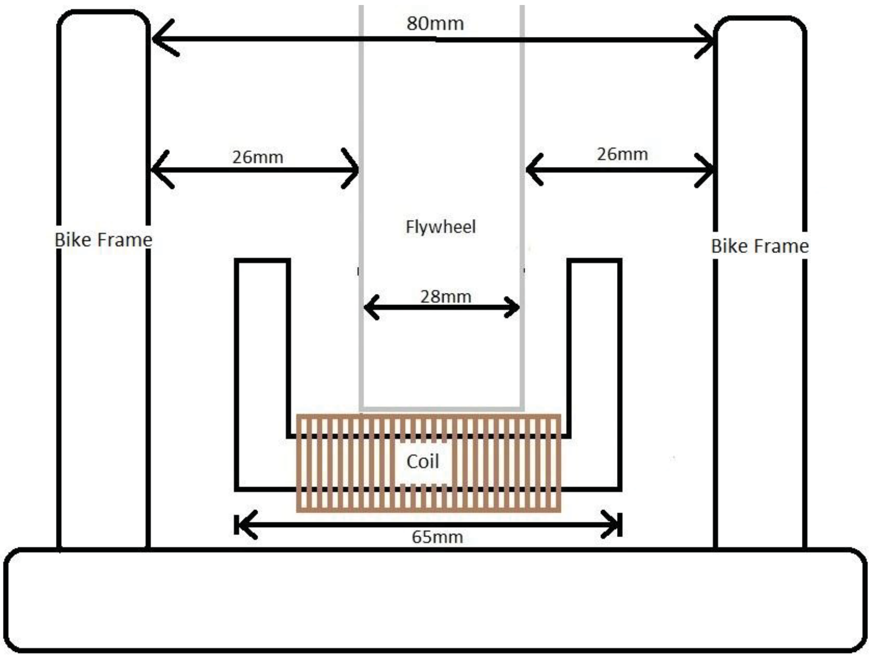


**Figure 4.14:** Dimensions of area under the flywheel for the electromagnet

The mounts were designed using Solidworks. Initially the mount was designed such that the steel plates bolted on to the side of the bike frame would press in on the sides of the electromagnet, to hold it in place. Figure 4.15 gives a 3D model view of the design. However this idea was not practical as this design did not allow enough space for the magnets when placed on the flywheel.

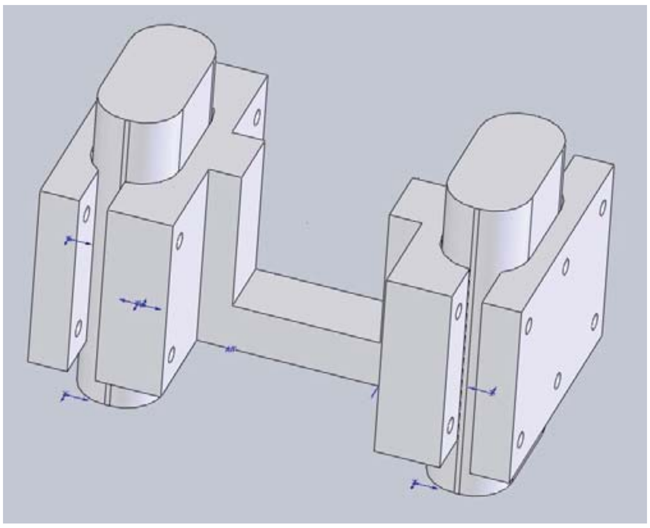

**Figure 4.15:** Initial 3D model design of the mount

A different method to hold the electromagnet had to designed, where the placement of the electromagnet under the flywheel was flexible. Therefore another design was made in Solidworks, this design is shown in Figure 4.16. The intention was to have two steel plates bolted from the front of the bike frame, where the plates pressed against the edge of the electromagnet. This method would provide the flexibility necessary if more of a gap was required on either side of the flywheel.

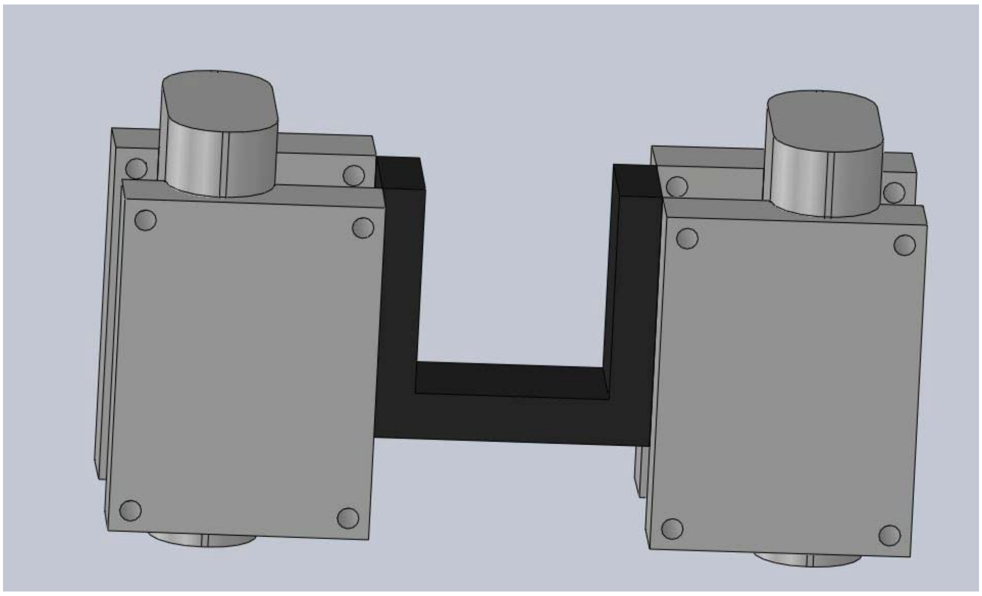

**Figure 4.16:** Final 3D design of the mount for the electromagnet

The frame of the bike where the mount would be put was an elliptical tube. A CNC machine was used to make the parts for the mount as per the unique shape of the bike frame. The code to machine the parts was generated in SolidCAM (3D model software). Figure 4.17 shows the mount being machined (on the left) and the machined product (to the right).

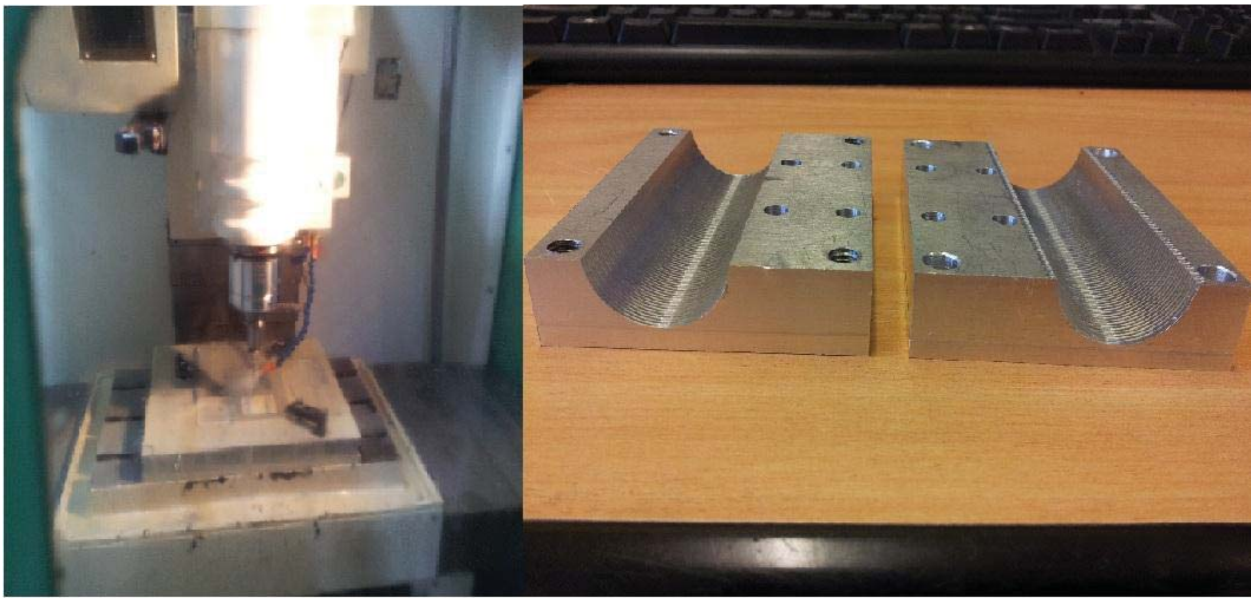

**Figure 4. 17:** CNC machining of the mount and the finished product

Figures 4.18 and 4.19 show the mounts fitted onto the bike frame holding the electromagnet right under the flywheel. Loosening the bolts reduced the pressure pushing against the electromagnet, allowing for the electromagnet to be moved around if necessary. Tightening these bolts would secure the hold of the electromagnet.

**Figure 4.18:** Side view of the Electromagnet mount


**Figure 4.19:** Front view of the Electromagnet mount

## 4.4. Magnets

Since a prominent feature of this project is to generate power using magnets, it was important to have good quality magnets. This would help give an accurate idea of the amount of energy that this technique of EH could generate.

Neodymium disc shaped, axially magnetized magnets were chosen for this project. Magnets with axial magnetization direction have its poles on the flat ends of the magnet [55]. Figure 4.20 shows the nature of a magnet axially magnetized. These were necessary since the magnets were going to be placed flat on the flywheel of the stationary bike.

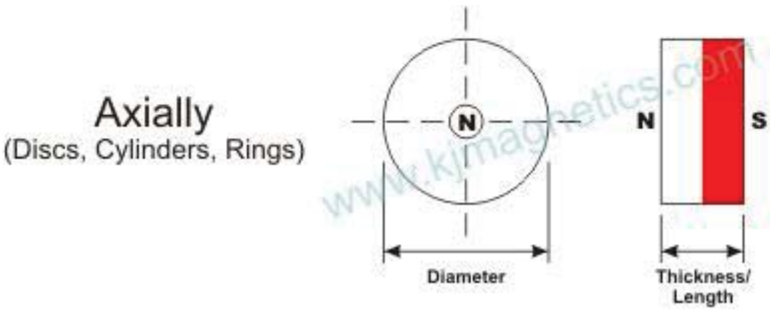


**Figure 4. 20:** Magnetization Direction for Disc magnets

Two kinds of magnets were bought from K&J Magnetics. Both magnets were of the same diameter but the thicknesses of the magnets differed. Magnets with different thicknesses were used to test the effect it would have on the output generated from the electromagnet.

Table 4.1 gives the specifications of both magnets used in this project. Both magnets were 22.225mm in diameter, Magnet 1 (M1) was 6.35mm thick and Magnet 2 (M2) was 9.53mm thick. One of the key factors to note is the pull force of a magnet. This is the force required to pull a particular magnet off a steel plate. Figures 4.21 shows the magnetic field generated by each magnet, it is evident that M2 is a lot stronger than M1.

| Magnet 1 (M1) | Magnet 2 (M2) |
|---|---|
| Dimensions: 22.225mm dia. x 6.35mm thick | Dimensions: 22.225mm dia. x 9.53mm thick |
| Tolerances: ±0.004" x ±0.004" | Tolerances: ±0.004" x ±0.004" |
| Material: NdFeB, Grade N42 | Material: NdFeB, Grade N42 |
| Plating/Coating: Ni-Cu-Ni (Nickel) | Plating/Coating: Ni-Cu-Ni (Nickel) |
| Magnetization Direction: Axial | Magnetization Direction: Axial |
| Weight: 0.652 oz. (18.5 g) | Weight: 0.978 oz. (27.7 g) |
| Pull Force, Case 1: 22.87 lbs | Pull Force, Case 1: 31.85 lbs |
| Surface Field: 3275 Gauss | Surface Field: 4295 Gauss |
| Max Operating Temp: 176°F (80°C) | Max Operating Temp: 176°F (80°C) |
| Brmax: 13,200 Gauss | Brmax: 13,200 Gauss |
| BHmax: 42 MGOe | BHmax: 42 MGOe |

**Table 4. 1: Magnet Specifications**

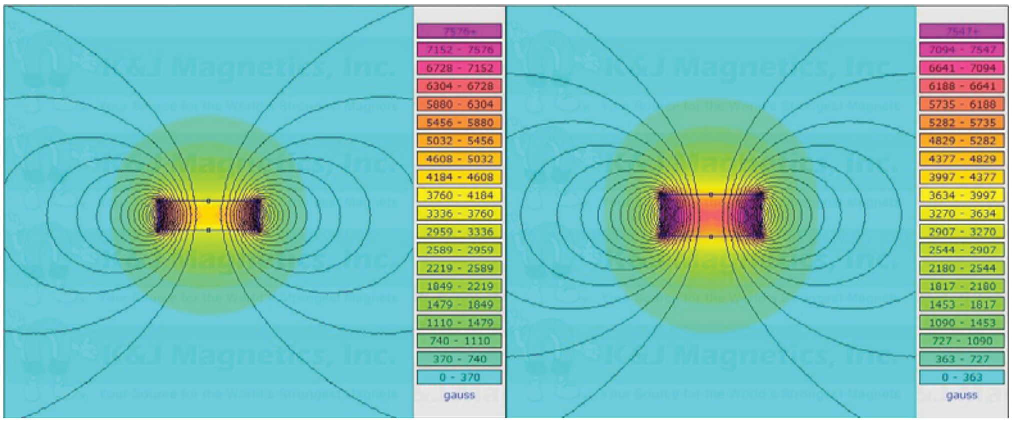


**Figure 4.21:** Magnetic Field Strength of M1 and M2 on the left and right respectively.

## 4.5. Circuits

A buck-boost converter had to be designed for this project as the output of the electromagnet varies depending on the person riding the bike. Different topologies were considered and researched, and the LTC3433 high voltage step up-step down converter was selected. This converter has a high frequency current mode switching regulator that provides both step-up and step-down regulation using a single inductor [64]. The IC operates over a wide range of 4V-60V input voltage making it suitable for applications such as this, where the input varies dependent on the person riding the bike. Control circuitry present in the IC monitors the input and either steps down the voltage or boosts it [64]. Figure 4.22 shows the block diagram of the IC.

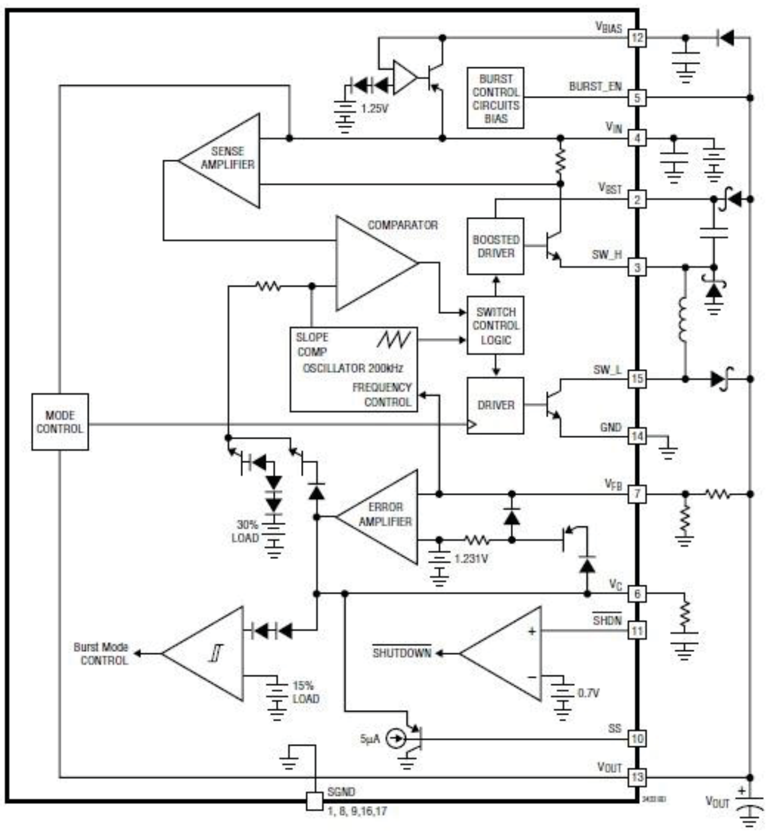


**Figure 4.22:** Block Diagram of LTC3433

Figure 4.23 is a schematic acquired from the data sheet (see appendix B). It depicts a circuit for an application with a varied input producing an output of 12 volts.

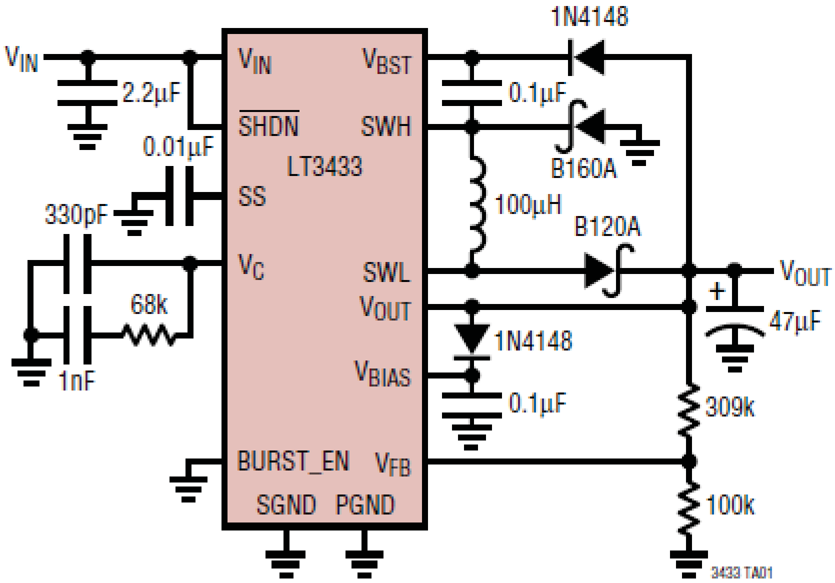


**Figure 4. 23: Schematic of a Step-up and Step-down circuit**

The regulated output for this circuit can be easily changed to give the necessary output. Changing the feedback resistors connected to pin 7, which is the Voltage feedback helps give the necessary output. As the output from this was going to be used to charge a 12V rechargeable battery, the output of the buck boost converter was set to 14V. Equation 4.11 was used to set the desired output voltage

$$V_{out} = 0.8 * \left(1 + \frac{R_3}{R_2}\right) \qquad \text{Equation (4.11)}$$

Where $R_2$ and $R_3$ are part of the resistor feedback network, connected from the output and to pin 7 of the IC. In order to achieve the desired voltage of 14 volts, a 7.5kohm resistor was choosen for $R_2$ and a 124kohm for $R_3$. Inserting these values into Equation 4.11 gave

$$V_{out} = 0.8 * \left(1 + \frac{124}{7.5}\right)$$

$$V_{out} = 14\ V$$

.

Figure 4.24 shows the schematic of the circuit designed. This was done in Altium designer. Diode SD1 switches the $V_{IN}$ side of the inductor making it a buck converter and SD2 switches the $V_{OUT}$ side of the inductor to make it a boost converter.

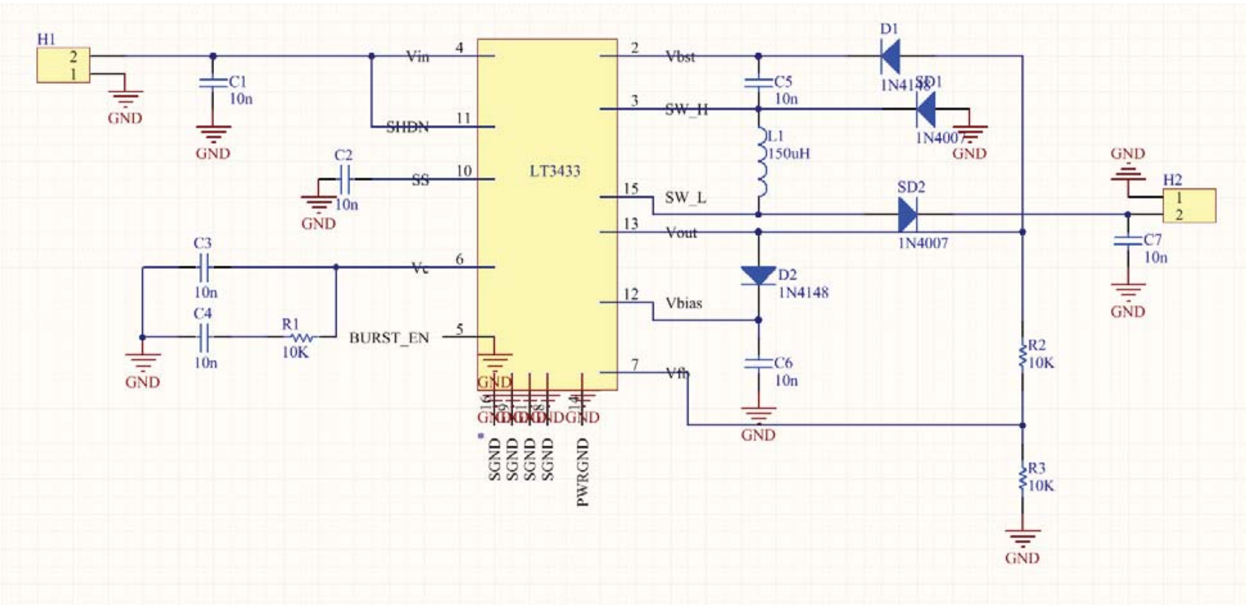


**Figure 4.24:** Buck-Boost Circuit Schematic

After the circuit schematic was designed the next step was to design the PCB for the converter. The PCB layout for this schematic is shown in figure 4.25

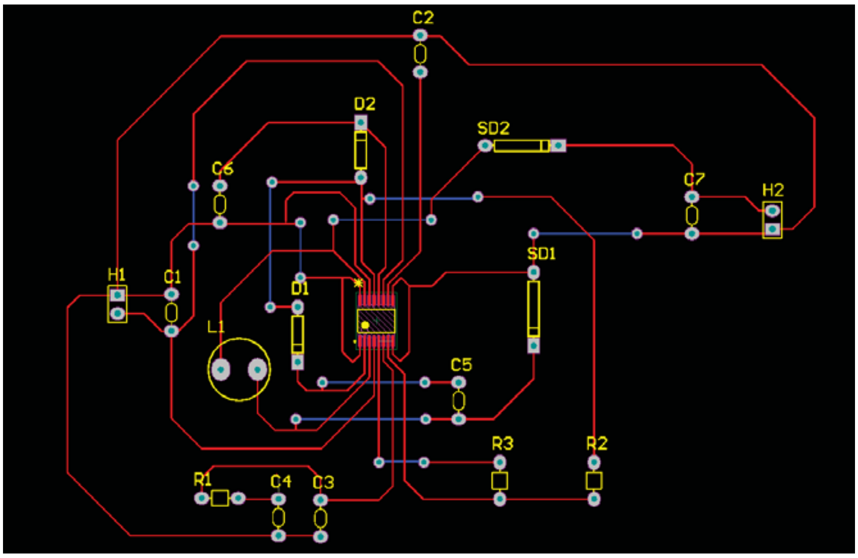


**Figure 4.25:** PCB design layout of the Buck-Boost converter

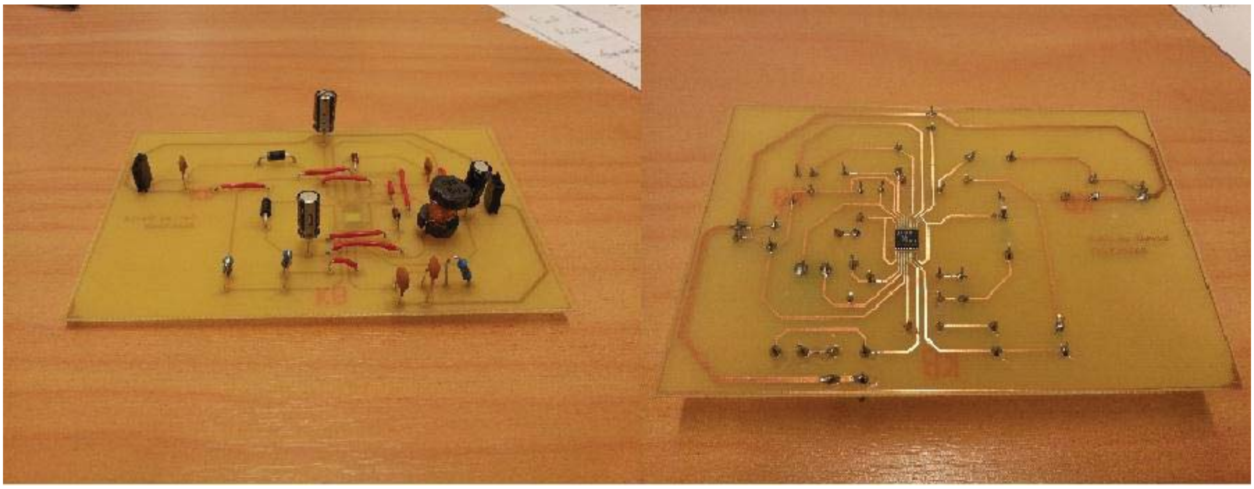

**Figure 4.26:** Buck-Boost PCB

Figure 4.26 shows the circuit board after all the components were soldered on the board. This was then tested to see if the converter worked and output the desired voltage. To check the functionality of the converter, the converter was connected to the output coming from the electromagnet. Figure 4.27 shows the setup for this experiment. The bike was pedalled with 18M1 magnets placed on the flywheel of the bike. Waveforms were captured at the output of the electromagnet and the output that came out of the Buck-Boost converter.

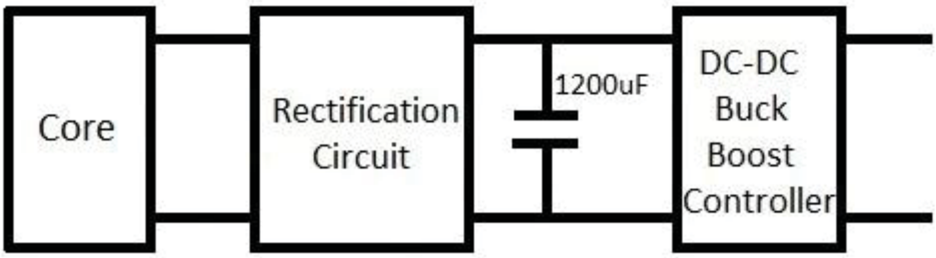


**Figure 4.27:** Setup to check functionality of the Buck-Boost converter

Figure 4.28 shows the waveforms captured from the experiment. One channel of the oscilloscope was connected to the output of the electromagnet (yellow signal in the waveform) and the other channel was connected to the output of the Buck-Boost converter (blue signal in the waveform). The waveforms show that though the input was different the output of the converter remains the same.

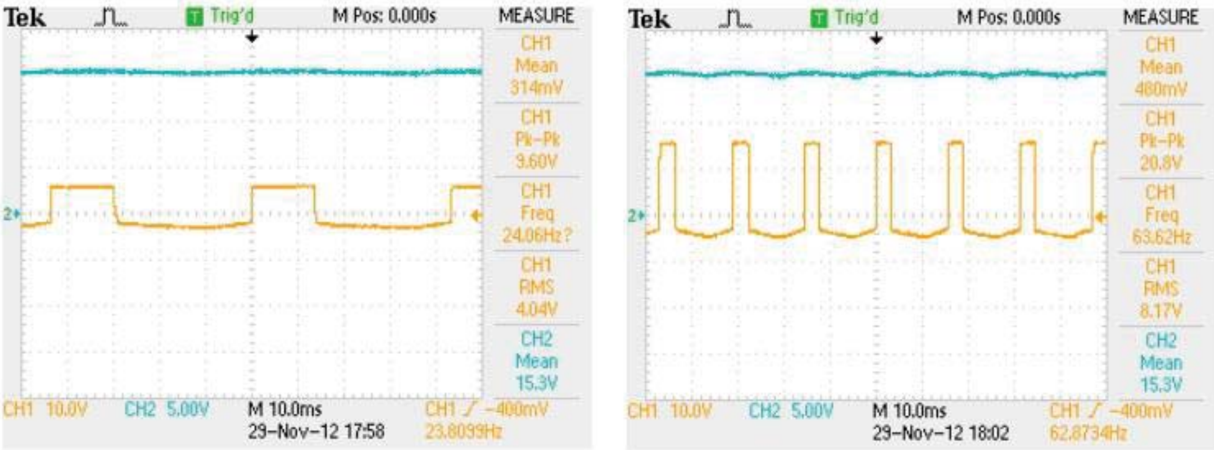


S10 S30

**Figure 4.28:** Waveforms of signal from the electromagnet and the output of the Buck-Boost Converter

The experiments and results of the stationary bike are discussed in the following chapter.

# Chapter 5. THE STATIONARY BIKE: EXPERIMENTS, RESULTS AND ANALYSIS

## 5.1. Introduction

The previous chapter outlined the method this project used to harvest energy from a stationary bike using magnets and an electromagnet. This section discusses the implementation of this method and analyses the results acquired from various experiments that were conducted. Experiments were conducted to check the relationship of the factors listed below and the effect these factors had on the power output.

- The material of the Electromagnet core
- Magnet Pole orientation
- The number of magnets used
- The thickness or strength of the magnets used
- Air gap

To achieve the best possible setup for this method of EH, experiments were conducted and adjustments were made based on results in each area listed above. Experiments were also conducted to note the maximum power that could be generated and the amount of energy that could be harvested, implementing the proposed method of EH.

## 5.2. Relationship of the electromagnet material on the Output

The first factor tested was the effect of the material of the electromagnet core had on the output generated. As mentioned in the previous chapter two identical electromagnets were made for this project. One was made out of mild steel and the other was made out of electrical steel.

### 5.2.1. Experimental Setup

Two experiments were conducted with each electromagnet to check the relationship between the core material and the output. The only difference between the two experiments was the magnets used for the experiment. Magnet 1 (M1) was used first and then magnet 2 (M2) was used for the second experiment. The experimental setup for both magnets M1 and M2 is shown in Figure 5.1.

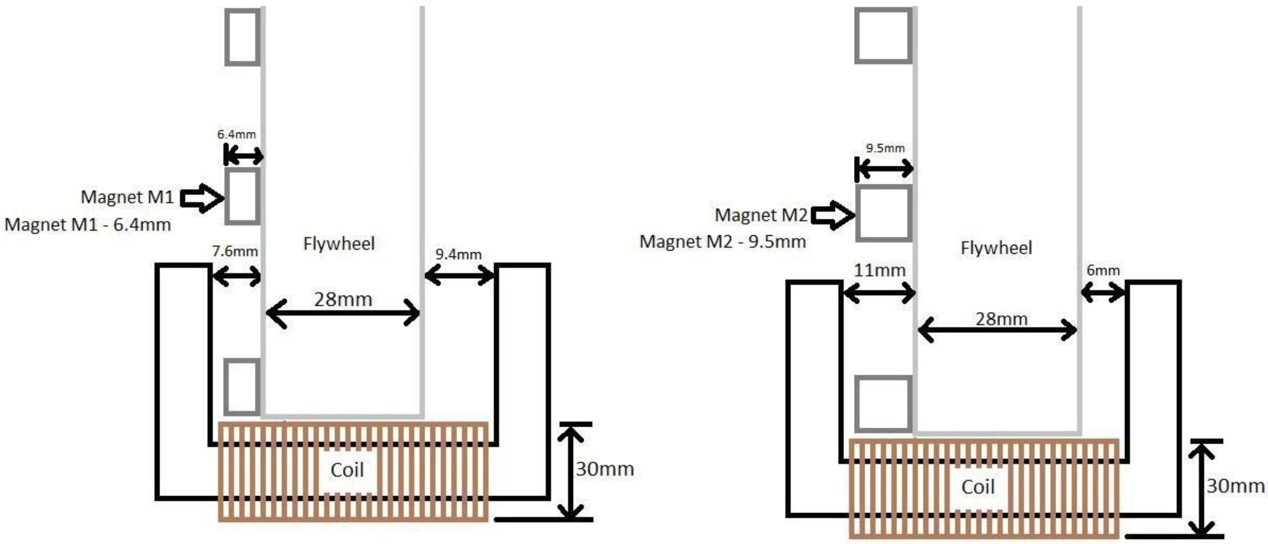


**Figure 5.1:** Setup for M1 and M2 magnets

To test this, experiments were run with 18 magnets placed equally apart on the flywheel. First it was tested with 18 M1 magnets and later with M2 magnets. Figure 5.2 shows the process followed to conduct the experiment.

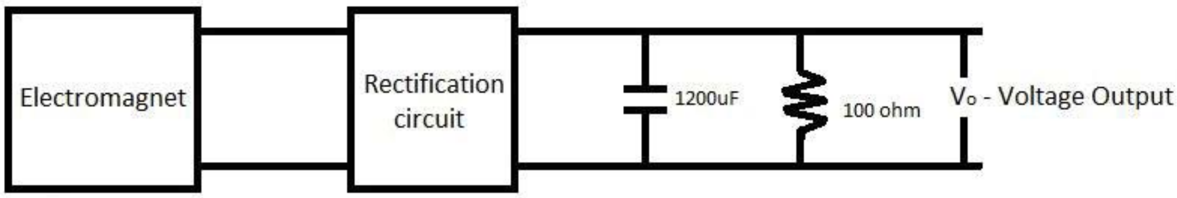


**Figure 5.2:** Block diagram of the setup for the experiment

As the bike is pedalled the flywheel (with the magnets) passed through the electromagnet generating an AC signal. This AC signal was connected to a rectification circuit which converts the AC signal to a DC signal. Schotky diodes were used for the rectification to keep the losses to a minimum. A capacitor was used to smooth out the power coming out of the rectification circuit. This output was then connected to a load of 100ohm. The output was hooked to a multimeter. Voltage readings were taken and power output calculated. The bike was pedalled at various speeds and the voltage output was noted along with the speed of the bike. Figure 5.3 shows the setup of the system.

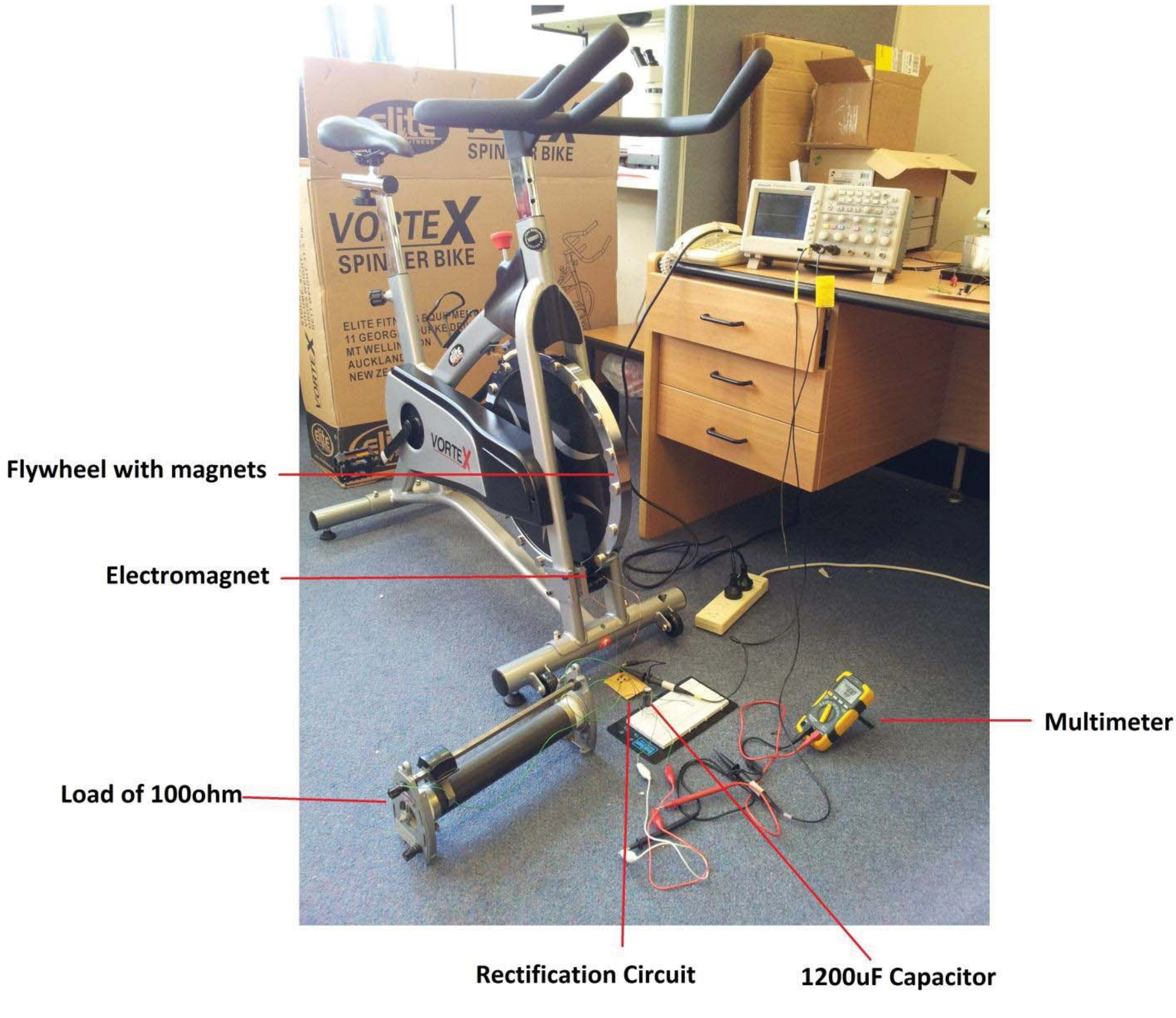


**Figure 5.3:** Bike Setup

### 5.2.2. Effect of Mild Steel

Two experiments were done using the electromagnet made out of mild steel. First experiment was done using M1 magnets and the second with M2 magnets. The bike was pedalled at various speeds ranging from riding the bike slowly to riding it at as fast as possible. The output voltage at various speeds was noted from the multi-meter connected to the system.

| | **Mild Steel Electromagnet** | | | |
|---|---|---|---|---|
| | **M1 Magnets** | | **M2 Magnets** | |
| **Speed (RPM)** | **Output Voltage (V)** | **Power output (W)** | **Output Voltage (V)** | **Power output (W)** |
| 20 | 1.3 | 0.0169 | 1.9 | 0.0361 |
| 30 | 2.3 | 0.0529 | 2.9 | 0.0841 |
| 37 | 3 | 0.09 | 3.6 | 0.1296 |
| 45 | 3.8 | 0.1444 | 4.7 | 0.2209 |
| 54 | 4.6 | 0.2116 | 5.6 | 0.3136 |
| 64 | 5.4 | 0.2916 | 6.1 | 0.3721 |
| 72 | 6 | 0.36 | 7.2 | 0.5184 |
| 79 | 6.5 | 0.4225 | 8.5 | 0.7225 |
| 90 | 7.3 | 0.5329 | 9.2 | 0.8464 |
| 99 | 8 | 0.64 | 10 | 1 |
| 109 | 8.6 | 0.7396 | 10.5 | 1.1025 |
| 121 | 9.5 | 0.9025 | 11.4 | 1.2996 |

**Table 5.1:** Generated Voltage and Power outputs using a mild steel electromagnet

Table 5.1 shows the Voltage and the Power outputs coming out from the system using both M1 and M2 magnets, at different speeds. The power output was calculated using Equation 5.1 derived from the combination of Joules law and Ohms law.

$$P = \frac{V^2}{R} \qquad \text{Equation (5.1)}$$

Where *P* is the instantaneous power, which is measured in Watts, *V* is the potential difference across the component measured in Volts and *R* is the resistance measured in ohms.

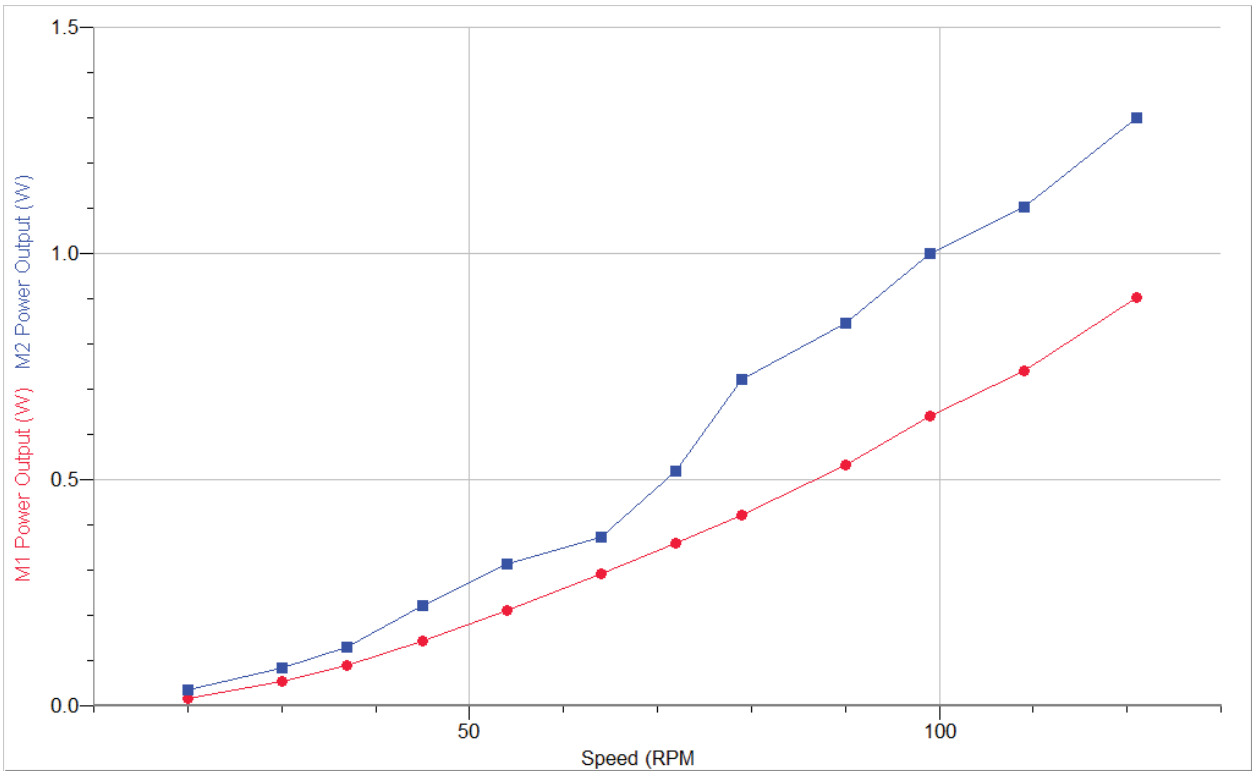


**Figure 5.4:** Power characteristics of M1 and M2 magnets at different speeds

Figure 5.4 shows the power characteristics of both M1 and M2 magnets at different speeds across a load of 100ohm. It shows that there was a steady increase in the power output as the speed was increased. The use of M2 magnets, blue line in the graph, gave a slightly higher output than M1 magnets, so it can be concluded that an electromagnet made of mild steel having stronger magnets would give a higher output.

### 5.2.3. Effect of Electrical steel

Similar experiments were done using the electromagnet made out of electrical steel. First experiment was done with M1 magnets and the second with M2 magnets. The bike was pedalled at various speeds ranging from riding the bike slowly to riding it at as fast as possible. The output voltage was noted, from the multi-meter connected to the system, at various speeds. Table 5.2 shows the Voltage and Power outputs generated.

| | Electrical Steel Electromagnet | | | |
|---|---|---|---|---|
| | M1 Magnets | | M2 Magnets | |
| **Speed (RPM)** | **Output Voltage (V)** | **Power output (W)** | **Output Voltage (V)** | **Power output (W)** |
| 20 | 3.1 | 0.0961 | 3.9 | 0.1521 |
| 29 | 4.9 | 0.2401 | 5.5 | 0.3025 |
| 36 | 5.9 | 0.3481 | 6.1 | 0.3721 |
| 48 | 7.3 | 0.5329 | 7.8 | 0.6084 |
| 53 | 8.9 | 0.7921 | 8.4 | 0.7056 |
| 65 | 10.6 | 1.1236 | 10.5 | 1.1025 |
| 69 | 11.3 | 1.2769 | 11.2 | 1.2544 |
| 79 | 12 | 1.44 | 12.1 | 1.4641 |
| 90 | 13.9 | 1.9321 | 13.8 | 1.9044 |
| 100 | 15.1 | 2.2801 | 15 | 2.25 |
| 107 | 15.9 | 2.5281 | 16.1 | 2.5921 |
| 125 | 17.8 | 3.1684 | 17.4 | 3.0276 |

**Table 5.2:** Generated Voltage and Power outputs using a electrical steel electromagnet

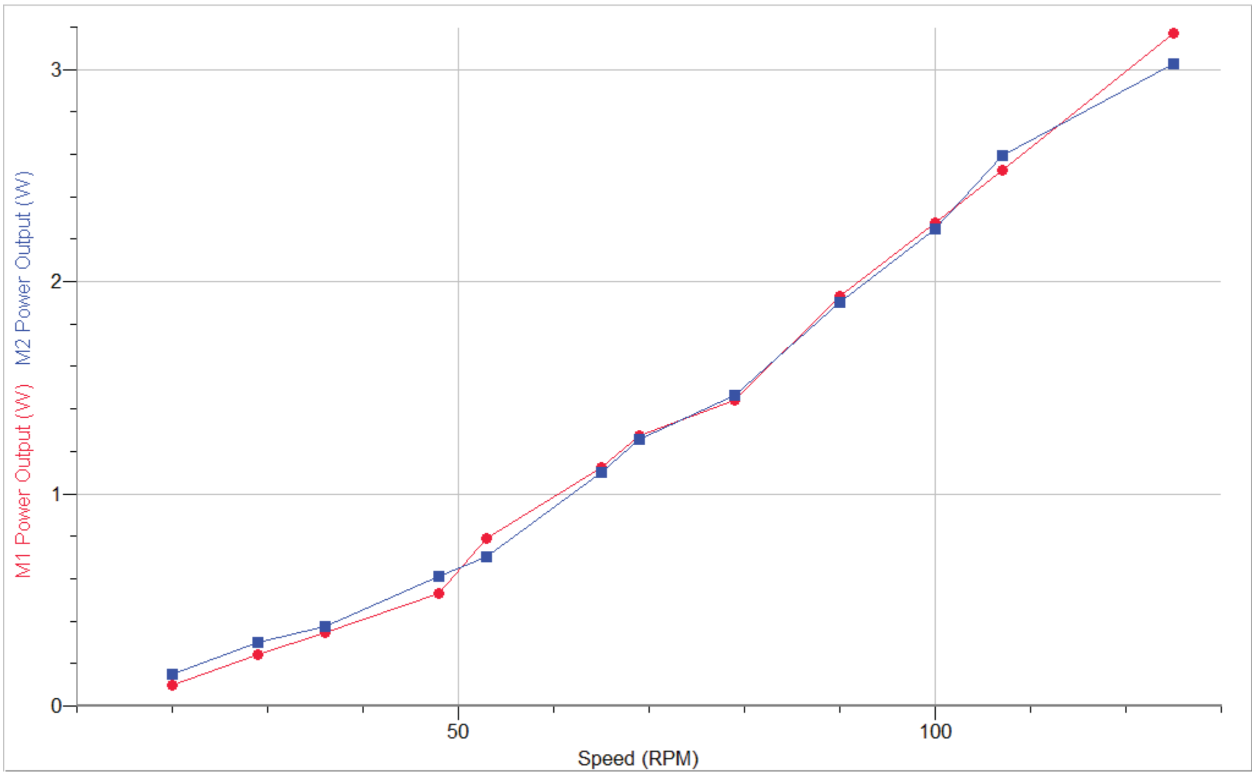


**Figure 5.5:** Power characteristics of M1 and M2 magnets at different speeds

Figure 5.5 gives the power characteristics of both M1 and M2 magnets at different speeds when connected across a load of 100ohm. The figure shows that there is a steady increase in the power output as the speed is increased, and that both M1 and M2 magnets give very similar outputs. This shows that stronger magnets do not necessarily give higher power outputs. Having stronger magnets on the flywheel increases the air gap present between the flywheel and one side of the electromagnet. Magnetic flux is reluctant to travel through air. Therefore a larger air gap results in losses in the winding and increases eddy current losses, which might cause the output to drop. The effects of air gaps are discussed in detail further in this chapter [59]. So, from this experiment it can be concluded that stronger magnets increase the air gap which in turn reduces the power output.

### 5.2.4. Comparison of Results

Comparing the results of both the electromagnets, it is evident that the output of the electrical steel electromagnet is far greater than that of the mild steel. Power values for both electrical and mild steel electromagnets using both M1 and M2 magnets are shown in Table 5.3. It shows that at every speed checked the output is always higher with the electrical steel electromagnet.

| | M1 Magnets | | M2 Magnets | |
|---|---|---|---|---|
| | Mild steel | Electrical Steel | Mild steel | Electrical Steel |
| Speed (RPM) | Power output (W) | Power output (W) | Power output (W) | Power output (W) |
| 20 | 0.0169 | 0.0961 | 0.0361 | 0.1521 |
| 30 | 0.0529 | 0.2401 | 0.0841 | 0.3025 |
| 37 | 0.09 | 0.3481 | 0.1296 | 0.3721 |
| 45 | 0.1444 | 0.5329 | 0.2209 | 0.6084 |
| 54 | 0.2116 | 0.7921 | 0.3136 | 0.7056 |
| 64 | 0.2916 | 1.1236 | 0.3721 | 1.1025 |
| 72 | 0.36 | 1.2769 | 0.5184 | 1.2544 |
| 79 | 0.4225 | 1.44 | 0.7225 | 1.4641 |
| 90 | 0.5329 | 1.9321 | 0.8464 | 1.9044 |
| 99 | 0.64 | 2.2801 | 1 | 2.25 |
| 109 | 0.7396 | 2.5281 | 1.1025 | 2.5921 |
| 121 | 0.9025 | 3.1684 | 1.2996 | 3.0276 |

**Table 5. 3:** Power outputs of both M1 & M2 magnets using mild steel & electrical steel electromagnet

Considering the permeability (μ) of both the materials provides reason for the power generated using one material being higher than the other. Permeability (μ) is the measure of the ease at which a magnetic field can be set up in a material [60]. The higher the μ value of the material the lesser the reluctance present in the material.

The relationship between permeability and reluctance is given by

$$R = \frac{l}{\mu_0 \mu_r * A}$$

Equation (5.2)

Where *R* is the reluctance of the circuit, *l* is the length of the magnetic circuit, $\mu$ is the permeability of the material and *A* is the cross sectional area of the magnetic circuit. So from equation 5.2 it can be concluded that to have a magnetic circuit with low reluctance the length of the electromagnet should be kept short, the material chosen should have a high permeability and the cross section of the area of the circuit should be large.

The only difference between the two electromagnets used in this experiment is the materials used. Therefore considering the permeability of the materials provides the reason for the electrical steel electromagnet giving a higher power output. The permeability of mild steel is known to be $\mu_{\text{Mild Steel}}$ - 200-800, and electrical steel has a value of $\mu_{\text{Electrical Steel}}$ 1000 – 5000 [61]. As the μ is a lot higher in electrical steel than mild steel, the reluctance is a lot higher in mild steel. This is reflected in the results of Figure 5.6 which shows that the power generated using the electrical steel electromagnet is a lot higher than that of the mild steel electromagnet.

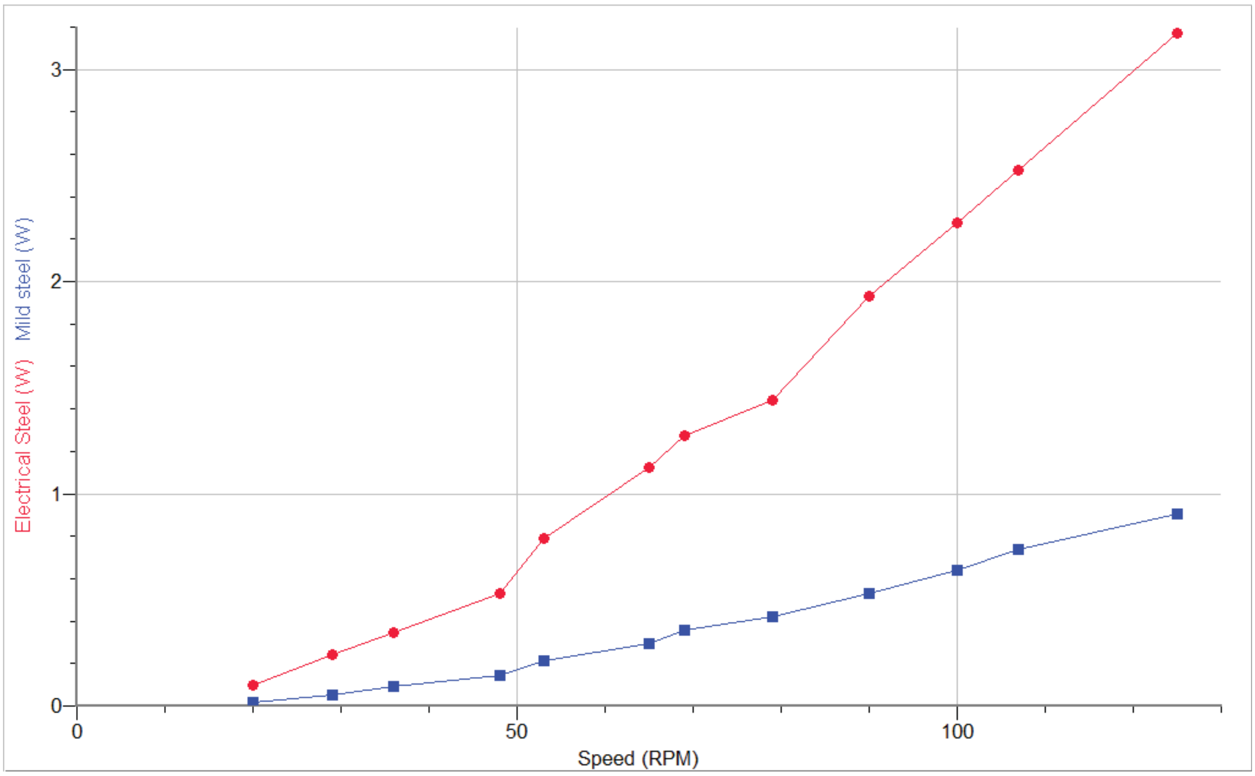


**Figure 5.6:** M1 magnets power output of electrical steel and mild steel

## 5.3. Effect of the orientation of the magnet pole

The second factor tested was the effect that the pole orientation of the magnets had on the output generated. Experiments were conducted to check if there would be a difference in output, if the poles of the magnets were changed.

### 5.3.1. Experimental Setup

Two experiments were run with 18 M1 magnets placed on the flywheel. First experiment was done with all the magnets being placed with their south pole facing the flywheel. The second experiment had the same setup as the first but the poles of the magnets alternated. Figure 5.7 shows this setup.

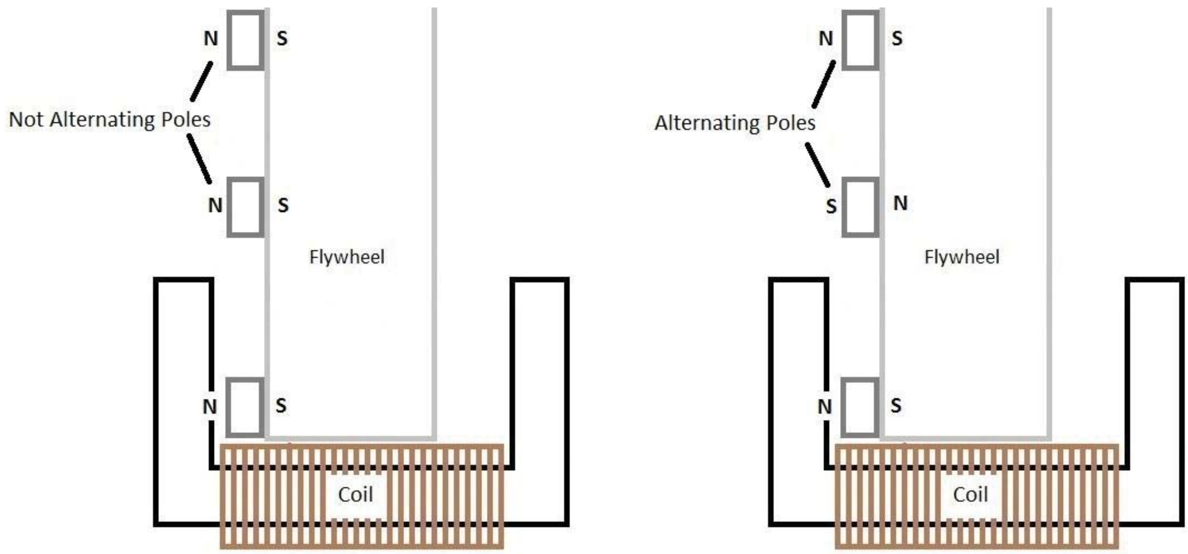


**Figure 5.7:** Setup for pole orientation of magnet poles

To calculate the power generated the output of the electromagnet was connected to a rectification circuit and then connected across a load of 100ohm. Waveforms of the outputs at different sections of this process were captured for analysis. Figure 5.8 shows a block diagram of the process used to carry out this experiment.

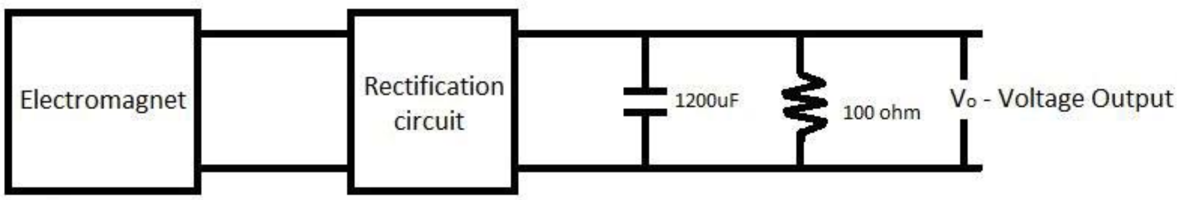


**Figure 5.8:** Block diagram of the setup for the experiment

### 5.3.2. Results and Discussion

As the experiments were run, an oscilloscope probe was connected to the output from the electromagnet and waveforms were captured at various speeds. The peak-peak voltages were noted from the waveforms captured.


**Figure 5.9:** Peak-Peak voltage waveform of magnets with different pole orientation at 110 RPM

Figure 5.9 shows a waveform comparison of when the bike was pedalled at a speed of 110RPM. The waveforms clearly indicate that having magnets with alternating poles give a higher output.

The output voltage, across the load, from both experiments was noted. From this the power generated by the system was calculated. Table 5.4 gives the Voltage and Power outputs generated by the system.

| | **Not Alternating Poles** | | **Alternating Poles** | |
|---|---|---|---|---|
| **Speed (RPM)** | **Voltage output (V)** | **Power output (W)** | **Voltage output (V)** | **Power output (W)** |
| 35 | 5.8 | 0.3364 | 7.1 | 0.5041 |
| 70 | 9.3 | 0.8649 | 12.5 | 1.5625 |
| 110 | 12.5 | 1.5625 | 16.8 | 2.8224 |

**Table 5.4:** Power Generated by having magnets with different pole orientation

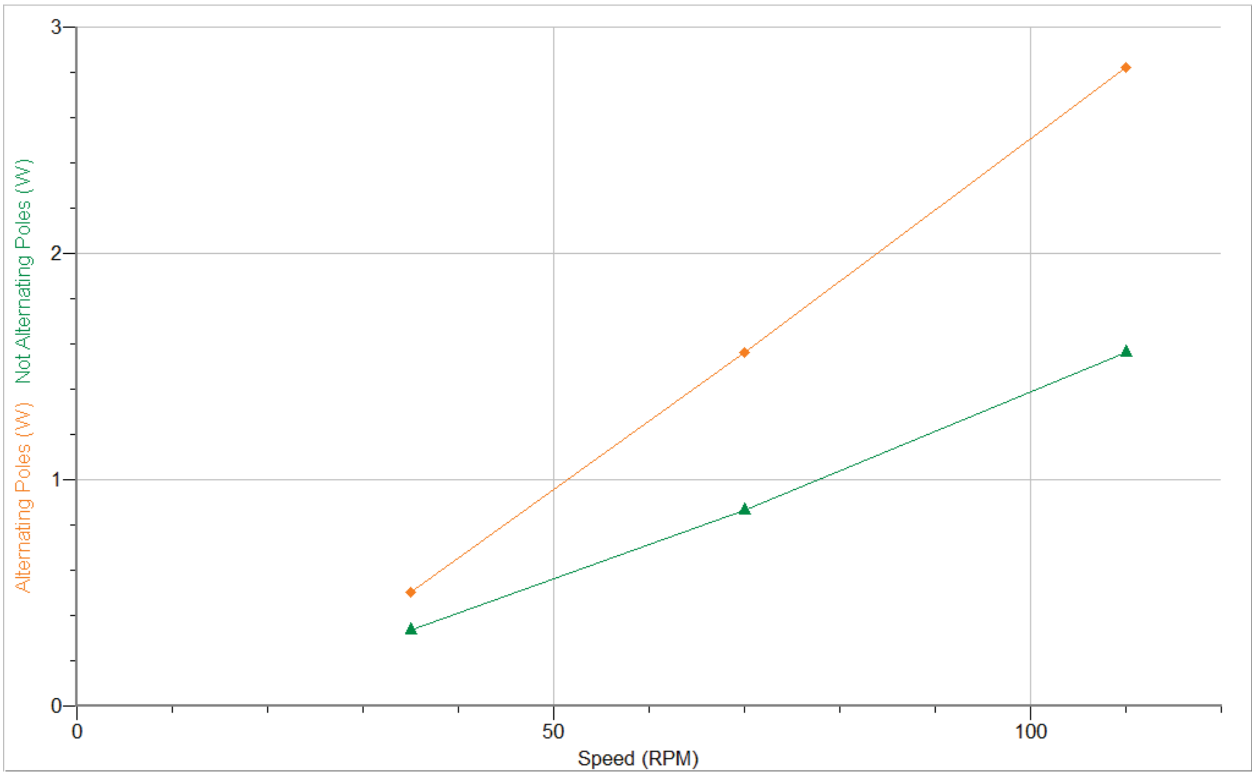


**Figure 5.10:** Relationship of magnet pole orientation and speed

The power characteristics of the magnet pole orientation and the speed is plotted in Figure 5.10. The figure shows that having magnets with alternating poles would give a higher output than having all the magnets placed facing the same way.

If all the magnets are placed having the same poles, the only change is that the magnetic field varies in strength. As a magnet approaches the coil the magnetic strength increases and as the magnet passes the strength decreases. This continues to happen as each magnet passes through. Because of this there is only a small amount of EMF being generated.

However when the magnets are placed where the poles alternate, not only does the magnetic strength change but also the direction of the magnetic field changes and hence creates more flux.

## 5.4. Effect of the number of magnets

The third factor tested was the effect that the number of magnets on the flywheel had on the output generated. As discussed in the previous chapter the power increases with the number of magnets used but this has a limit. Experiments were done to see how many magnets could be placed on the flywheel to get the best possible output.

### 5.4.1. Experimental Setup

Two experiments were run with different number of M1 magnets, with alternating poles, placed on the flywheel. The first experiment consisted of 18M1 magnets and the second with 20 M1 magnets. The magnets were spaced apart equally on the flywheel. Figure 5.11 shows the process for this experiment and Figure 5.12 shows the setup for this experiment.

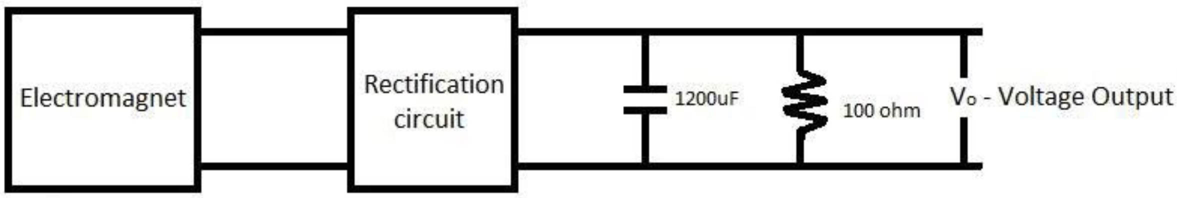


**Figure 5.11:** Block diagram of the setup for the experiment

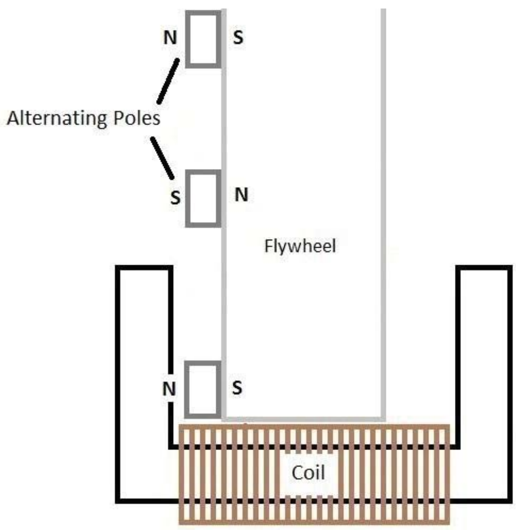


**Figure 5.12:** Experimental setup for the effect of the number of magnets used

### 5.4.2. Results and Discussion

As the experiments were run waveforms of the outputs were captured using an oscilloscope. The mean voltage output by the system was noted from the waveforms for further analysis.


**Figure 5. 13:** Waveforms of 18 and 20 M1 magnets at a speed of 110RPM

Figure 5.13 is the waveforms captured at the output of the load at a speed of 110RPM. The waveforms show that the output voltage with 18 magnets at 110RPM is 16.8V and with 20 magnets at the same speed the output voltage is 19.4V. Table 5.5 gives the Voltage and Power outputs at various speeds.

| | 18 M1 Magnets | | 20 M1 Magnets | | 22 M1 Magnets | |
|---|---|---|---|---|---|---|
| Speed (RPM) | Voltage Output (V) | Power Output (W) | Voltage Output (V) | Power Output (W) | Voltage Output (V) | Power Output (W) |
| 35 | 7.1 | 0.5041 | 8.02 | 0.643204 | 4.3 | 0.1849 |
| 70 | 12.5 | 1.5625 | 14.2 | 2.0164 | 5.9 | 0.3481 |
| 110 | 16.8 | 2.8224 | 19.4 | 3.7636 | 7 | 0.49 |

**Table 5.5:** Voltage and Power output for 18, 20 and 22 M1 magnets

The power characteristics of the relationship between the number of magnets and the speed of the bike is shown in Figure 5.14. As the speed increases the output increases. The output is slightly higher when 20 magnets are used instead of 18. Increasing the number of magnets past 20 drops the voltage drastically. So the ideal number of magnets on the flywheel for this experiment is 20.

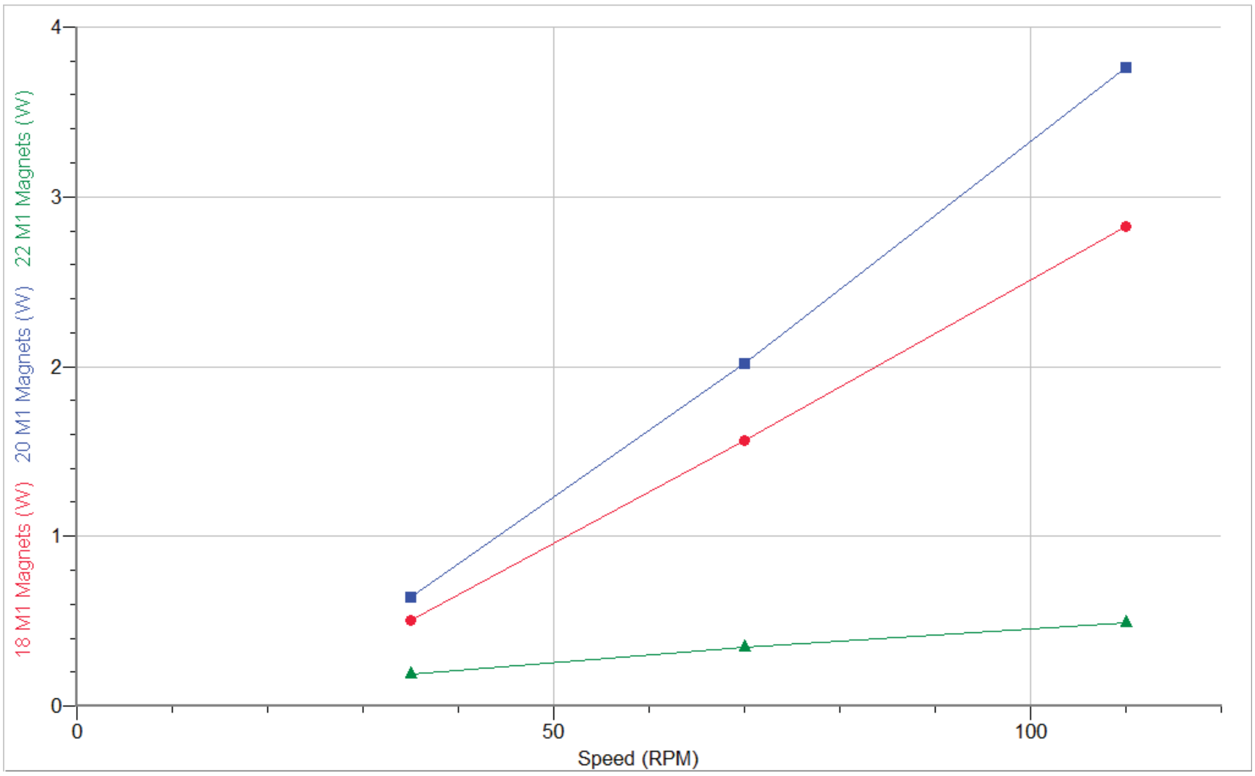


**Figure 5.14:** Power output with 18, 20 and 22 magnets at different speeds

The greater the number of magnets the greater the change in the magnetic field strength and direction. This in turn creates more flux which in turn generates more EMF [61]. However, the results of this experiment shows that having too many magnets very close together produces very little flux.

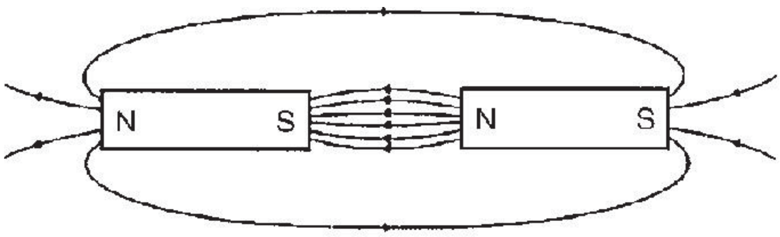


**Figure 5. 15:** Behaviour of magnetic field lines when they are too close to each other

Figure 5.15 shows how the magnetic field lines can travel in a straight line if the magnets are too close. The magnetic field lines of a magnet always go from North to South. So when the magnets are placed where the poles alternate and the magnets are too close, the magnetic field lines will go from a magnet to the opposite magnet. From this can be concluded that the cause of the huge drop in output when 22 magnets are used is due to the fact that there is very little space between the magnets.

## 5.5. Effect of the strength of the magnet

The fourth factor tested was the effect that magnets with different strengths would have on the output generated. Two magnets of different strength but same diameter were used for this project. The two magnets used are referred to as Magnet 1 (M1) and Magnet 2 (M2). M1 had a thickness of 6.35mm and had a surface field strength of 3275 Gauss. M2 was slightly stronger than M1, which was 9.5mm thick and had a surface field strength of 4295 Gauss. In theory, M2 should produce a higher power output based on its surface field strength.

### 5.5.1. Experimental Setup

Two experiments were conducted with each electromagnet to check the relation between the magnet strength and the output. 20 magnets placed with alternating poles were used for both experiments. The only difference between the two experiments was the magnets used. Figure 5.16 shows how the output voltage was acquired and Figure 5.18 is a visual on the setup used for both magnets.

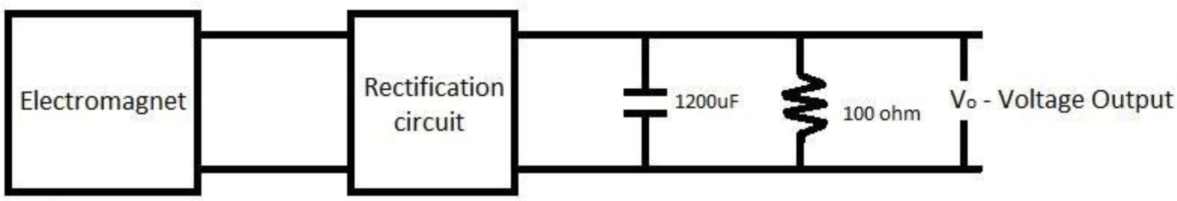


**Figure 5.16:** Block diagram of the setup for the experiment t

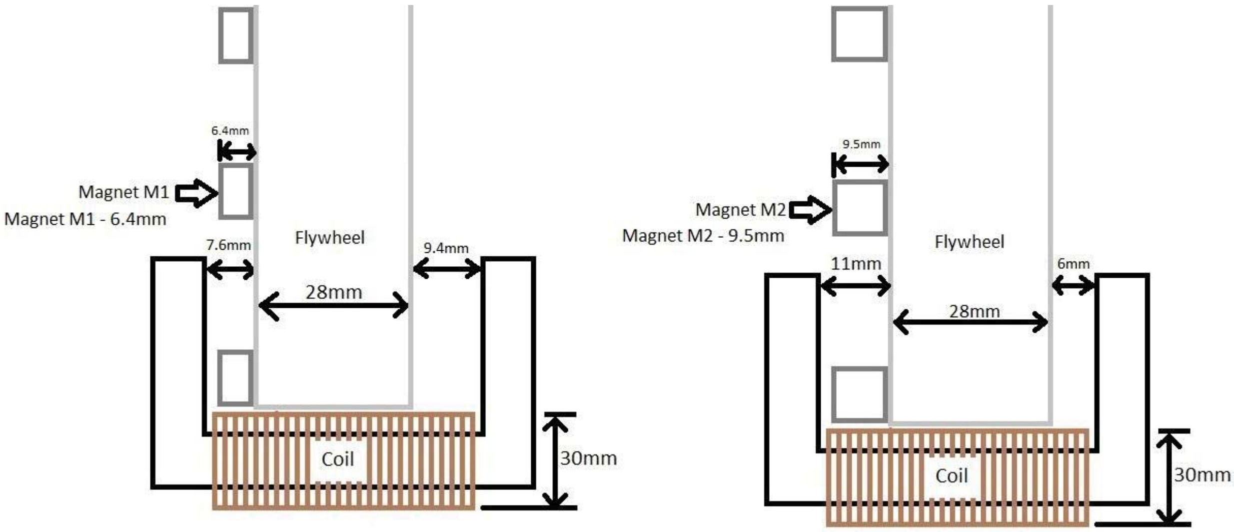


**Figure 5.17:** Experimental setup for the effect of the strength of the magnet on the output

### 5.5.2. Results and Discussion

As the experiments were run, waveforms of the outputs were captured using an oscilloscope. The mean voltage output by the system was noted from the waveforms for further analysis. Figure 5.18 shows the waveforms of the voltage output at 110RPM for both the magnets.

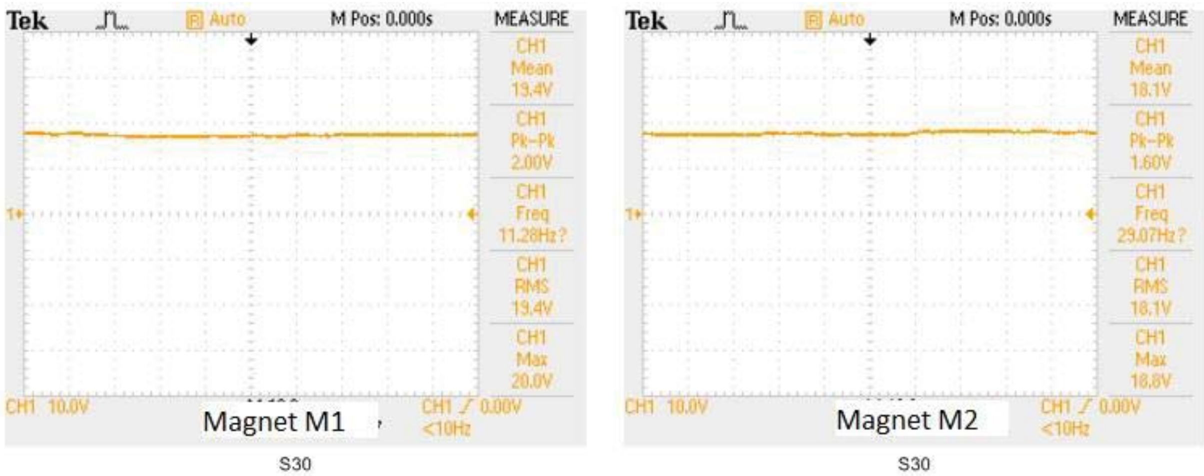


**Figure 5.18:** Waveform of voltage output for different magnets at 110RPM

In theory, the voltage and power output is expected to be more when stronger magnets are used. However, in this experiment stronger magnet M2 did not give a higher output compared to M1. M1 gave a slightly higher voltage output than M2. The results of the experiments are shown in Table 5.6.

| | **Magnet M1** | | **Magnet M2** | |
|---|---|---|---|---|
| **Speed (RPM)** | **Voltage Output (V)** | **Power Output (W)** | **Voltage Output (V)** | **Power Output (W)** |
| 35 | 8.02 | 0.643204 | 7.36 | 0.541696 |
| 55 | 10.7 | 1.1449 | 10.7 | 1.1449 |
| 70 | 14.2 | 2.0164 | 13.2 | 1.7424 |
| 90 | 16.5 | 2.7225 | 16.2 | 2.6244 |
| 110 | 19.4 | 3.7636 | 18.1 | 3.2761 |

**Table 5.6:** Voltage & Power outputs for magnets of different strength at various speeds

Figure 5.19 shows the power characteristics in relation to the speed and magnet strength.

M1 has a slightly higher power output compared to the output of M2. Though M2 is the stronger magnet the output shows that M1 gives a slightly higher power output. This can be the result of a bigger air gap present in the setup when magnet M2 is used. As M2 is approximately 4mm thicker than M1, this increases the air gap by that distance. Even a gap of a few millimeters can cause a drop in the output since the strength of the magnetic field drops exponentially with distance [62]. Because of this M1 produces a higher power output than M2, as is the case in this experiment.

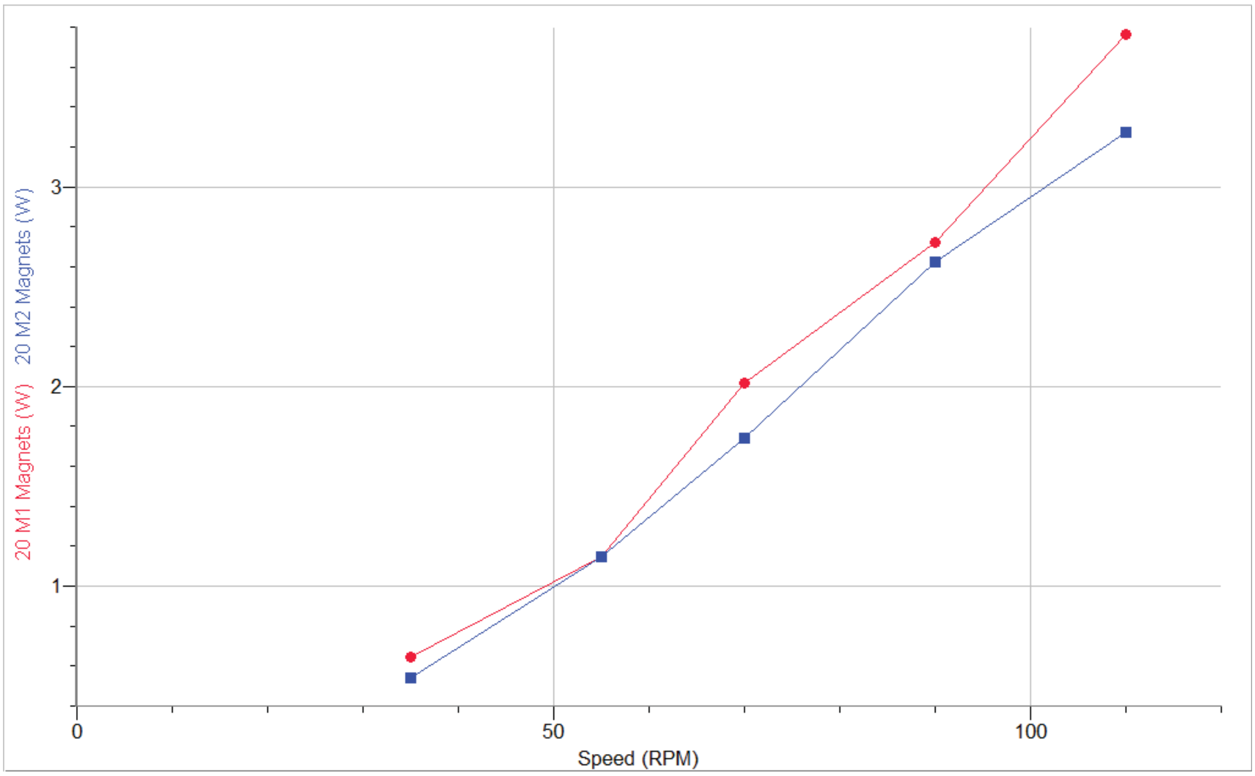


**Figure 5. 19:** Power output of M1 and M2 magnets at different speeds

## 5.6. Effect of an air gap

The fifth and last factor tested was the effect that an air gap present in the electromagnet would have on the output generated. Having an air gap in this experiment was unavoidable but could be reduced. The presence of an air gap increases the reluctance in a magnetic circuit and causes the flux generated to spread into the surrounding medium. This is referred to as the flux-fringing effect [63] and figure 5.20 shows this in an electromagnet. Experiments were run to see the difference in power output when the air gap present in this system was reduced.

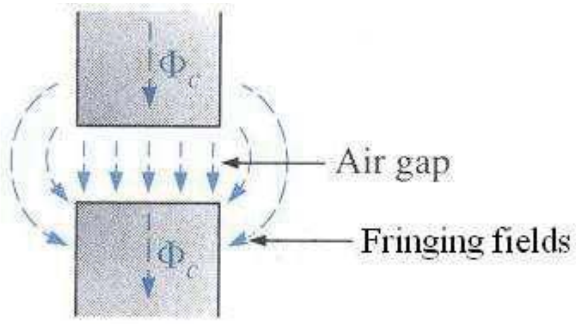


**Figure 5.20:** Fringing effect caused by an air gap

### 5.6.1. Experimental Setup

Air gaps present in this circuit were the gaps present on either side of the flywheel. The side with the magnets had an air gap of 7.6mm, and the side without the magnets had an air gap of 9.4mm. Figure 5.21 shows these air gaps.

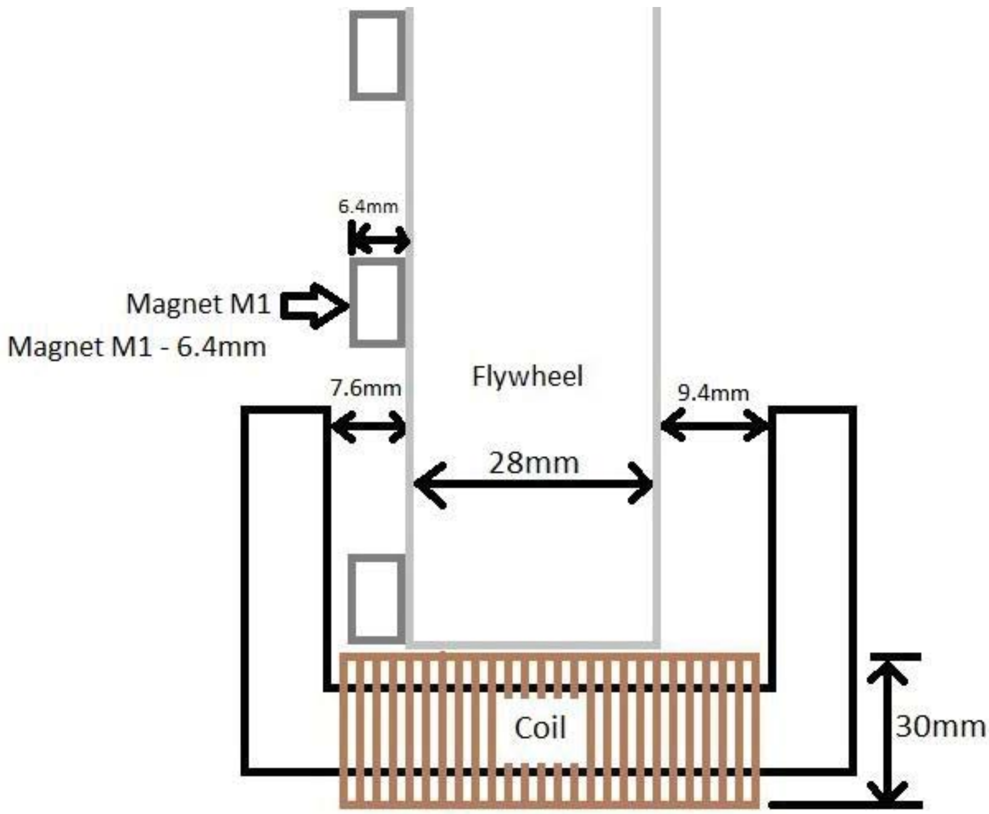


**Figure 5. 21:** Experimental setup for effect of air gap on the output

The air gap on the side with the magnets could not be reduced further. Doing so would cause the magnets on the flywheel to hit the electromagnet which would in turn cause the flywheel to stop spinning. However, the air gap on the opposite side of the flywheel could be reduced as this would not affect the spinning of the flywheel. The air gap was reduced by putting a small stack of I shaped electrical steel sheets between the flywheel and the electromagnet.

Figure 5.22 shows a stack of I shaped electrical steel held together by electrical tape. This was made 8mm thick so that it fit snugly in the air gap of 9.4mm. A gap of about 1mm was given between the stack of electrical steel and the flywheel because that would cause the stack of electrical steel to rub against the flywheel.

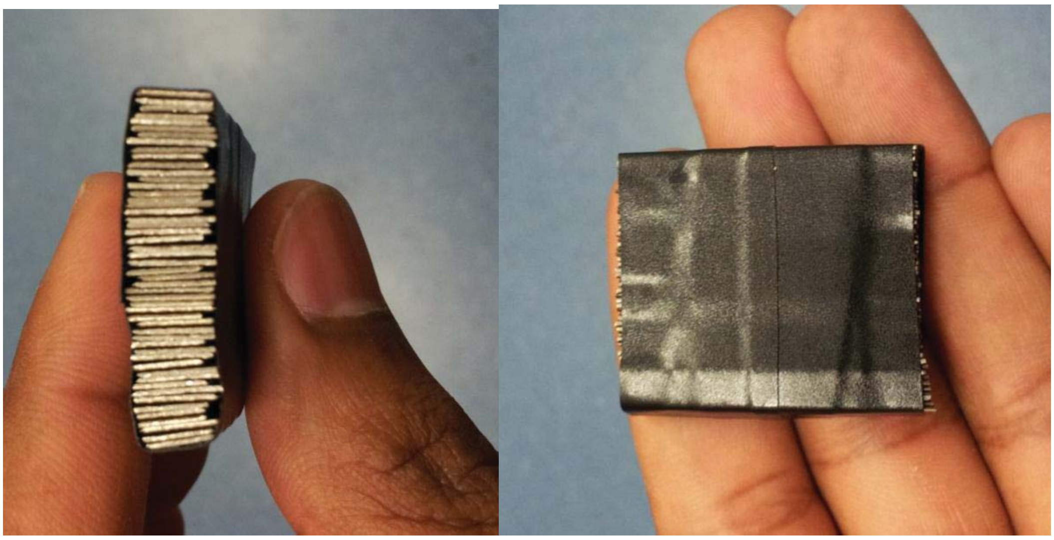

**Figure 5. 22:** Stack of I shaped electrical steel sheets

Figure 5.23 shows the electromagnet with an air gap of 9.4mm. Figure 5.24 shows the electromagnet with the air gap reduced by the insertion of the I shaped electrical steel stack. The experiment was run with the same process as the previous experiment. This is shown in Figure 5.25.

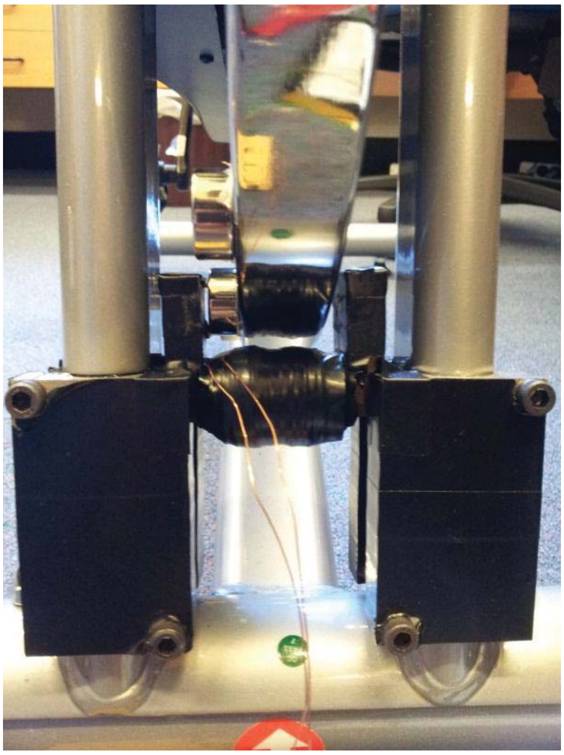

**Figure 5.23:** Setup with air gap

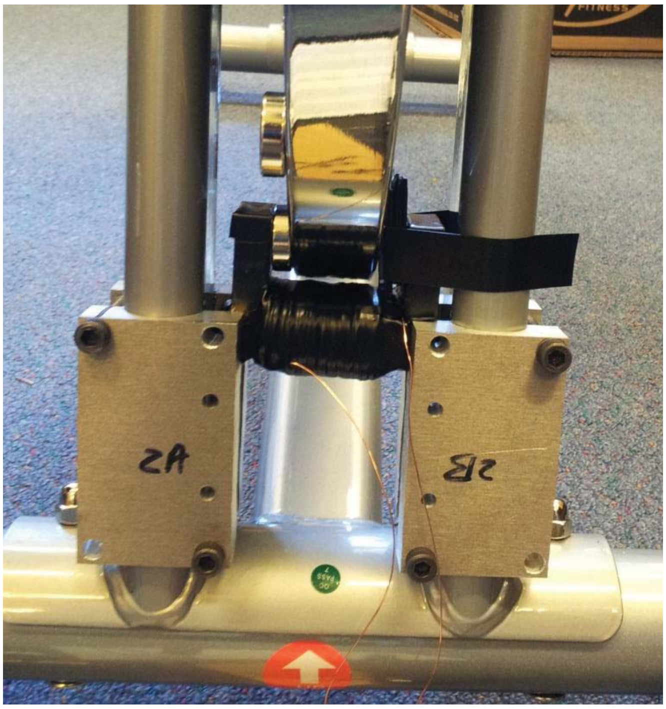


**Figure 5. 24:** Setup with reduced air gap

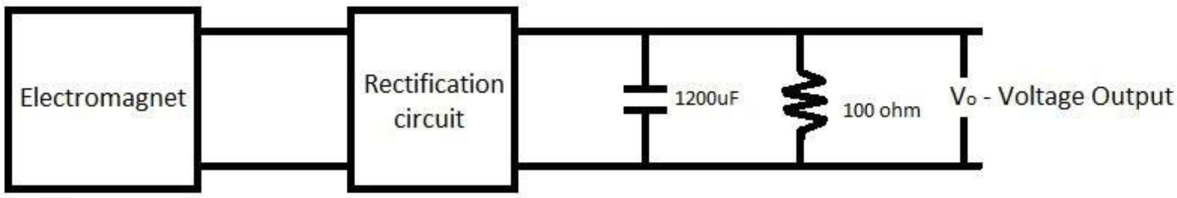


**Figure 5.25:** Block diagram of the setup for the experiment

### 5.6.2. Results and Discussion

Two experiments were run to see the relationship between the air gap present in the system and the power output. Both experiments had 20 M1 magnets with alternating poles placed on the flywheel. Experiments were done with the system having an air gap of 9.4mm and then a reduced air gap of 1mm. The voltage and power outputs for both these experiments are shown in Table 5.7.

| | Air Gap of 8.5mm | | Air Gap of 1mm | |
|---|---|---|---|---|
| **Speed (RPM)** | **Voltage Output (V)** | **Power Output (W)** | **Voltage Output (V)** | **Power Output (W)** |
| 35 | 8.02 | 0.643204 | 9.11 | 0.829921 |
| 55 | 10.7 | 1.1449 | 11.5 | 1.3225 |
| 70 | 14.2 | 2.0164 | 15.3 | 2.3409 |
| 90 | 16.5 | 2.7225 | 17.9 | 3.2041 |
| 110 | 19.4 | 3.7636 | 21.1 | 4.4521 |

**Table 5. 7:** Voltage and Power output when an air gap is reduced

By looking at the power values generated, it is evident that reducing the air gap gives a higher output. Figure 5.26 shows the power characteristics in relation to the speed and the air gap present in the system. The strength of the magnetic field drops exponentially with distance because having an air gap in the circuit increases the reluctance in the circuit [62]. A Larger air gap means more reluctance in the circuit. Reducing the air gap reduces the reluctance in the circuit which in turn increases the amount of power generated. This provides a clear indication that reducing the air gap in this system has increased the power generated.

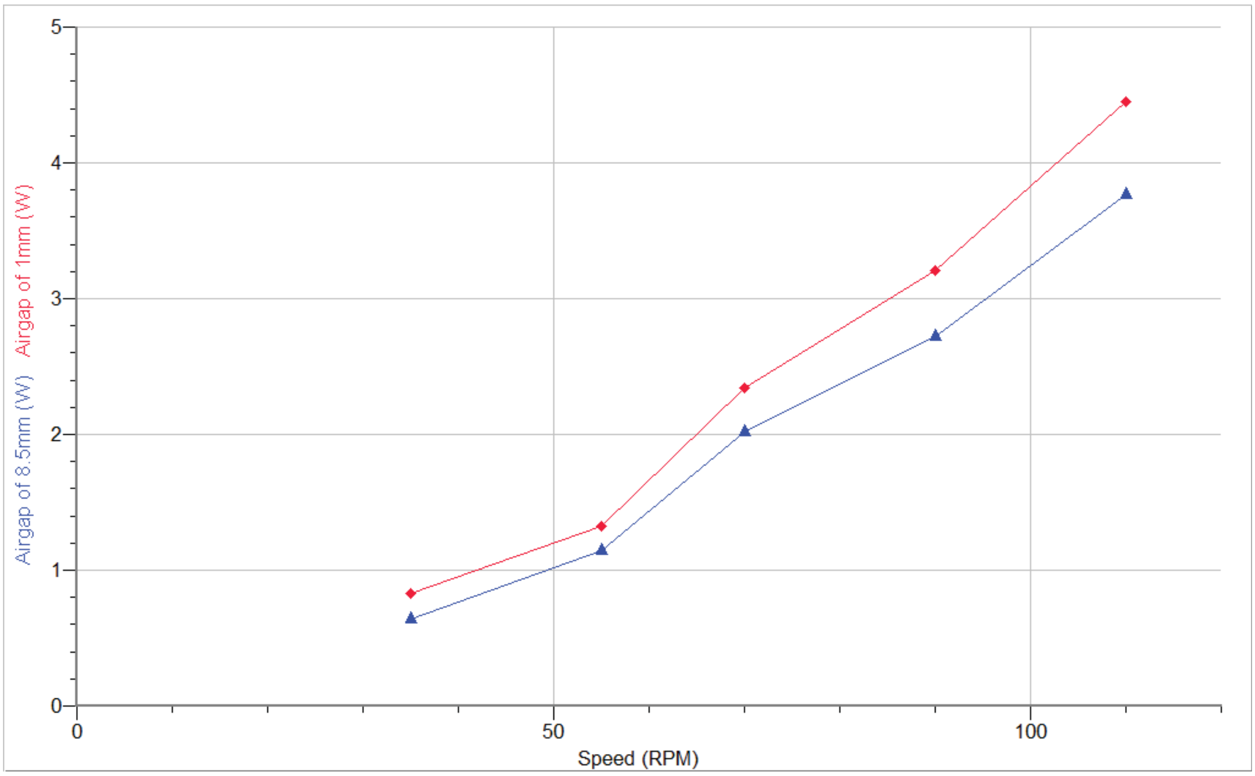


**Figure 5.26:** Power characteristics of the speed of the bike and the air gap present in the system

## 5.7. Maximum Power and Energy Calculations

After all the variables that could affect the output were investigated the best possible setup for harvesting energy using this method was determined. The experiments showed that an electromagnet made with high Permeability (μ) material would increase the power output. It was also found that the orientation of the poles of the magnets used is important. Having magnets with their poles alternating produced more flux in the circuit. Results showed that there is a limit to the number of magnets that can be placed on the flywheel at a given time, as having too many magnets on the disc would cause the power generated to drop drastically. The experiment also indicated that a stronger magnet does not necessarily increase the output. The stronger the magnet the thicker it is and creates a larger air gap in the circuit. This in turn causes the output to drop when compared to a magnet with smaller thickness. This showed that as the air gap in the circuit increased the reluctance in the circuit also increased causing the output to drop. Reducing the air gap resulted in higher power output.

### 5.7.1. Experimental Setup

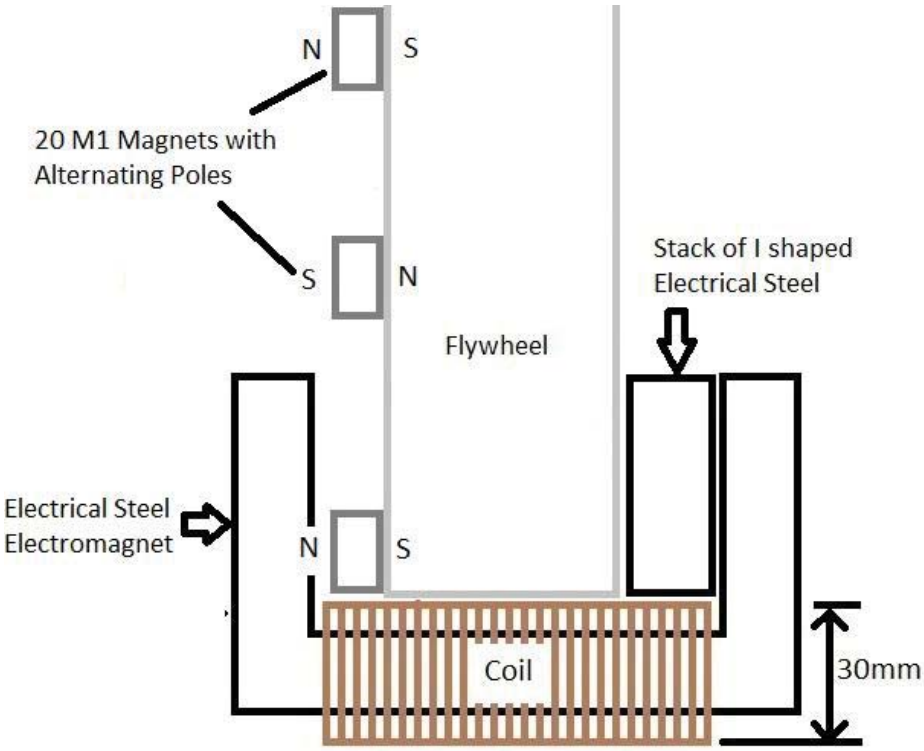


**Figure 5.27:** Final Experimental Setup

Figure 5.27 shows the final setup of the system. This was based on the results and findings of the previous experiments. This system was used to conduct experiments to investigate the Energy (E) and Power (W) that could be generated using this method of EH. To do this, the output from the coil/electromagnet was connected to a rectification circuit which was passed through a capacitor to smooth out the signal. The signal was then connected to a Buck-Boost converter which would either boost the incoming voltage to 15V or limit it to 15V. The output of the Buck-Boost converter was then used to charge a 12V rechargeable battery. Figure 5.28 shows a block diagram of the setup and figure 5.29 is a picture of the actual setup of the whole system.

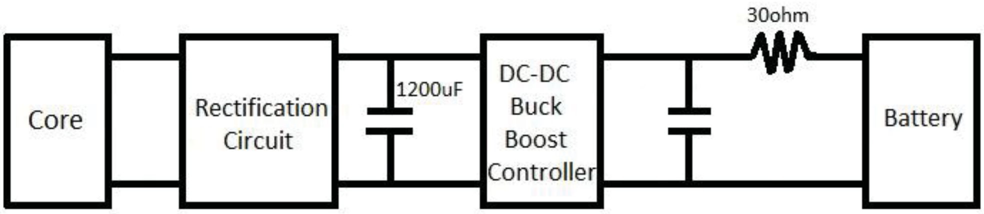


**Figure 5.28:** Block diagram of the setup for the experiment

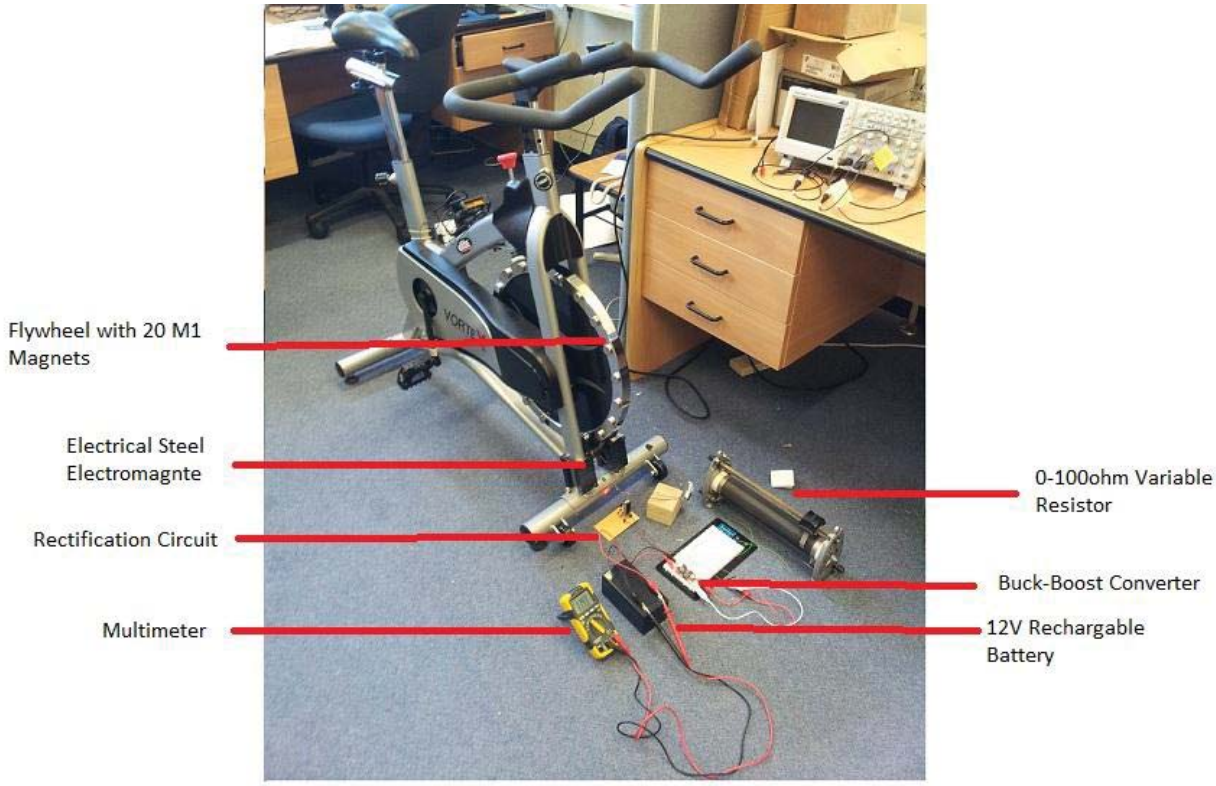


**Figure 5.29:** Setup of the stationary bike to charge a battery

To calculate the Energy (E) generated, the output from the Buck-Boost controller was used to connect a 12V rechargeable battery as shown in Figure 5.28. The intent was to charge the battery for certain periods of time and record the charge of the battery. The following equations were used to record this. For this the battery voltage $(V_B)$ was noted at the start and then noted every 5minutes as the bike was pedalled.

The equation to calculate Energy (E) is

$$E = P_o * t_{charging} \qquad \text{Equation (5.3)}$$

Where $P_o$ is the Power output measured in Watts and $t_{charging}$ is the time the battery has been charged measured in seconds. The power output ($P_O$) was calculated using equation 5.4

$$P_o = V_B * I_{charging} \qquad \text{(Equation 5.4)}$$

Where, $V_B$ is the battery voltage measured in Volts and $I_{charging}$ is the charging current of the battery measured in Amps. The charging current ($I_{charging}$) was calculated using equation 5.5

$$I_{charging} = \frac{V_{in} - V_B}{R} \qquad \text{Equation (5.5)}$$

Where, $V_{IN}$ is the voltage coming in to the battery from the Buck-Boost converter measured in volts, $V_B$ is the battery voltage measured in Volts and $R$ is the resistance measured in ohms.

Inserting equation 5.5 and 5.4 into equation 5.3 gives us

$$E = V_B * \left(\frac{V_{in} - V_B}{R}\right) * t_{charging} \qquad \text{Equation (5.6)}$$

Where $E$ is the energy generated by the system measured in Joules, $V_B$ is the battery voltage measured in Volts, $V_{out}$ is the voltage out of the Buck Boost converter measured in Volts, $R$ is the resistance between the Buck Boost converter and the battery measured in ohms and $t$ is the time the battery has been charged measured in seconds.

### 5.7.2. Maximum Power ($P_{MAX}$) Calculations

Before connecting the system to a battery experiments were done to check the maximum power output from the system. The system was setup as shown in figure 5.27. Experiments were run by varying the load resistance of the system and the Voltage and Power outputs were noted.

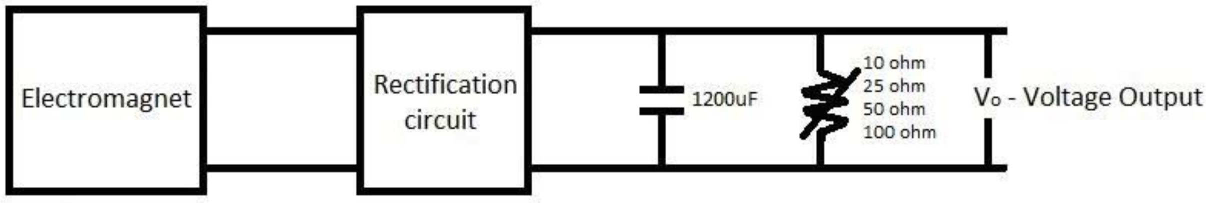


**Figure 5.30:** Block diagram of the setup for the experiment

Figure 5.30 shows the process of this experiment in a block diagram. A variable resistor was connected to the output of the rectification circuit. Experiments were done with the resistance being set to 10ohm, 25ohm, 50ohm and 100ohm. The bike was pedalled at different speeds and the voltage output noted. The results from these experiments are shown in Table 5.8. It was found that the voltage output increased as the speed and resistance in the system increased. Figure 5.31 shows the results of this experiment graphically. It clearly shows that the voltage output increases when the bike is pedalled faster. It also shows that the voltage increases as the resistance in the circuit is increased.

| **Resistance (ohm)** | **Voltage ($V_O$) 35 RPM** | **Voltage ($V_O$) 55 RPM** | **Voltage ($V_O$) 70 RPM** | **Voltage ($V_O$) 90 RPM** | **Voltage ($V_O$) 110 RPM** |
|---|---|---|---|---|---|
| 10 | 3.42 | 4.05 | 4.09 | 4.45 | 4.46 |
| 25 | 5.43 | 7.16 | 8.92 | 9.32 | 10.2 |
| 50 | 6.78 | 9.38 | 11.5 | 13 | 14.7 |
| 100 | 7.9 | 11.3 | 14.1 | 16.6 | 19.4 |

**Table 5.8:** Voltage output with different Load resistance

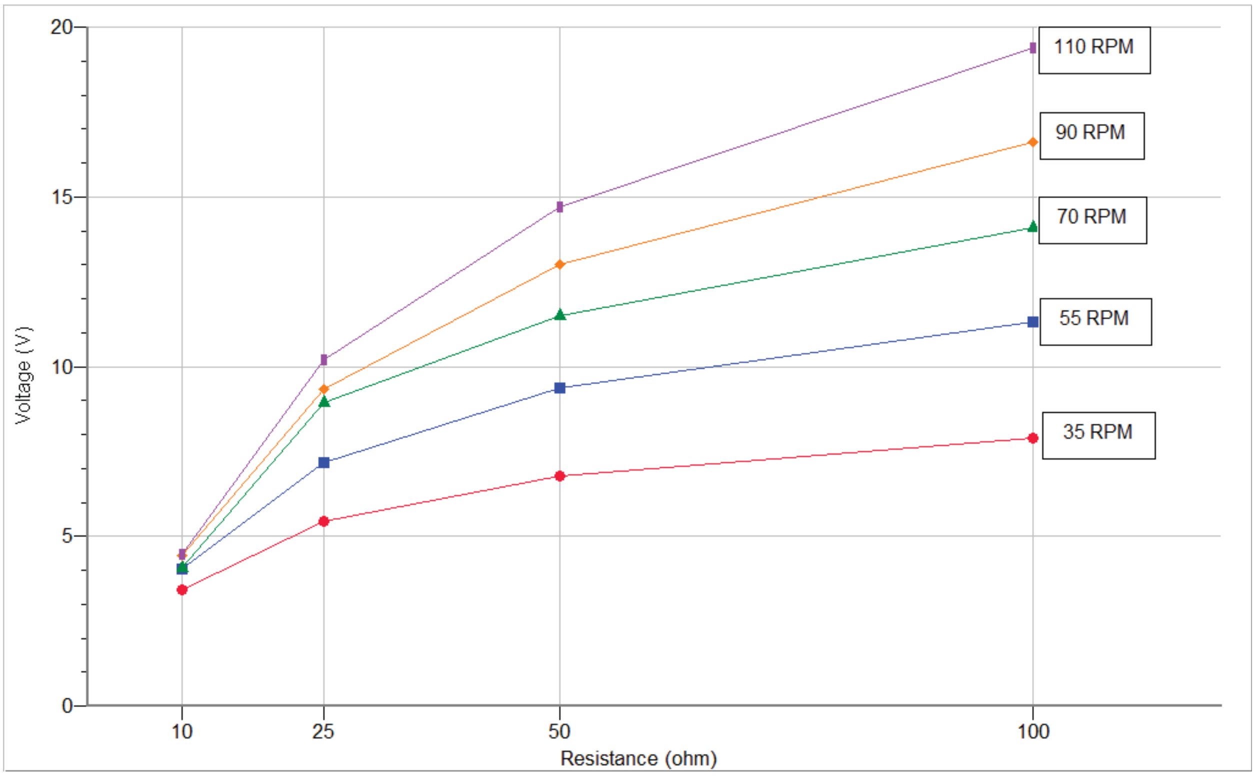


**Figure 5.31:** Voltage output with different load resistance at various speeds

From the output voltages the power output of the system was calculated using Equation 5.1. Table 5.9 gives the calculated power outputs when the speed and resitance in the system was varied.

| Resistance (ohm) | Power ($P_O$) 35 RPM | Power ($P_O$) 55 RPM | Power ($P_O$) 70 RPM | Power ($P_O$) 90 RPM | Power ($P_O$) 110 RPM |
|---|---|---|---|---|---|
| 10 | 1.16964 | 1.64025 | 1.67281 | 1.98025 | 1.98916 |
| 25 | 1.179396 | 2.050624 | 3.182656 | 3.474496 | 4.1616 |
| 50 | 0.919368 | 1.759688 | 2.645 | 3.38 | 4.3218 |
| 100 | 0.6241 | 1.2769 | 1.9881 | 2.7556 | 3.7636 |

**Table 5.9:** Power outputs across varied loads at different speeds

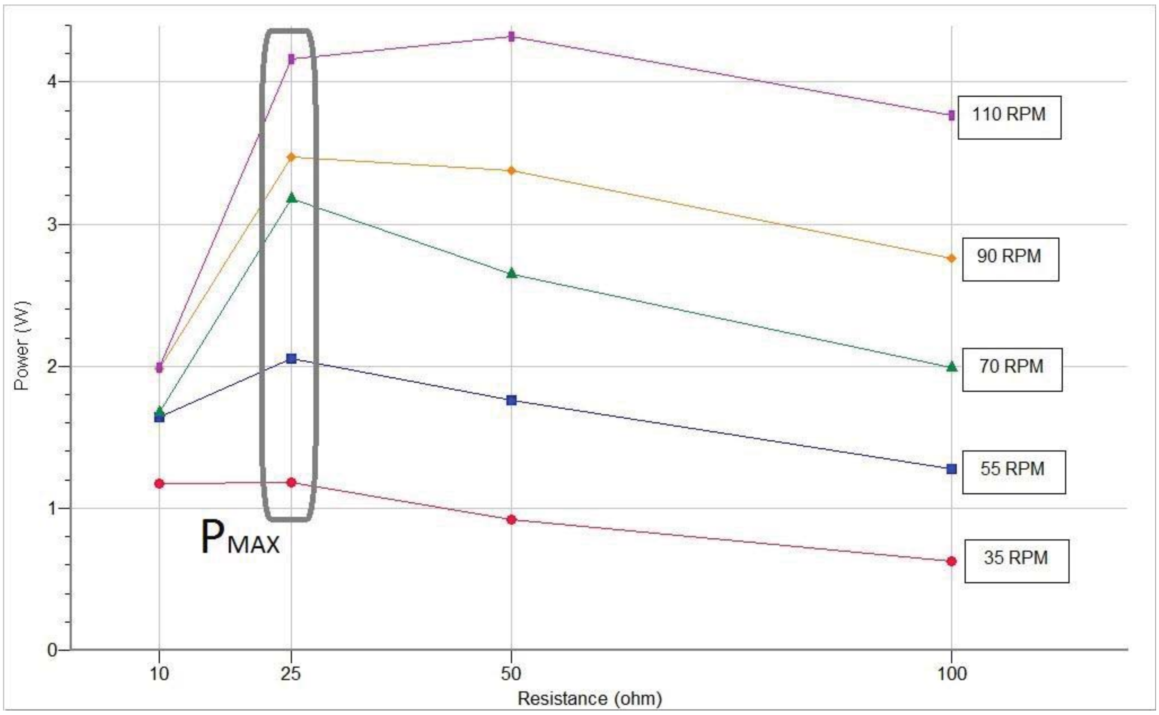


**Figure 5.32:** Power output with different load resistance at various speeds

Figure 5.32 gives a visual display of the power outputs plotted against the resistance at different speeds. It highlights that the maximum power $P_{MAX}$ is acheived when the system has a load resistance of about 25ohm. It shows that the power increases with the load to a certain point and then begins to decrease as the resistance in the circuit is increased.

### 5.7.3. Energy Calculations

For the experiment the bike was pedalled for 30 minutes at a constant speed of 70RPM. The Buck-Boost converter was set to output 15V. The resistor between the Buck-Boost converter and the battery was a 100ohm. The initial battery voltage $V_B$ was 11.49V. As the bike was being pedalled the battery voltage $V_B$ was noted every 5 minutes. The results of the experiment are shown in Table 5.10 and graphically in Figure 5.33-5.36. The charging current, power and energy was calculated using equations 5.5, 5.4 and 5.6 respectively.

| Time | Battery Voltage ($V_B$) | Charging Current (I) | Power (W) | Energy (J) |
|---|---|---|---|---|
| 0 | 11.49 | 0.361 | 4.14789 | 0 |
| 300 | 11.71 | 0.339 | 3.96969 | 1190.907 |
| 600 | 11.77 | 0.333 | 3.91941 | 2351.646 |
| 900 | 11.81 | 0.329 | 3.88549 | 3496.941 |
| 1200 | 11.84 | 0.326 | 3.85984 | 4631.808 |
| 1500 | 11.87 | 0.323 | 3.83401 | 5751.015 |
| 1800 | 11.9 | 0.32 | 3.808 | 6854.4 |

**Table 5.10:** Energy outputs from experiment

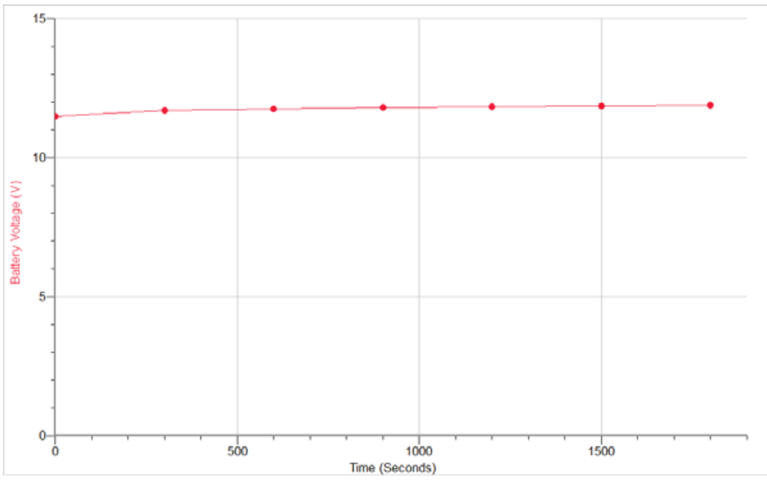


**Figure 5.33:** Battery voltage over time

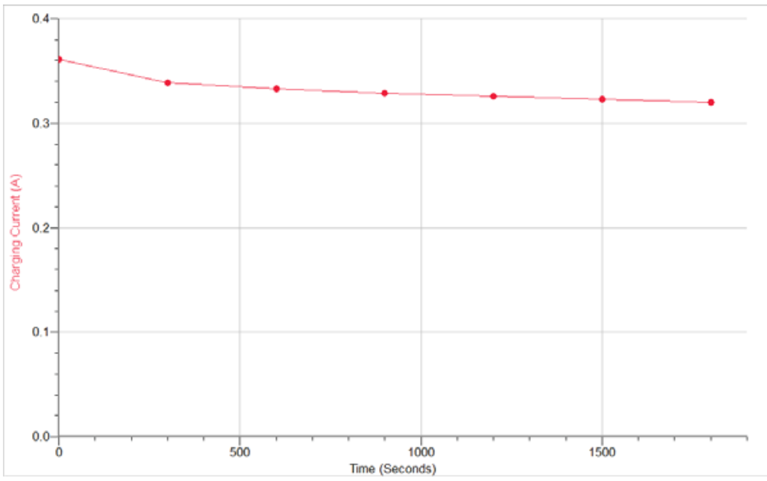


**Figure 5.34:** Charging current over time

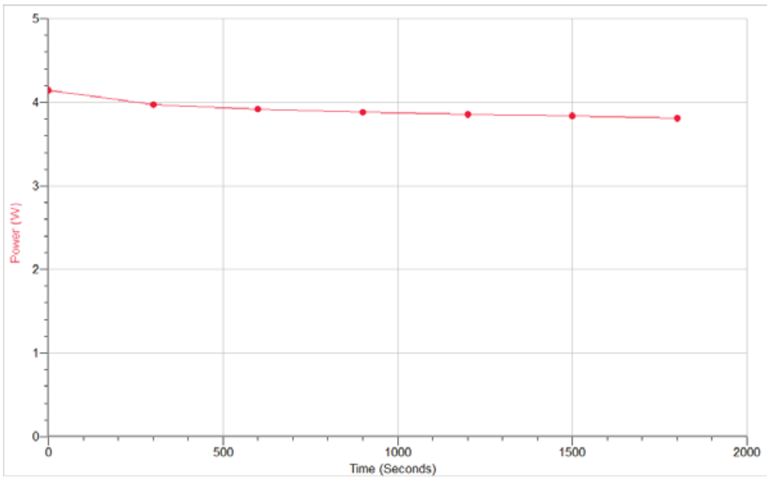


**Figure 5.35:** Power generated by EH in 30 minutes

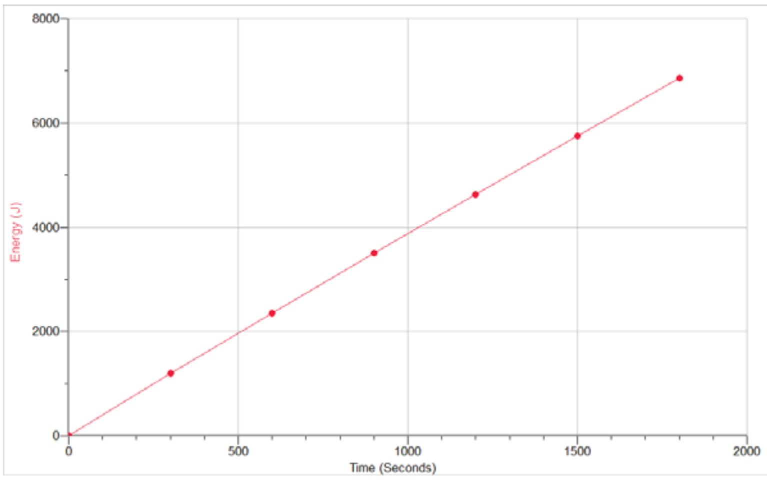


**Figure 5.36:** Energy generated by EH in 30minutes

This experiment shows that when the bike is pedalled at a speed of 70 RPM, the system generates 6854J of energy in 30mins. When the bike is pedalled the battery voltage increases with time and the charging current drops slightly (see Figure 5.33 and 5.34). Since the power generated is dependent on the charging current, power reduces slowly as the charging current decreases.

The battery was charged for half hour as stated above. Tests were then done to measure the length of time taken to discharge the battery. For this a 12V 50W bulb was connected to the battery and the battery voltage was monitored using a multimeter. Figure 5.37 shows the setup used to discharge the battery and Table 5.11 gives the battery voltage for the charging and discharging process.

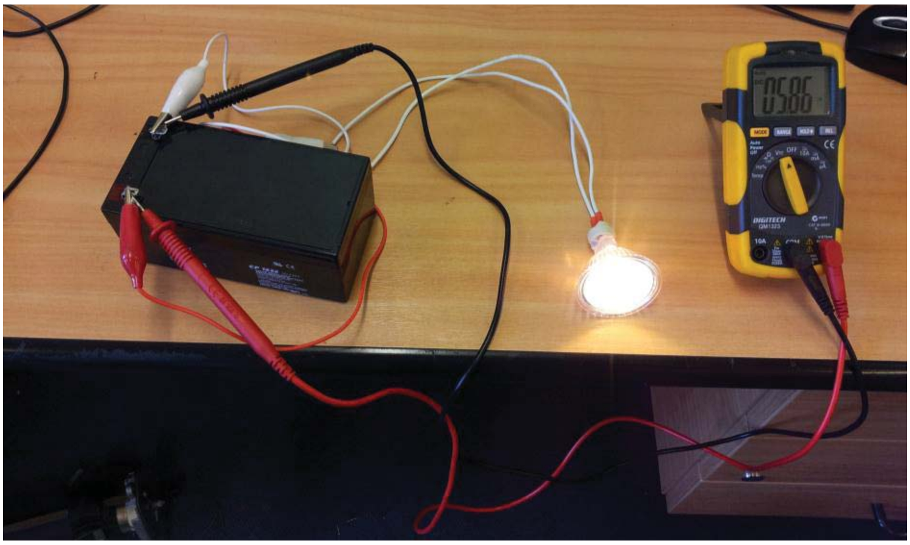

**Figure 5. 37: Discharging Battery using 12V 50W bulb**

| Time (Minutes) | Battery Voltage ($V_B$) |
|---|---|
| 0 | 11.49 |
| 5 | 11.71 |
| 10 | 11.77 |
| 15 | 11.81 |
| 20 | 11.84 |
| 25 | 11.87 |
| 30 | 11.9 |
| 31 | 11.88 |
| 32 | 11.83 |
| 33 | 11.79 |
| 34 | 11.74 |
| 35 | 11.67 |
| 36 | 11.6 |
| 37 | 11.54 |
| 38 | 11.46 |
| 39 | 11.39 |
| 40 | 11.26 |

**Table 5.11:** Charge and Discharge of Battery voltage over time

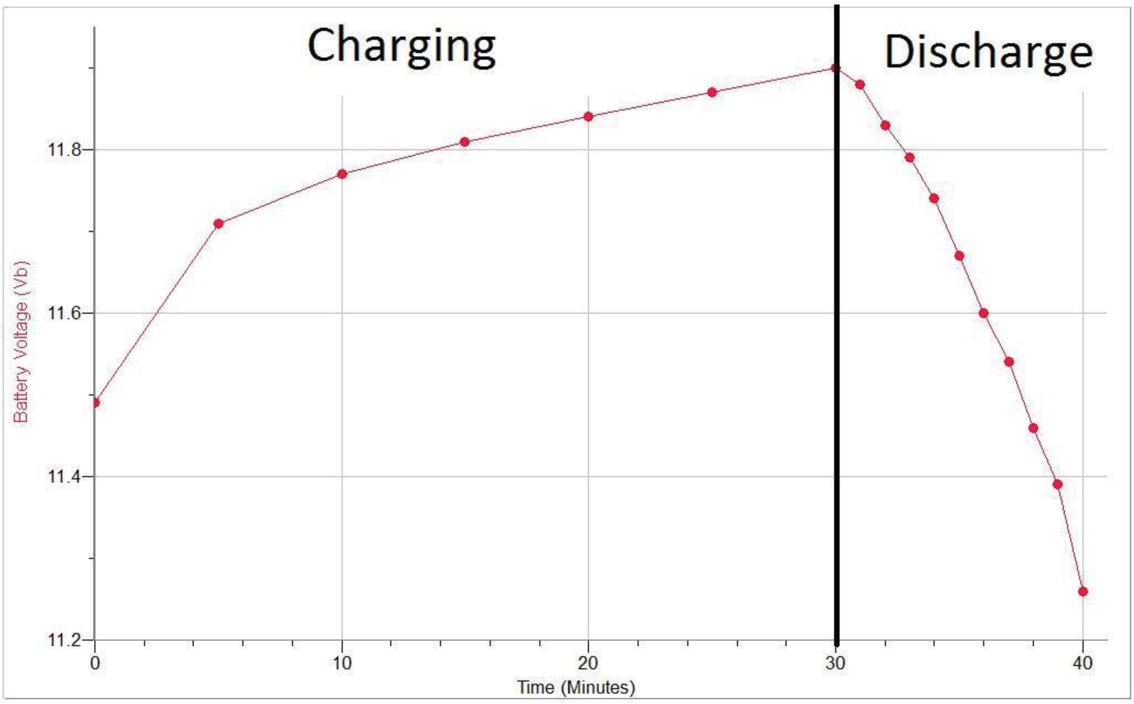


**Figure 5.38:** Charging and Discharging of Battery Voltage over time

Figure 5.38 is a graphical display of the battery being charged by the system for 30 minutes and then discharged for 10 minutes. Charging the battery for half hour powers a 50W bulb for around 8 minutes.

The energy generated by pedalling the bike at 70 RPM is enough energy to power a 50W bulb for about 8 minutes. Previous experiments have shown that increasing the speed that the bike is ridden at would increase the amount of power that could be generated. This implemented on a stand-alone machine will not produce a significant output. Therefore implementing this in a gym with more machines fitted with more than one electromagnet could increase the amount of energy created, thus making it a significant method of EH. Further research is required to test this.

# Chapter 6. RECOMMENDATIONS FOR FUTURE WORK AND CONCLUSION

## 6.1. Recommendation for future work

In the area of EH on a stationary bike using magnets there is scope for future work. Implementing the method used in the current project but with more than one machine or using more than one electromagnet is one area for further research.

The aim of not wanting to modify the bike put certain constraints on the methods that could be used for EH. Making certain inexpensive modifications to the bike to improve EH could also be an avenue for further research.

Future work could be conducted building on the understanding acquired from this research on this method of EH.

## 6.2. Conclusion

The aim of this project was to develop an EH system that could be fitted onto any stationary bike with a flywheel. The literature review conducted gave a clear understanding of EH and the ways in which it could be used in real world applications. Information and knowledge gained from the study of electromagnetic energy harvesting helped in the understanding of how EH could be applied in a gym setting.

A prototype model was developed for this project to ascertain the feasibility of using magnets to produce energy using a stationary bike. The experiments conducted showed that it is possible to harvest energy by placing magnets on a flywheel and spinning it through an electromagnet. The most effective way to harvest energy using magnets was having the magnets placed with their poles alternating and having the magnets close to the coil. A specially designed DC-DC boost converter for low power applications was used to boost the low voltages generated by the harvester. Developments of such converters in EH is important as most EH methods output small amounts of energy.

The aim of not needing to modify or change the existing stationary bike was made possible with this method of EH. However this created the need to make design adjustments to fit the system around the bike.

Six different factors were considered to examine their effect on the generated output. The experiments showed that an electromagnet made with high Permeability (μ) material would increase the power output. It was also found that having magnets with their poles alternating produced more flux in the circuit. However there is a limit to the number of magnets that can be placed on the flywheel at a given time, as having too many magnets on the disc would cause the power generated to drop drastically. The experiment also indicated that a stronger magnet doesn't necessarily increase the output. Finally it was found that as the air gap in the circuit increased the reluctance in the circuit also increased causing the output to drop. Reducing the air gap resulted in higher power output.

This method of EH implemented on a stand-alone machine will not produce a significant output. However implementing this in a gym with more machines or a machine fitted with more than one electromagnet could increase the amount of energy created, thus making it a significant method of EH. Further research is required to test this.

With the increasing need for alternative sources of energy the field of EH in its entirety is vast and has incredible scope for further research. The above recommendations focus on extending the research conducted in the current project. The rationale for these recommendations are that while this project has successfully found a method for EH it needs to be extended to capture more power to make it a significant source of EH. However in the meantime it could be used in conjunction with other methods of EH since it is a step in the direction of reducing the wastage of untapped energy.

# Chapter 7. REFERENCES


[1] Institute of Physics. (n.d.).*Energy Harvesting.* Retrieved from https://www.iop.org/resources/energy/index.html

[2] Yildiz, F. (2009). Potential Ambient Energy-Harvesting Sources and Techniques. *The Journal of Technology Studies, 35*(1), 40-48.

[3] Pimentel, D., Herz, M., Glickstein, M., Zimmerman, M., Allen, R., Becker, K., et al. (2002, December). Renewable Energy: Current and Potential Issues. *Bioscience* , pp. 1111-1120.

[4] Schneider SH, E. W. (2000). Adaptation: Sensitivity to natural variability, agent assumptions, and dynamic climate changes. *Climatic Change*, *45*: 203-221.

[5] Energy Harvesting Forum. (2012). *Energy Harvesting Electronic Solutions for Wireless Sensor Networks & Control Systems.* Retrieved from http://www.energyharvesting.net/

[6] Institute of Physics. (n.d.).*Energy Harvesting.* Retrieved from https://www.iop.org/resources/energy/index.html

[7] Harrop, P., & Das, R. (2012). Energy Harvesting and Storage for Electronic Devices 2012-2022: Forecasts, Technologies, Players. *IDTechEx*.

[8] Bickerstaffe, J. (2011). Energy Harvesting. *Sagentia*.

[9] Park, G. (2009). *Overview of Energy Harvesting Systems (for low-power systems).* Retrieved August 5, 2013, from LANL Institutes Office: http://institutes.lanl.gov/ei/_docs/Annual_Workshops/Overview_of_energy_harvesting_systemsLA-UR_8296.pdf

[10] Das, R. (2013). Energy harvesting comes to market. *Energy Harvesting journal.* Retrieved from - http://www.energyharvestingjournal.com/articles/energy-harvesting-comes-to-market-00005163.asp

[11] Priya, S., & Inman, D. J. (2009). *Energy Harvesting Technologies.* New York: Springer.

[12] Brush, L. ( 2007, October 8). Portable Devices: The Benefits from Energy Harvesting. *EDN Network.* Retrieved from http://www.edn.com/electronics-news/4314501/Portable-Devices-The-Benefits-From-Energy-Harvesting

[13] Ambio Systems. (2013). *Concept of energy harvesting*. Retrieved from http://www.ambiosystems.com/index.php/energy-harvesting.html

[14] Texas Instruments. (2013). *Energy Harvesting.* Retrieved from http://www.ti.com/solution/energy_harvesting

[15] Prakash, N. (2011). Green gyms, turning sweat into watts. *Huff Post Healthy Living.* Retrieved from http://www.thatsfit.com/2011/04/28/green-gyms-turning-sweat-into-watts/

[16] Gibson, T. (2011). These exercise machines you're your sweat into electricity. *IEEE Spectrum.* Retrieved from http://spectrum.ieee.org/green-tech/conservation/these-exercise-machines-turn-your-sweat-into-electricity

[17] Trigaux, R. (2009, May 19). Hudson Harr searches for renewable energy. *St.Petersburg Times.*

[18] Solomon, S. D., Qin, M., Manning, Z., Chen, M., Marquis, K. B., Averyt, M, and Miller, H. L. (2007). Climate change 2007, the physical science. *Fourth Assessment Report*. Retrieved from the Intergovernmental Panel on Climate Change website http://www.ipcc.ch/pdf/assessment-report/ar4/wg1/ar4_wg1_full_report.pdf

[19] Pickup, D. (2010). *Human Powered Gyms.* Retrieved from http://energythoughtspickup.blogspot.co.nz/2010/12/essay-on-human-powered-gym.html

[20] Runnymede Borough Council. (2010). Addlestone Leisure Centre Information. Retrieved from

http://www.runnymede.gov.uk/portal/site/alc/menuitem.0283cc2d9e7dbe9b1512d754af8ca028/

[21] MacKay, D. (2008). *Sustainable Energy – without the hot air.* Retrieved from www.withouthotair.com

[22] Human dynamo. (n.d.).*Technical Information.* Retrieved from http://www.humandynamo.com/technical_info.html

[23] CNET (n.d.) *HDTV Power consumption compared.* Retrieved from http://reviews.cnet.com/green-tech/tv-consumption-chart/

[24] Ho, E. (n.d.). *Gadget Power Usage.* Retrieved from http://www.edho.com/power/

[25] Bowes, P. (2009, 2 January). A gym powered by sweat and tears. *BBC News.* Retrieved from http://news.bbc.co.uk/1/hi/technology/7796215.stm

[26] Alternative Energy, (2009). *Human Powered Workout Gym Concept.* Retrieved from http://www.alternative-energy-news.info/human-powered-workout-gym-concept/

[27] Byrne, C. (2012). *A Brief History of Electromagnetism.* University of Massachusetts Lowell, USA. Retrieved from http://faculty.uml.edu/cbyrne/EMHIST.pdf

[28] Arnold, D. P. (2007). Review of microscale magnetic power generation. *IEEE Transactions on Magnetics, 43*(1), 3940-3951.

[29] Mitcheson, P.D., Green, T. C., Yeatman, E. M. and Holmes, A. S. (2004). Architectures for vibration-driven micropower generators. *Journal of Microelectromechanical Systems,13*( 3), 429-440.

[30] Mitcheson, P. D. (2005). *Analysis and optimisation of energy-harvesting micro-generator systems*.

[31] Williams, C. B. & Yates, R.B. (1995). *Analysis of a micro-electric generator for microsystems*. Stockholm, Sweden: Eurosensors IX.

[32] Williams, C. B. & Yates R. B. (1996) Analysis of a micro-electric generator for microsystems. *Sensors and Actuators A: Physical, 52,* 8-11.

[33] Williams, C. B., Shearwood, C., Harradine, M. A. , Mellor, P. H., Birch, T. S. & Yates, R. B. (2001) Development of an electromagnetic micro-generator. *IEEE Proc. - Circuit Devices Syst.,148*(6), 337-342.

[34] Amirtharajah, R & Chandrakasan, A. P. (1998). Self-powered signal processing using vibration based power generation. *IEEE Journal of Solid-state Circuits, 33*(5), 687-695.

[35] Zuo, L., Scully, B., Shestani, J. & Zhou, Y. (2010) Design and characterization of an electromagnetic energy harvester for vehicle suspensions. *Smart Materials and Structures, 19*.

[36] Prudell, J., Stoddard, M., Amon, E., Brekken, T. K. A., &. von Jouanne, A. A permanentmagnet tubular linear generator for ocean wave energy conversion. *IEEE Transactions on Industry Applications,* 46( 6), 2392-2400.

[37] Danielsson, O. (2003) *Design of a linear generator for wave energy plant*.

[38] Polinder, H., Damen, M. & Gardner, F. (2004) Linear PM generator system for wave energy conversion in the AWS. *IEEE Transactions on Energy Conversion, 19*( 3), 583-589.

[39] Seiko (n.d.) *Seiko Kinetic*. Retrieved from http://www.seikowatches.com/technology/kinetic/.

[40] Yeatman, E. M. (2008). Energy harvesting from motion using rotating and gyroscopic proof masses. Proc. IMechE, Part C: J. *Mechanical Engineering Science, 222*(1), 27-36.

[41] Trimble, A. Z., Lang, J, H., Pabon, J. & Slocum, A. (2010) A device for harvesting energy from rotational vibrations. *Journal of Mechanical Design, 132*.

[42] Spreemann, D., Folker, B., Mintenbeck, D. & Manoli, Y. (2005) *Novel non-resonant vibration transducer for energy harvesting.* Retrieved from PowerMEMS database.

[43] El-hami, M., Glynne-Jones, P., White, N. M., Hill, M., Beeby, S., James, E., Brown, A. D., & Ross, J. N. (2001). Design and fabrication of a new vibration-based electromechanical power generator. *Sensors and Actuators A: Physical 92*, 335-342.

[44] Yang, B., Lee, C., Xiang, W., Xie, J., He, J. H.,. Kotlanka, R. K., Low, S. P. &.Feng, H. (2009). Electromagnetic energy harvesting from vibrations of multiple frequencies. *Journal of Micromechanics and Microengineering,19*.

[45] Challa, V. R., Prasad, M. G., & Fisher, F. T. (2009). A coupled piezoelectric-electromagnetic energy harvesting technique for achieving increased power output through damping matching. *Smart Materials and Structures, vol. 18.*

[46] Yang, B., Lee, C., Kee, T. W. & Lim, S. P. (2010). Hybrid energy harvester based on piezoelectric and electromagnetic mechanisms. J. Micro/Nanolith. *MEMS MOEMS, 9*( 2).

[47] Eitel, J. (2013). *The differences in stationery bikes flywheel weights.* Retrieved from http://www.livestrong.com/article/372857-differences-flywheel-weights-stationary-bikes/

[48] Drak, M. & Dobrzanski, L.A. (2007). Corrosion of Nd-Fe-B Permanent Magnets. *Journal of Achievements in Materials and Manufacturing Engineering, 20*(239).

[49] Herbst, J. F. (1991). Neodymium-Iron-Boron Permanent Magnets. *Journal of Magnetism and Magnetic Materials* 100(57).

[50] *Shapes, Properties and Magnetization Directions of Magnets.* (n.d.). Retrieved from http://www.6pie.com/shapesofmagnets.php

[51] Moir, A. (2010). *The Chemistry, Economics and Politics of Neodymium.* Coursework Stanford University. Retrieved from http://large.stanford.edu/courses/2010/ph240/moir2/

[52] Levesque, T. (2007). *Human-Powered Gyms in Hong Kong*. Retrieved from http://www.inhabitat.com/2007/03/08/human-powered-gyms-in-hong-kong/

[53] Bowes, P. (2009, 2 January). A gym powered by sweat and tears. *BBC News.* Retrieved from http://news.bbc.co.uk/1/hi/technology/7796215.stm

[54] Field, S. Q. (n.d.) *Magnetism*. Retrieved from http://sci-toys.com/scitoys/scitoys/magnets/calculating/calculating.html

[55] K & J Magetics Inc. (n.d.). Magnetization Directions for Neodymium Magnets. Retrieved from http://www.kjmagnetics.com/magdir.asp

[56] Linear Technology. (n.d.). *400m A Step-up DC/DC Converter with Maximum Power Point Control and 250mV Start-Up*. Retrieved from http://cds.linear.com/docs/en/datasheet/3105fa.pdf

[57] Anderson, J. (2013). *Indoor Cycling Exercise Bikes – How to Choose and What to Buy*. Retrieved from http://janderson99.hubpages.com/hub/Indoor-Cycling-Exercise-Bikes-How-to-Choose-and-What-to-Buy

[58] AK Steel. (2007). Selection of Electrical Steels for Magnetic Cores. Retrieved from http://www.aksteel.com/pdf/markets_products/electrical/Mag_Cores_Data_Bulletin.pdf

[59] Chao, K. Y. (2006). Magnetic Circuit. In *Field Theory.* Retrieved from http://www.ee.up.ac.za/main/_media/en/undergrad/subjects/eir211/eir211_additional_reference_on_electromagnetism_-_ect1026_em.pdf

[60] Morris, M. J. (2003). *Permeability.* Retrieved from http://www.science-campus.com/physics/magnetism/basic_theory/permeability.html

[61] *Magnetic Circuits.* (n.d.) Retrieved from http://v5.books.elsevier.com/bookscat/samples/9780750685566/9780750685566.pdf

[62] Integrated Magnetics (2013). *Magnet Frequently Asked Questions.* Retrieved from http://www.intemag.com/faqs.html#equation.

[63] Chao, K. Y. (2006). Magnetic Circuit. In *Field Theory.* Retrieved from http://www.ee.up.ac.za/main/_media/en/undergrad/subjects/eir211/eir211_additional_reference_on_electromagnetism_-_ect1026_em.pdf

[64] Linear Technology. (n.d.). *High Voltage Step-up/Step-Down DC/DC Converter.* Retrieved from http://cds.linear.com/docs/en/datasheet/3433f.pdf

[65] EIIT. (n.d.). *Module 6: Magnetic Circuits & Core Losses.* [Web Course Slides]. Kharagpur, EIIT. Retrieved from http://www.nptel.iitm.ac.in/courses/Webcourse-contents/IIT%20Kharagpur/Basic%20Electrical%20Technology/pdf/L-21(TB)(ET)%20((EE)NPTEL).pdf

[66] *Magnetic Materials and Magnetic Circuit Analysis.* (n.d.). Retrieved from http://services.eng.uts.edu.au/cempe/subjects_JGZ/ems/ems_ch7_nt.pdf

[67] Jefferson Lab. (n.d.). *Science Education: Questions and Answers.* Retrieved from http://education.jlab.org/qa/electromagnet_is.html

# Appendix A

# 400mA Step-Up DC/DC Converter with Maximum Power Point Control and 250mV Start-Up

## FEATURES

- **Low Start-Up Voltage: 250mV**
- **Maximum Power Point Control**
- **Wide $V_{IN}$ Range: 225mV to 5V**
- **Auxiliary 6mA LDO Regulator**
- **Burst Mode® Operation: $I_Q$ = 24µA**
- Output Disconnect and Inrush Current Limiting
- $V_{IN} > V_{OUT}$ Operation
- Antiringing Control
- Soft Start
- Automatic Power Adjust
- Power Good Indicator
- 10-Lead 3mm × 3mm × 0.75mm DFN and 12-Lead MSOP Packages

## APPLICATIONS

- Solar Powered Battery/Supercapacitor Chargers
- Energy Harvesting
- Remote Industrial Sensors
- Low Power Wireless Transmitters
- Cell Phone, MP3, PMP and GPS Accessory Chargers

## DESCRIPTION

The LTC®3105 is a high efficiency step-up DC/DC converter that can operate from input voltages as low as 225mV. A 250mV start-up capability and integrated maximum power point controller (MPPC) enable operation directly from low voltage, high impedance alternative power sources such as photovoltaic cells, TEGs (thermoelectric generators) and fuel cells. A user programmable MPPC set point maximizes the energy that can be extracted from any power source. Burst Mode operation, with a proprietary self adjusting peak current, optimizes converter efficiency and output voltage ripple over all operating conditions.

The AUX powered 6mA LDO provides a regulated rail for external microcontrollers and sensors while the main output is charging. In shutdown, $I_Q$ is reduced to 10µA and integrated thermal shutdown offers protection from overtemperature faults. The LTC3105 is offered in 10-lead 3mm × 3mm × 0.75mm DFN and 12-lead MSOP packages.



## TYPICAL APPLICATION

**Single Photovoltaic Cell Li-Ion Trickle Charger**

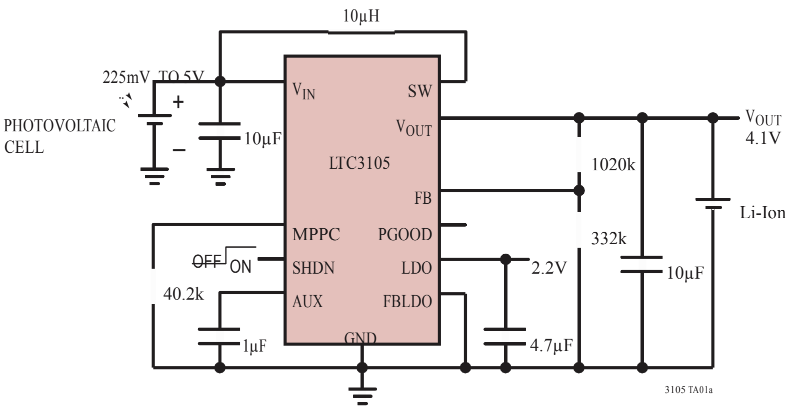


**Output Current vs Input Voltage**

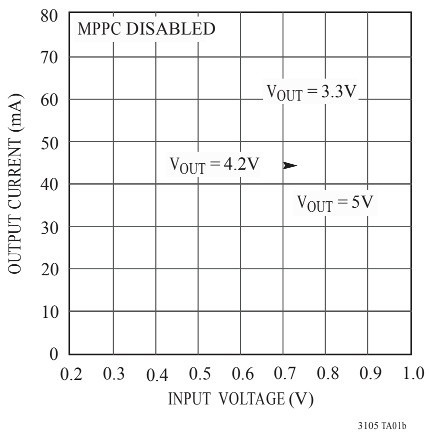

## ABSOLUTE MAXIMUM RATINGS (Note 1)

SW Voltage
 DC .......................................................... –0.3V to 6V
 Pulsed (<100ns) .......................................... –1V to 7V
Voltage, All Other Pins ................................ –0.3V to 6V
Operating Junction Temperature
Range (Note 2) ........................................ –40°C to 85°C

Maximum Junction Temperature (Note 4) ............ 125°C
Storage Temperature ............................ –65°C to 150°C
Lead Temperature (Soldering, 10 sec.)
 MS Package .................................................... 300°C

## PIN CONFIGURATION

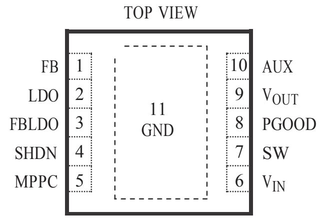


DD PACKAGE
10-LEAD (3mm × 3mm) PLASTIC DFN
$T_{JMAX}$ = 125°C, $\theta_{JA}$ = 43°C/W, $\theta_{JC}$ = 3°C/W
EXPOSED PAD (PIN 11) IS GND, MUST BE SOLDERED TO PCB

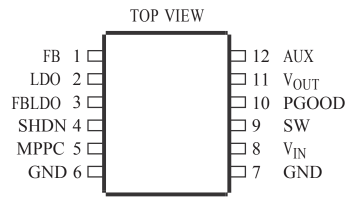


MS PACKAGE
12-LEAD PLASTIC MSOP
$T_{JMAX}$ = 125°C, $\theta_{JA}$ = 130°C/W, $\theta_{JC}$ = 21°C/W

## ORDER INFORMATION

| LEAD FREE FINISH | TAPE AND REEL | PART MARKING | PACKAGE DESCRIPTION | TEMPERATURE RANGE |
|---|---|---|---|---|
| LTC3105EDD#PBF | LTC3105EDD#TRPBF | LFQC | 10-Lead (3mm × 3mm) Plastic DFN | –40°C to 85°C |
| LTC3105EMS#PBF | LTC3105EMS#TRPBF | 3105 | 12-Lead Plastic MSOP | –40°C to 85°C |

Consult LTC Marketing for parts specified with wider operating temperature ranges.
Consult LTC Marketing for information on non-standard lead based finish parts.
For more information on lead free part marking, go to: http://www.linear.com/leadfree/
For more information on tape and reel specifications, go to: http://www.linear.com/tapeandreel/

## ELECTRICAL CHARACTERISTICS

**The 1 denotes the specifications which apply over the full operating junction temperature range, otherwise specifications are at $T_A$ = 25°C (Note 2). $V_{AUX}$ = $V_{OUT}$ = 3.3V, $V_{LDO}$ = 2.2V, $V_{IN}$ = 0.6V, unless otherwise noted.**

| PARAMETER | CONDITIONS | | MIN | TYP | MAX | UNITS |
|---|---|---|---|---|---|---|
| **Step-Up Converter** | | | | | | |
| Input Operating Voltage | | 1 | 0.225 | | 5 | V |
| Input Start-Up Voltage | (Note 5)<br>$T_J$ = 0°C to 85°C (Note 5) | 1 | | 0.25 | 0.4<br>0.36 | V<br>V |
| Output Voltage Adjust Range | | 1 | 1.5 | | 5.25 | V |
| Feedback Voltage (FB Pin) | | 1 | 0.984 | 1.004 | 1.024 | V |
| $V_{OUT}$ $I_Q$ in Operation | $V_{FB}$ = 1.10V | | | 24 | | µA |
| $V_{OUT}$ $I_Q$ in Shutdown | SHDN = 0V | | | 10 | | µA |
| MPPC Pin Output Current | $V_{MPPC}$ = 0.6V | | 9.72 | 10 | 10.28 | µA |
| SHDN Input Logic High Voltage | | 1 | 1.1 | | | V |
| SHDN Input Logic Low Voltage | | 1 | | | 0.3 | V |
| N-Channel SW Pin Leakage Current | $V_{IN}$ = $V_{SW}$ = 5V, $V_{SHDN}$ = 0V | | | 1 | 10 | µA |
| P-Channel SW Pin Leakage Current | $V_{IN}$ = $V_{SW}$ = 0V, $V_{OUT}$ = $V_{AUX}$ = 5.25V | | | 1 | 10 | µA |
| N-Channel On-Resistance: SW to GND | | | | 0.5 | | Ω |
| P-Channel On-Resistance: SW to $V_{OUT}$ | | | | 0.5 | | Ω |
| Peak Current Limit | $V_{FB}$ = 0.90V, $V_{MPPC}$ = 0.4V (Note 3) | | 0.4 | 0.5 | | A |
| Valley Current Limit | $V_{FB}$ = 0.90V, $V_{MPPC}$ = 0.4V (Note 3) | | 0.275 | 0.35 | | A |
| PGOOD Threshold (% of Feedback Voltage) | $V_{OUT}$ Falling | | 85 | 90 | 95 | % |
| **LDO Regulator** | | | | | | |
| LDO Output Adjust Range | External Feedback Network, $V_{AUX}$ > $V_{LDO}$ | 1 | 1.4 | | 5 | V |
| LDO Output Voltage | $V_{FBLDO}$ = 0V | 1 | 2.148 | 2.2 | 2.236 | V |
| Feedback Voltage (FBLDO Pin) | External Feedback Network | 1 | 0.984 | 1.004 | 1.024 | V |
| Load Regulation | $I_{LDO}$ = 1mA to 6mA | | | 0.40 | | % |
| Line Regulation | $V_{AUX}$ = 2.5V to 5V | | | 0.15 | | % |
| Dropout Voltage | $I_{LDO}$ = 6mA, $V_{OUT}$ = $V_{AUX}$ = 2.2V | | | 105 | | mV |
| LDO Current Limit | $V_{LDO}$ 0.5V Below Regulation Voltage | 1 | 6 | 12 | | mA |
| LDO Reverse-Blocking Leakage Current | $V_{IN}$ = $V_{AUX}$ = $V_{OUT}$ = 0V, $V_{SHDN}$ = 0V | | | 1 | | µA |

**Note 1:** Stresses beyond those listed under Absolute Maximum Ratings may cause permanent damage to the device. Exposure to any Absolute Maximum Rating condition for extended periods may affect device reliability and lifetime.

**Note 2:** The LTC3105 is tested under pulsed load conditions such that $T_J$ H $T_A$. The LTC3105E is guaranteed to meet specifications from 0°C to 85°C junction temperature. Specifications over the –40°C to 85°C operating junction temperature range are assured by design, characterization and correlation with statistical process controls. Note that the maximum ambient temperature consistent with these specifications is determined by specific operating conditions in conjunction with board layout, the rated package thermal impedance and other environmental factors.

**Note 3:** Current measurements are performed when the LTC3105 is not switching. The current limit values measured in operation will be somewhat higher due to the propagation delay of the comparators.

**Note 4:** This IC includes over temperature protection that is intended to protect the device during momentary overload conditions. Junction temperature will exceed 125°C when overtemperature protection is active. Continuous operation above the specified maximum operating junction temperature may impair device reliability.

**Note 5:** The LTC3105 has been optimized for use with high impedance power sources such as photovoltaic cells and thermoelectric generators. The input start-up voltage is measured using an input voltage source with a series resistance of approximately 200mΩ and MPPC enabled. Use of the LTC3105 with lower resistance voltage sources or with MPPC disabled may result in a higher input start-up voltage.

## TYPICAL PERFORMANCE CHARACTERISTICS $T_A$ = 25°C, $V_{AUX}$ = $V_{OUT}$ = 3.3V, $V_{LDO}$ = 2.2V, $V_{IN}$ = 0.6V, unless otherwise noted.

**Minimum Input Start-Up Voltage vs Temperature**

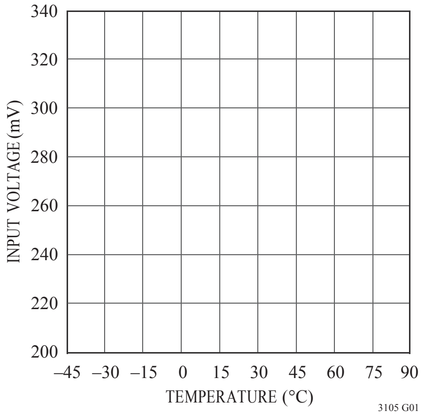


**Shutdown Thresholds vs Input Voltage**

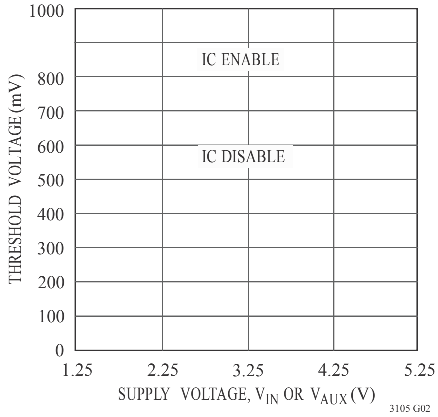


**IC Enable Delay vs Input Voltage**

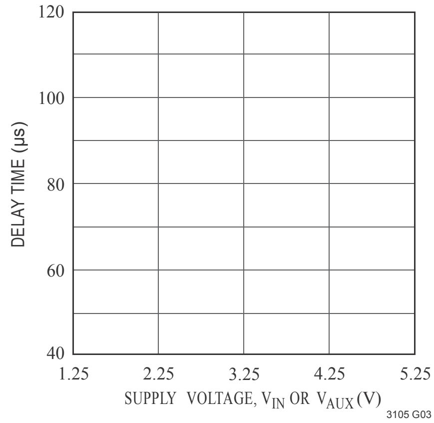


**MPPC Current Variation vs Temperature**

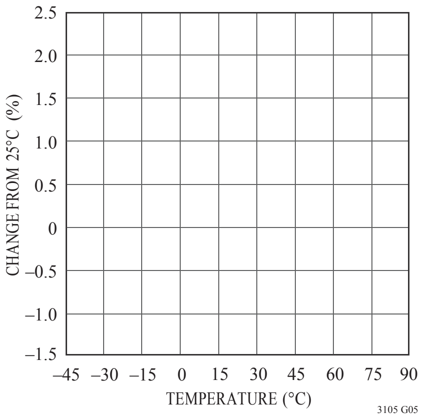


**LDO Soft-Start Duration vs LDO Load**

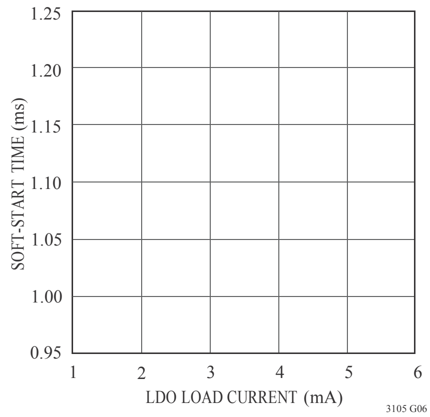


**$V_{OUT}$ $I_Q$ vs Temperature During Shutdown**

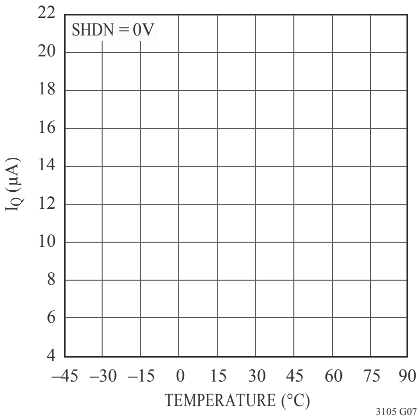


**$V_{IN}$ for Synchronous Operation**

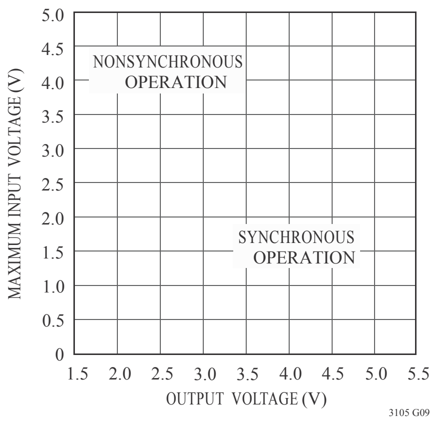

## TYPICAL PERFORMANCE CHARACTERISTICS $T_A$ = 25°C, $V_{AUX}$ = $V_{OUT}$ = 3.3V, $V_{LDO}$ = 2.2V, $V_{IN}$ = 0.6V, unless otherwise noted.

**Exiting MPPC Control on Input Voltage Step**

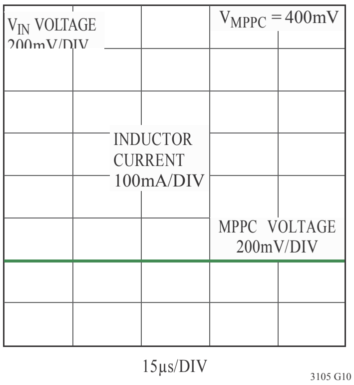


**$I_{PEAK}$ and $I_{VALLEY}$ Current Limit Change vs Temperature**

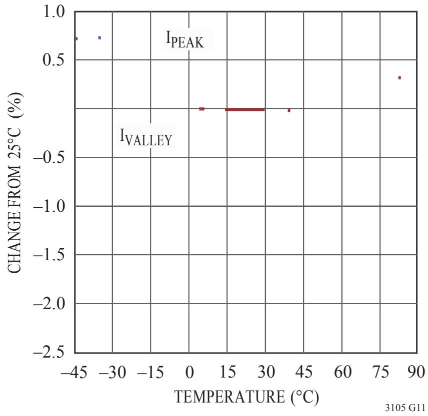


**Efficiency vs $V_{IN}$**

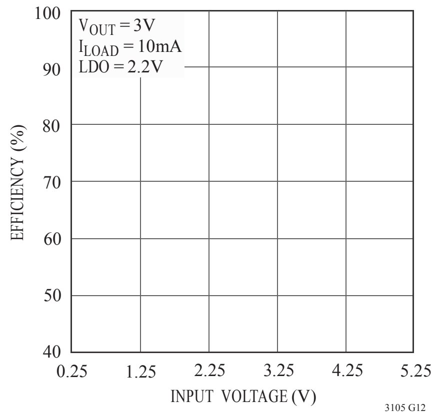


**Input and Output Burst Ripple**

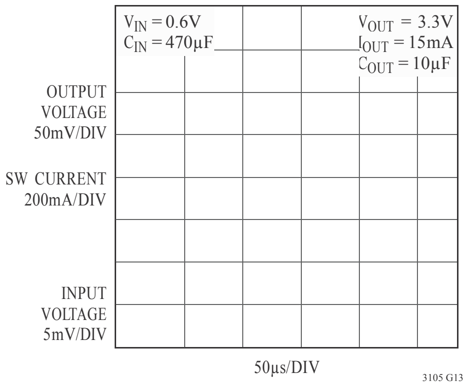


**Efficiency vs Output Current and Power Loss, $V_{OUT}$ = 3.3V**

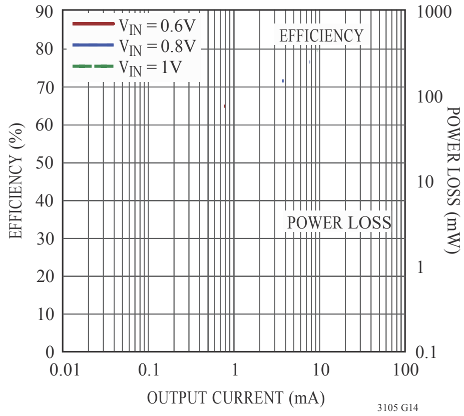


**Efficiency vs Output Current and Power Loss, $V_{OUT}$ = 5V**

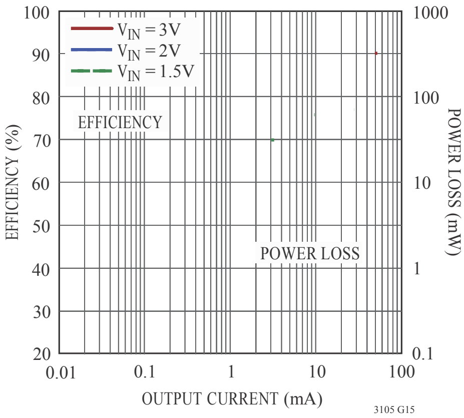


**No-Load Input Current vs Input Voltage**

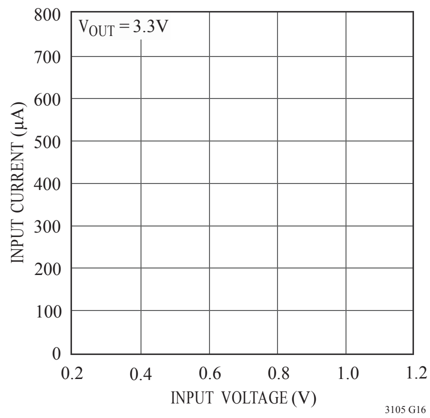

## PIN FUNCTIONS (DFN/MSOP)

**FB (Pin 1/Pin 1):** Step-Up Converter Feedback Input. Connect the $V_{OUT}$ resistor divider tap to this input. The output voltage can be adjusted between 1.5V and 5.25V.

**LDO (Pin 2/Pin 2):** LDO Regulator Output. Connect a 4.7µF or larger capacitor between LDO and GND.

**FBLDO (Pin 3/Pin 3):** LDO Feedback Input. Connect the LDO resistive divider tab to this input. Alternatively, connecting FBLDO directly to GND will configure the LDO output voltage to be internally set at 2.2V (nominal).

**SHDN (Pin 4/Pin 4):** Logic Controlled Shutdown Input. With SHDN open, the converter is enabled by an internal 2MΩ pull-up resistor. The SHDN pin should be driven with an open-drain or open-collector pull-down and floated until the converter has entered normal operation. Excessive loading on this pin may cause a failure to complete start-up.

SHDN = Low: IC Disabled

SHDN = High: IC Enabled

**MPPC (Pin 5/Pin 5):** Set Point Input for Maximum Power Point Control. Connect a resistor from MPPC to GND to program the activation point for the MPPC loop. To disable the MPPC circuit, connect MPPC directly to GND.

**$V_{IN}$ (Pin 6/Pin 8):** Input Supply. Connect a decoupling capacitor between this pin and GND. The PCB trace length from the $V_{IN}$ pin to the decoupling capacitor should be as short and wide as possible. When used with high impedance sources such as photovoltaic cells, this pin should have a 10µF or larger decoupling capacitor.

**GND (Exposed Pad Pin 11/Pins 6, 7) :** Small Signal and Power Ground for the IC. The GND connections should be soldered to the PCB ground using the lowest impedance path possible.

**SW (Pin 7/Pin 9):** Switch Pin. Connect an inductor between SW and $V_{IN}$. PCB trace lengths should be as short as possible to reduce EMI. While the converter is sleeping or is in shutdown, the internal antiringing switch connects the SW pin to the $V_{IN}$ pin in order to minimize EMI.

**PGOOD (Pin 8/Pin 10):** Power Good Indicator. This is an open-drain output. The pull-down is disabled when $V_{OUT}$ has achieved the voltage defined by the feedback divider on the FB pin. The pull-down is also disabled while the IC is in shutdown or start-up mode.

**$V_{OUT}$ (Pin 9/Pin 11):** Step-Up Converter Output. This is the drain connection of the main output internal synchronous rectifier. A 10µF or larger capacitor must be connected between this pin and GND. The PCB trace length from the $V_{OUT}$ pin to the output filter capacitor should be as short and wide as possible.

**AUX (Pin 10/Pin 12):** Auxiliary Voltage. Connect a 1µF capacitor between this pin and GND. This pin is used by the start-up circuitry to generate a voltage rail to power internal circuitry until the main output reaches regulation. AUX and $V_{OUT}$ are internally connected together once $V_{OUT}$ exceeds $V_{AUX}$.

## BLOCK DIAGRAM (Pin Numbers for DFN Package Only)

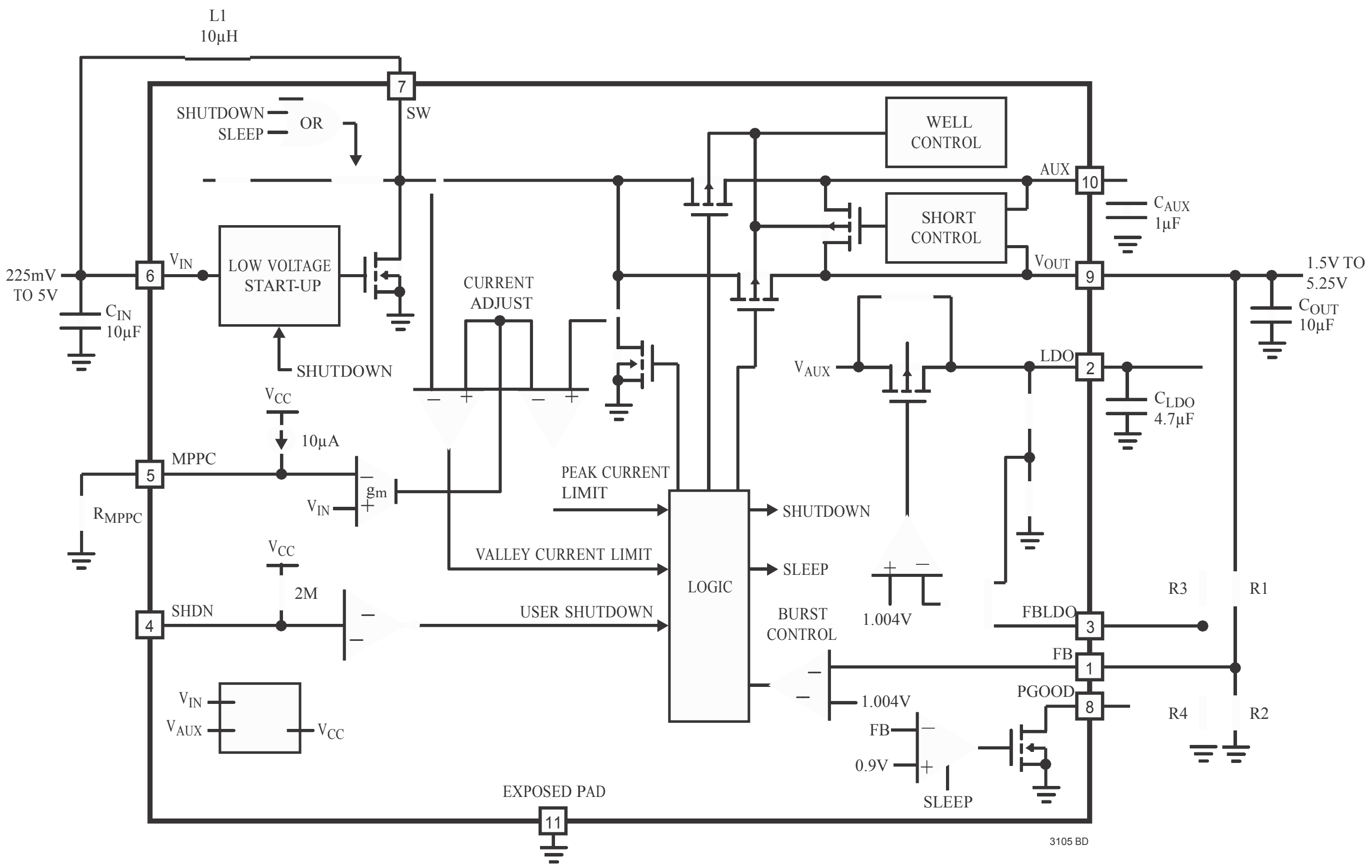

# OPERATION

### Introduction

The LTC3105 is a unique, high performance, synchronous boost converter that incorporates maximum power point control, 250mV start-up capability and an integrated LDO regulator. This part operates over a very wide range of input voltages from 225mV to 5V. Its Burst Mode architecture and low 24µA quiescent current optimize efficiency in low power applications.

An integrated maximum power point controller allows for operation directly from high impedance sources such as photovoltaic cells by preventing the input power source voltage from collapsing below the user programmable MPPC threshold. Peak current limits are automatically adjusted with proprietary techniques to maintain operation at levels that maximize power extraction from the source.

The 250mV start-up voltage and 225mV minimum operating voltage enable direct operation from a single photovoltaic cell and other very low voltage, high series impedance power sources such as TEGs and fuel cells.

Synchronous rectification provides high efficiency operation while eliminating the need for external Schottky diodes. The LTC3105 provides output disconnect which prevents large inrush currents during start-up. This is particularly important for high internal resistance power sources like photovoltaic cells and thermoelectric generators which can become overloaded if inrush current is not limited during start-up of the power converter. In addition, output disconnect isolates $V_{OUT}$ from $V_{IN}$ while in shutdown.

### $V_{IN} > V_{OUT}$ Operation

The LTC3105 includes the ability to seamlessly maintain regulation if $V_{IN}$ becomes equal to or greater than $V_{OUT}$. With $V_{IN}$ greater than or equal to $V_{OUT}$, the synchro- nous rectifiers are disabled which may result in reduced efficiency.

### Shutdown Control

The SHDN pin is an active low input that places the IC into low current shutdown mode. This pin incorporates an internal 2MΩ pull-up resistor which enables the converter if the SHDN pin is not controlled by an external circuit. The SHDN pin should be allowed to float while the part is in start-up mode. Once in normal operation, the SHDN pin may be controlled using an open-drain or open-collector pull-down. Other external loads on this pin should be avoided, as they may result in the part failing to reach regulation. In shutdown, the internal switch connecting AUX and $V_{OUT}$ is enabled.

When the SHDN pin is released, the LTC3105 is enabled and begins switching after a short delay. When either $V_{IN}$ or $V_{AUX}$ is above 1.4V, this delay will typically range between 20µs and 100µs. Refer to the Typical Performance Characteristics section for more details.

### Start-Up Mode Operation

The LTC3105 provides the capability to start with voltages as low as 250mV. During start-up the AUX output initially is charged with the synchronous rectifiers disabled. Once $V_{AUX}$ has reached approximately 1.4V, the converter leaves start-up mode and enters normal operation. Maximum power point control is not enabled during start-up, however, the currents are internally limited to sufficiently low levels to allow start-up from weak input sources.

While the converter is in start-up mode, the internal switch between AUX and $V_{OUT}$ remains disabled and the LDO is disabled. Refer to Figure 1 for an example of a typical start-up sequence.

The LTC3105 is optimized for use with high impedance power sources such as photovoltaic cells. For operation from very low impedance, low input voltage sources, it may be necessary to add several hundred milliohms of series input resistance to allow for proper low voltage start-up.

### Normal Operation

When either $V_{IN}$ or $V_{AUX}$ is greater than 1.4V typical, the converter will enter normal operation.

The converter continues charging the AUX output until the LDO output enters regulation. Once the LDO output is in regulation, the converter begins charging the $V_{OUT}$ pin. $V_{AUX}$ is maintained at a level sufficient to ensure the LDO remains in regulation. If $V_{AUX}$ becomes higher than required to maintain LDO regulation, charge is transferred from the AUX output to the $V_{OUT}$ output. If $V_{AUX}$ falls too low, current is redirected to the AUX output instead of being used to charge the $V_{OUT}$ output. Once $V_{OUT}$ rises

# OPERATION

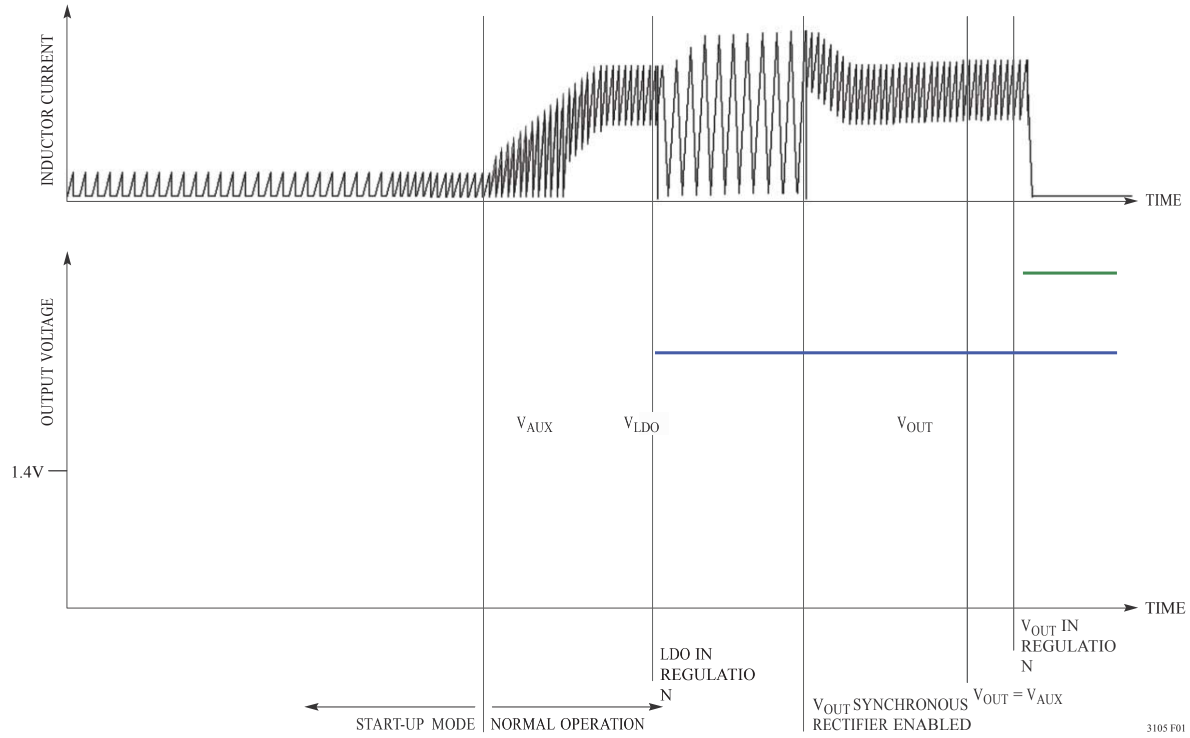


**Figure 1. Typical Converter Start-Up Sequence**

above $V_{AUX}$, an internal switch is enabled to connect the two outputs together.

If $V_{IN}$ is greater than the voltage on the driven output ($V_{OUT}$ or $V_{AUX}$), or the driven output is less than 1.2V (typical), the synchronous rectifiers are disabled. With the synchronous rectifiers disabled, the converter operates in critical conduction mode. In this mode, the N-channel MOSFET between SW and GND is enabled and remains on until the inductor current reaches the peak current limit. It is then disabled and the inductor current discharges completely before the cycle is repeated.

When the output voltage is greater than the input voltage and greater than 1.2V, the synchronous rectifier is enabled. In this mode, the N-channel MOSFET between SW and GND is enabled until the inductor current reaches the peak current limit. Once current limit is reached, the N-channel MOSFET turns off and the P-channel MOSFET between SW and the driven output is enabled. This switch remains on until the inductor current drops below the valley current limit and the cycle is repeated.

When $V_{OUT}$ reaches the regulation point, the N- and P-channel MOSFETs connected to the SW pin are disabled and the converter enters sleep.

### Auxiliary LDO

The integrated LDO provides a regulated 6mA rail to power microcontrollers and external sensors. When the input voltage is above the minimum of 225mV, the LDO is powered from the AUX output allowing the LDO to attain regulation while the main output is still charging. The LDO has a 12mA current limit and an internal 1ms soft-start to eliminate inrush currents. The LDO output voltage is set by the FBLDO pin. If a resistor divider is connected to this pin, the ratio of the resistors determines the LDO output voltage. If the FBLDO pin is connected directly to GND, the LDO will use a 2MΩ internal divider network to program a 2.2V nominal output voltage. The LDO should be programmed for an output voltage less than the programmed $V_{OUT}$.

## OPERATION

When the converter is placed in shutdown mode, the LDO is forced into reverse-blocking mode with reverse current limited to under 1µA. After the shutdown event has ended, the LDO remains in reverse-blocking mode until $V_{AUX}$ has risen above the LDO voltage.

### MPPC Operation

The maximum power point control circuit allows the user to set the optimal input voltage operating point for a given power source. The MPPC circuit dynamically regulates the average inductor current to prevent the input voltage from dropping below the MPPC threshold. When $V_{IN}$ is greater than the MPPC voltage, the inductor current is increased until $V_{IN}$ is pulled down to the MPPC set point. If $V_{IN}$ is less than the MPPC voltage, the inductor current is reduced until $V_{IN}$ rises to the MPPC set point.

### Automatic Power Adjust

The LTC3105 incorporates a feature that maximizes efficiency at light load while providing increased power capability at heavy load by adjusting the peak and valley of the inductor current as a function of load. Lowering the peak inductor current to 100mA at light load optimizes efficiency by reducing conduction losses. As the load increases, the peak inductor current is automatically increased to a maximum of 500mA. At intermediate loads, the peak inductor current can vary between 100mA to 500mA. This function is overridden by the MPPC function and will only be observed when the power source can deliver more power than the load requires.

### PGOOD Operation

The power good output is used to indicate that $V_{OUT}$ is in regulation. PGOOD is an open-drain output, and is disabled in shutdown. PGOOD will indicate that power is good at the beginning of the first sleep event after the output voltage has risen above 90% of its regulation value. PGOOD remains asserted until $V_{OUT}$ drops below 90% of its regulation value at which point PGOOD will pull low.

## APPLICATIONS INFORMATION

### Component Selection

Low DCR power inductors with values between 4.7µH and 30µH are suitable for use with the LTC3105. For most applications, a 10µH inductor is recommended. In applications where the input voltage is very low, a larger value inductor can provide higher efficiency and a lower start-up voltage. In applications where the input voltage is relatively high ($V_{IN}$ > 0.8V), smaller inductors may be used to provide a smaller overall footprint. In all cases, the inductor must have low DCR and sufficient saturation current rating. If the DC resistance of the inductor is too high, efficiency will be reduced and the minimum operating voltage will increase.

Input capacitor selection is highly important in low voltage, high source resistance systems. For general applications, a 10µF ceramic capacitor is recommended between $V_{IN}$ and GND. For high impedance sources, the input capacitor should be large enough to allow the converter to complete start-up mode using the energy stored in the input ca- pacitor. When using bulk input capacitors that have high ESR, a small valued parallel ceramic capacitor should be placed between $V_{IN}$ and GND as close to the converter pins as possible.

A 1µF ceramic capacitor should be connected between AUX and GND. Larger capacitors should be avoided to minimize start-up time. A low ESR output capacitor should be connected between $V_{OUT}$ and GND. The main output capacitor should be 10µF or larger. The main output can also be used to charge energy storage devices including tantalum capacitors, supercapacitors and batteries. When using output bulk storage devices with high ESR, a small valued ceramic capacitor should be placed in parallel and located as close to the converter pins as possible.

# APPLICATIONS INFORMATION

### Step-Up Converter Feedback Configuration

A resistor divider connected between the $V_{OUT}$ and FB pins programs the step-up converter output voltage, as shown in Figure 2. An optional 22pF feedforward capacitor, $C_{FF1}$, can be used to reduce output ripple and improve load transient response. The equation for $V_{OUT}$ is:

$$V_{OUT} = 1.004V \bullet \left(\frac{R1}{R2} + 1\right)$$

### LDO Regulator Feedback Configuration

Two methods can be used to program the LDO output voltage, as shown in Figure 3. A resistor divider connected between the LDO and FBLDO pins can be used to program the LDO output voltage. The equation for the LDO output voltage is:

$$V_{LDO} = 1.004V \bullet \left(\frac{R3}{R4} + 1\right)$$

Alternatively, the FBLDO pin can be connected directly to GND. In this configuration, the LDO is internally set to a nominal 2.2V output.

### MPPC Threshold Configuration

The MPPC circuit controls the inductor current to maintain $V_{IN}$ at the voltage on the MPPC pin. The MPPC pin voltage is set by connecting a resistor between the MPPC pin and GND, as shown in Figure 4. The MPPC voltage is determined by the equation:

$$V_{MPPC} = 10\mu A \bullet R_{MPPC}$$

In photovoltaic cell applications, a diode can be used to set the MPPC threshold so that it tracks the cell voltage over temperature, as shown in Figure 5. The diode should be thermally coupled to the photovoltaic cell to ensure proper tracking. A resistor placed in series with the diode can be used to adjust the DC set point to better match the maximum power point of a particular source if the selected diode forward voltage is too low. If the diode is located far from the converter inputs, a capacitor may be required to filter noise that may couple onto the MPPC pin, as shown in Figure 5. This method can be extended to stacked cell sources through use of multiple series connected diodes.

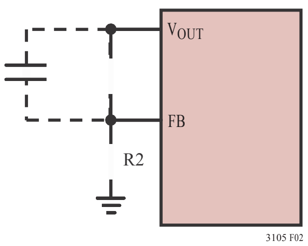


Figure 2. FB Configuration

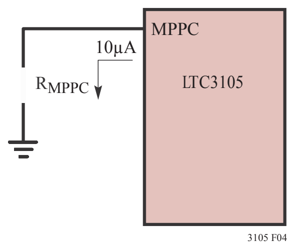


Figure 4. MPPC Configuration

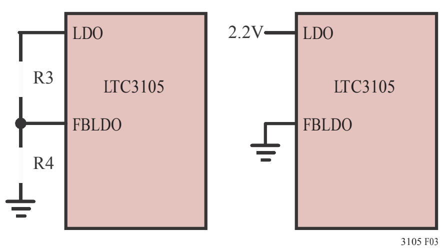


Figure 3. FBLDO Configuration

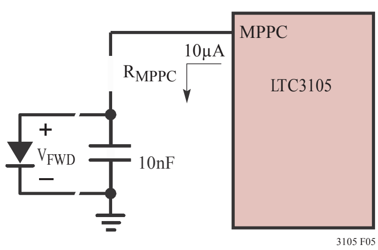


Figure 5. MPPC Configuration with Temperature Adjustment

# APPLICATIONS INFORMATION

### Industrial Current Loops

The low 250mV start-up and low voltage operation of the LTC3105 allow it to be supplied by power from a diode placed in an industrial sensor current loop, as shown in Figure 6. In this application, a large input capacitor is required due to the very low available supply current (less than 4mA). The loop diode should be selected for a minimum forward drop of 300mV. The MPPC pin voltage should be set for a value approximately 50mV below the minimum diode forward voltage.

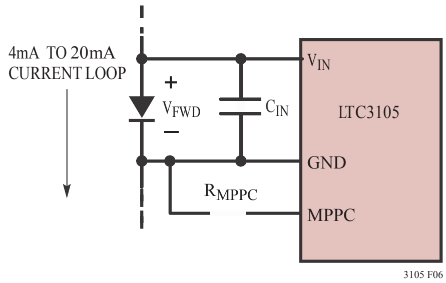


**Figure 6. Current Loop Power Tap**

# TYPICAL APPLICATIONS

**3.3V from a Single-Cell Photovoltaic Source with Temperature Tracking**

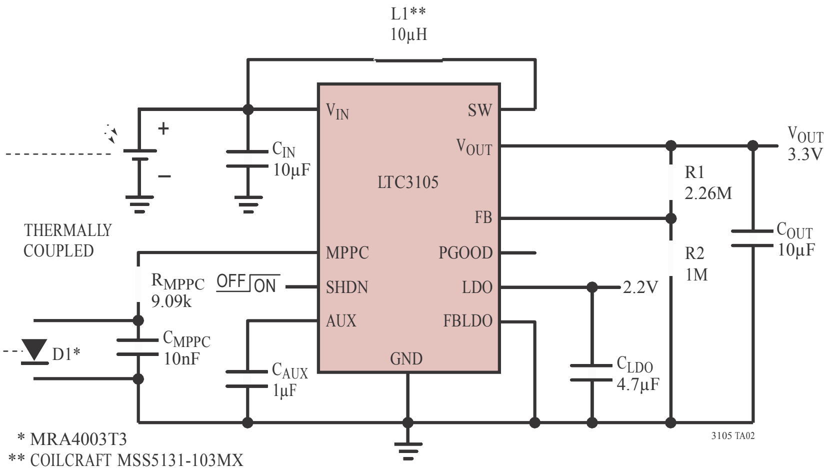


* MRA4003T3
** COILCRAFT MSS5131-103MX

**$V_{MPPC}$ vs Temperature**

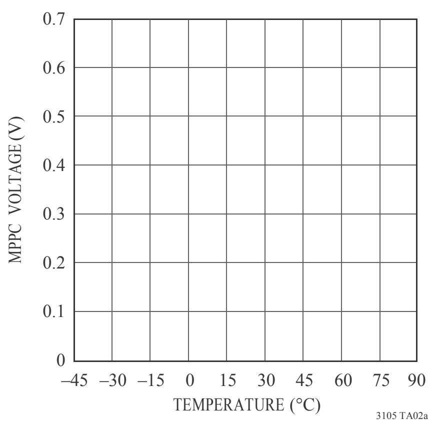


**MPPC Response to Input Source Current Step**

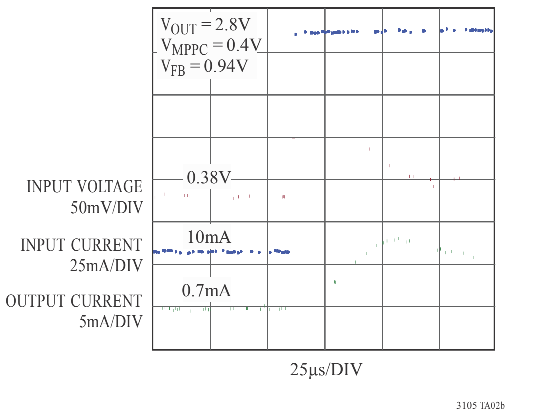

# TYPICAL APPLICATIONS

**3.3V from Multiple Stacked-Cell Photovoltaic with Source Temperature Tracking**

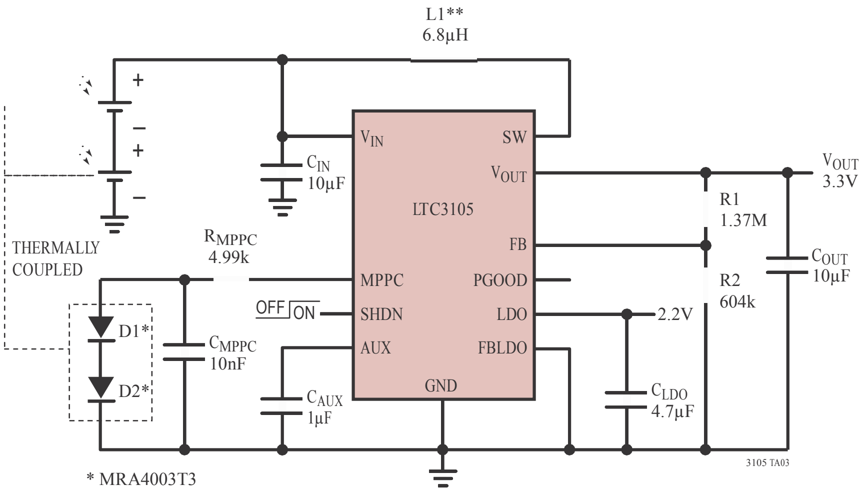


* MRA4003T3
** PANASONIC ELL-VEG6R8N

**Thermoelectric Generator to 2.4V Super Capacitor Charger**

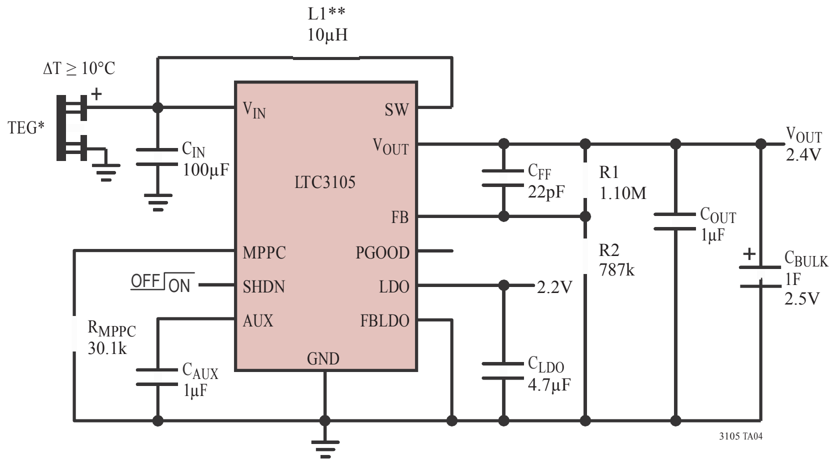


* MICROPELT MPG-D751
** COILCRAFT MSS5131-103MX

# TYPICAL APPLICATIONS

**Industrial Sensor 4mA to 20mA Current Loop Power Tap**

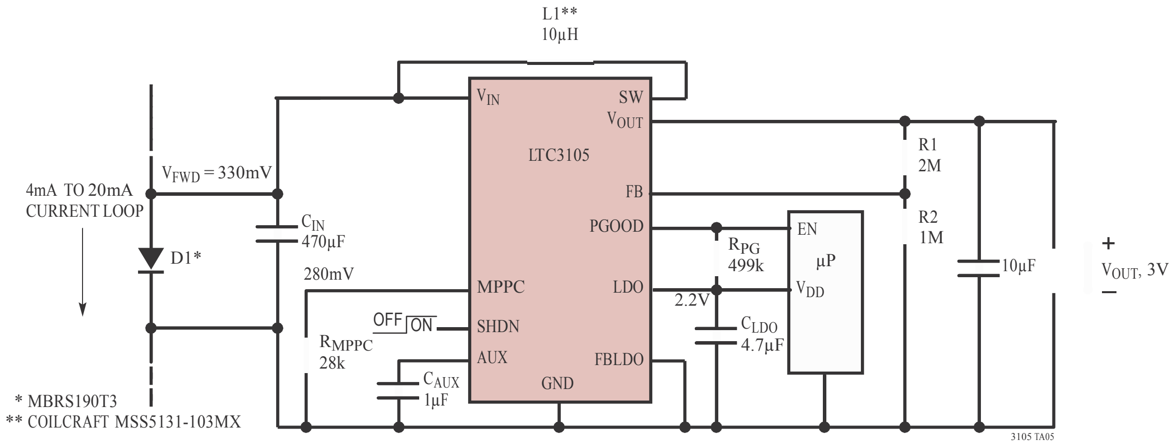


**Transient Response to Load Pulse with 4mA Loop Current**

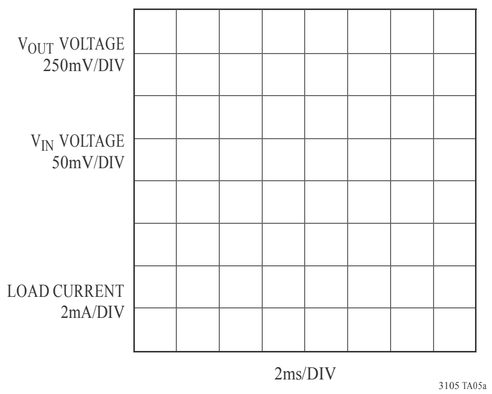


**Start-Up $V_{IN}$, $V_{OUT}$, $V_{LDO}$**

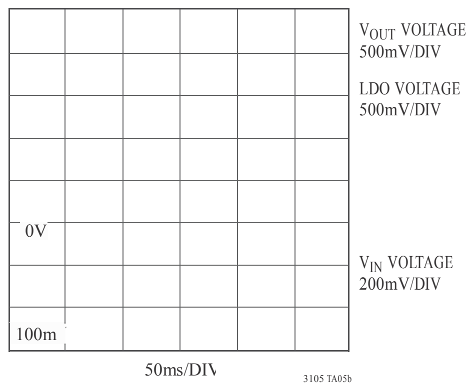


**Single-Cell Photovoltaic NiMH Trickle Charger**

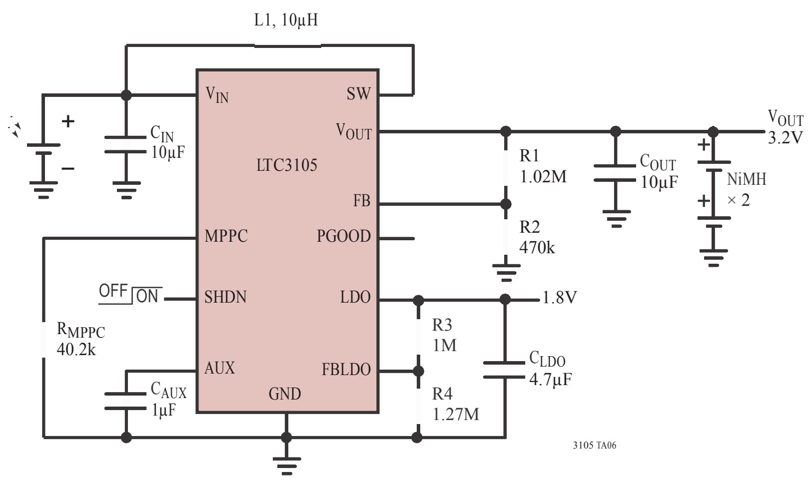

# PACKAGE DESCRIPTION

**DD Package**
**10-Lead Plastic DFN (3mm × 3mm)**
(Reference LTC DWG # 05-08-1699 Rev C)

**DD Package**
**10-Lead Plastic DFN (3mm × 3mm)**
(Reference LTC DWG # 05-08-1699 Rev C)

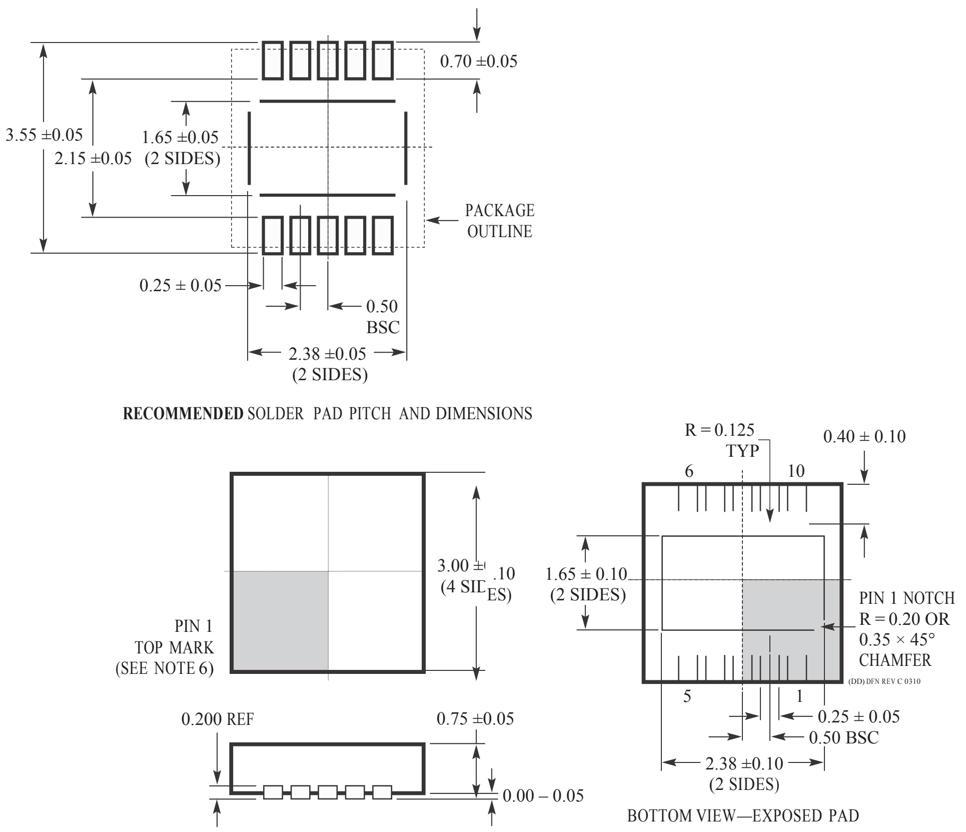


NOTE:
1. DRAWING TO BE MADE A JEDEC PACKAGE OUTLINE M0-229 VARIATION OF (WEED-2). CHECK THE LTC WEBSITE DATA SHEET FOR CURRENT STATUS OF VARIATION ASSIGNMENT
2. DRAWING NOT TO SCALE
3. ALL DIMENSIONS ARE IN MILLIMETERS
4. DIMENSIONS OF EXPOSED PAD ON BOTTOM OF PACKAGE DO NOT INCLUDE MOLD FLASH. MOLD FLASH, IF PRESENT, SHALL NOT EXCEED 0.15mm ON ANY SIDE
5. EXPOSED PAD SHALL BE SOLDER PLATED
6. SHADED AREA IS ONLY A REFERENCE FOR PIN 1 LOCATION ON THE TOP AND BOTTOM OF PACKAGE

# PACKAGE DESCRIPTION

**MS Package**
**12-Lead Plastic MSOP**
(Reference LTC DWG # 05-08-1668 Rev Ø)

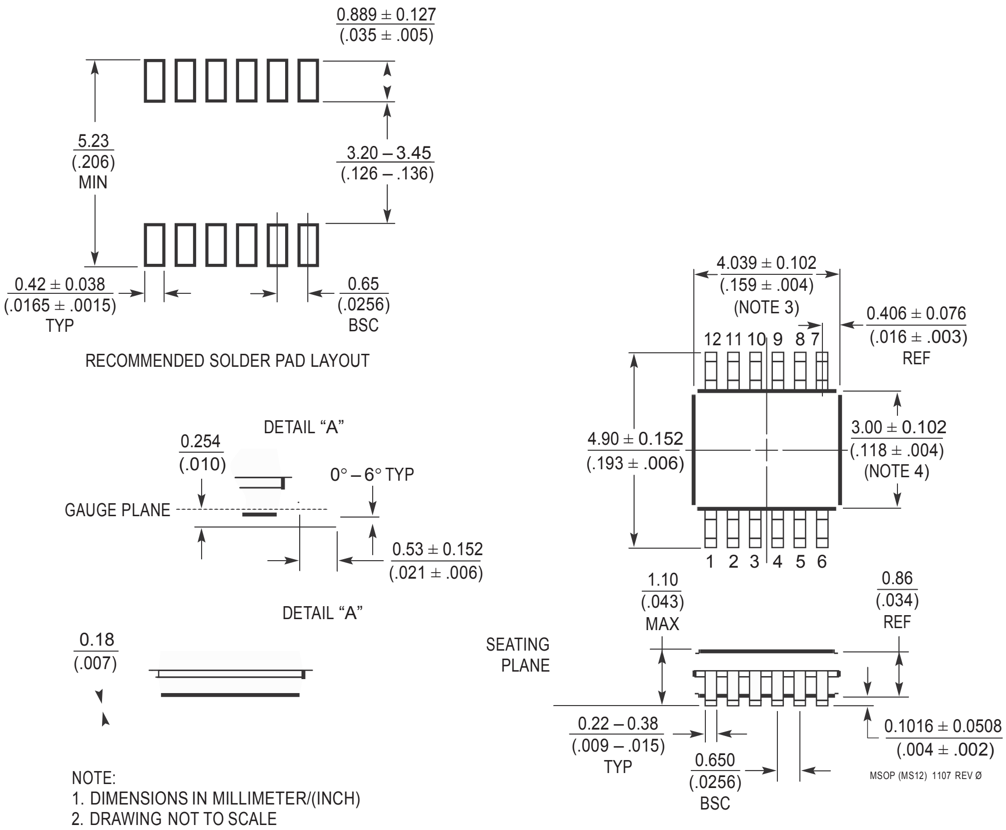


NOTE:
1. DIMENSIONS IN MILLIMETER/(INCH)
2. DRAWING NOT TO SCALE
3. DIMENSION DOES NOT INCLUDE MOLD FLASH, PROTRUSIONS OR GATE BURRS. MOLD FLASH, PROTRUSIONS OR GATE BURRS SHALL NOT EXCEED 0.152mm (.006") PER SIDE
4. DIMENSION DOES NOT INCLUDE INTERLEAD FLASH OR PROTRUSIONS. INTERLEAD FLASH OR PROTRUSIONS SHALL NOT EXCEED 0.152mm (.006") PER SIDE
5. LEAD COPLANARITY (BOTTOM OF LEADS AFTER FORMING) SHALL BE 0.102mm (.004") MAX

## REVISION HISTORY

| REV | DATE | DESCRIPTION | PAGE NUMBER |
|---|---|---|---|
| A | 02/11 | Added (Note 5) notation to Input Start-Up Voltage conditions | 3 |
| | | Added Note 5 | 3 |
| | | Updated Start-Up Mode Operation section | 8 |

## TYPICAL APPLICATION

**Single-Cell Powered Remote Wireless Sensor**

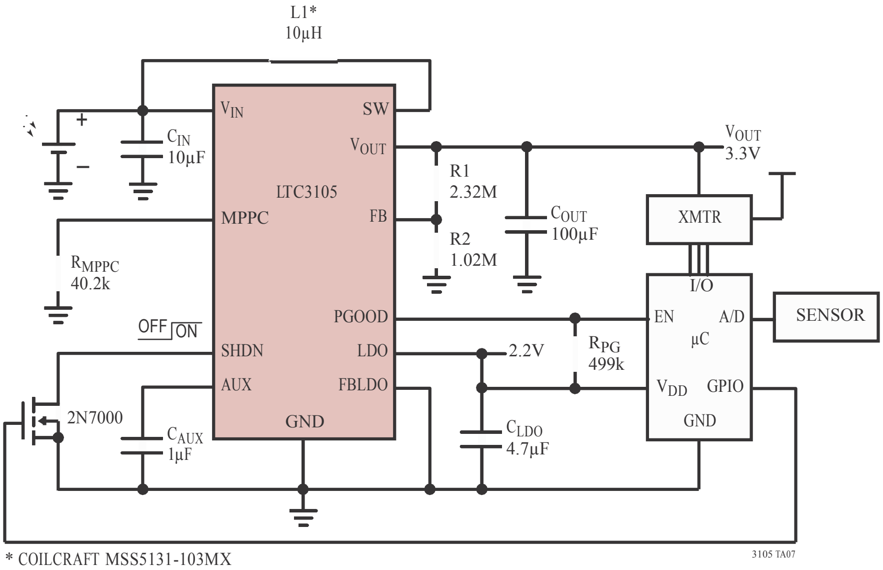


* COILCRAFT MSS5131-103MX

## RELATED PARTS

| PART NUMBER | DESCRIPTION | COMMENTS |
|---|---|---|
| LTC3108/LTC3108-1 | Ultralow Voltage Step-Up Converter and Power Manager | $V_{IN}$: 0.02V to 1V; $V_{OUT}$ = 2.2V, 2.35V, 3.3V, 4.1V, 5V; $I_Q$ = 6µA; 4mm × 3mm DFN-12, SSOP-16 Packages; LTC3108-1 $V_{OUT}$ = 2.2V, 2.5V, 3V, 3.7V, 4.5V |
| LTC3109 | Auto-Polarity, Ultralow Voltage Step-Up Converter and Power Manager | $\|V_{IN}\|$: 0.03V to 1V; $V_{OUT}$ = 2.2V, 2.35V, 3.3V, 4.1V, 5V; $I_Q$ = 7µA; 4mm × 4mm QFN-20, SSOP-20 Packages |
| LTC4070 | Li-Ion/Polymer Shunt Battery Charger System | 450nA $I_Q$; 1% Float Voltage Accuracy; 50mA Shunt Current 4.0V/4.1V/4.2V |
| LTC4071 | Li-Ion/Polymer Shunt Battery Charger System with Low Battery Disconnect | 550nA $I_Q$; 1% Float Voltage Accuracy; <10nA Low Battery Disconnect; 4.0V/4.1V/4.2V; 8-Lead 2mm × 3mm DFN and MSOP Packages |
| LTC3588-1/LTC3588-2 | Piezoelectric Energy Harvesting Power Supply | < 1µA $I_Q$ in Regulation; 2.7V to 20V Input Range; Integrated Bridge Rectifier |
| LTC3388-1/LTC3388-3 | 20V High Efficiency Nanopower Step-Down Regulator | 860nA $I_Q$ in Sleep; 2.7V to 20V Input; $V_{OUT}$: 1.2V to 5V; Enable and Standby Pins |
| LTC3225/LTC3225-1 | 150mA Super Capacitor Charger | Programmable Charge Current Up to 150mA; Constant-Frequency Charging of Two Series Supercapacitors; No Inductors; 2mm × 3mm DFN Package |
| LTC3525-3/LTC3525-3.3/ LTC3525-5/LTC3525L-3 | 400mA Micropower Synchronous Step-Up DC/DC Converter with Output Disconnect | 95% Efficiency; $V_{IN}$: 1V to 4.5V; $V_{OUT}$ = 3V, 3.3V or 5V; $I_Q$ = 7µA; $I_{SD}$ < 1µA; SC70 Package; LTC3525L-3 $V_{IN}$: 0.7V to 4.5V |
| LTC3526L/LTC3526L-2/ LTC3526LB/LTC3526LB-2 | 550mA, 1MHz/2MHz Synchronous Boost Converter | 95% Efficiency; $V_{IN}$: 0.7V to 5.5V; $V_{OUT(MAX)}$ = 5.25V; $I_Q$ = 9µA; $I_{SD}$ < 1µA; 2mm × 2mm DFN Package |
| LTC3527 | Dual 2.2MHz 800mA/400mA Synchronous Step-Up DC/DC Converters | $V_{IN}$: 0.5V to 5V; $V_{OUT}$: 1.6V to 5.25V; $I_Q$ = 12µA; $I_{SD}$ < 1µA; 3mm × 3mm QFN Package |
| LTC3528/LTC3528-2/ LTC3528B/LTC3528B-2 | 1A ($I_{SW}$), 1MHz/2MHz Synchronous Step-Up DC/DC Converter with Output Disconnect | 94% Efficiency; $V_{IN}$: 0.7V to 5.5V; $V_{OUT(MAX)}$ = 5.25V; $I_Q$ = 12µA; $I_{SD}$ < 1µA; 2mm × 3mm DFN-8 Package |
| LTC3537 | 2.2MHz, 600mA Synchronous Step-Up DC/DC Converter and 100mA LDO | $V_{IN}$: 0.68V to 5V; $V_{OUT}$: 1.5V to 5.25V; 3mm × 3mm QFN Package |
| LTC3539/LTC3539-2 | 2A ($I_{SW}$), 1MHz/2MHz Synchronous Step-Up DC/DC Converter with Output Disconnect | 94% Efficiency; $V_{IN}$: 0.7V to 5V; $V_{OUT(MAX)}$ = 5.25V; $I_Q$ = 10µA; $I_{SD}$ < 1µA; 2mm × 3mm DFN Package |


LT 0211 REV A • PRINTED IN USA

# Appendix B

LT3433

# High Voltage Step-Up/Step-Down DC/DC Converter

## FEATURES

- **Automatic Step-Up and Step-Down Conversion**
- **Uses a Single Inductor**
- **Wide 4V to 60V Input Voltage Range**
- **$V_{OUT}$ from 3.3V to 20V**
- **Dual Internal 500mA Switches**
- 100μA No-Load Quiescent Current
- Low Current Shutdown
- ±1% Output Voltage Accuracy
- 200kHz Operating Frequency
- Boosted Supply Pin to Saturate High Side Switch
- Frequency Foldback Protection
- Current Limit Foldback Protection
- Current Limit Unaffected by Duty Cycle
- 16-lead Thermally Enhanced TSSOP Package

## APPLICATIONS

- 12V Automotive Systems
- Wall Adapter Powered Systems
- Battery Power Voltage Buffering


U.S. patent number: 5731694

## DESCRIPTION

The LT®3433 is a 200kHz fixed-frequency current mode switching regulator that provides both step-up and step-down regulation using a single inductor. The IC operates over a 4V to 60V input voltage range making it suitable for use in various wide input voltage range applications such as automotive electronics that must withstand both load dump and cold crank conditions.

Internal control circuitry monitors system conditions and converts from single switch buck operation to dual switch bridged operation when required, seamlessly changing between step-down and step-up voltage conversion.

Optional Burst Mode® operation reduces no-load quiescent current to 100μA and maintains high efficiencies with light loads.

Current limit foldback and frequency foldback help prevent inductor current runaway during start-up. Programmable soft-start helps prevent output overshoot at start-up.

The LT3433 is available in a 16-lead thermally enhanced TSSOP package.

## TYPICAL APPLICATION

**4V to 60V to 5V DC/DC Converter with Burst Mode Operation**

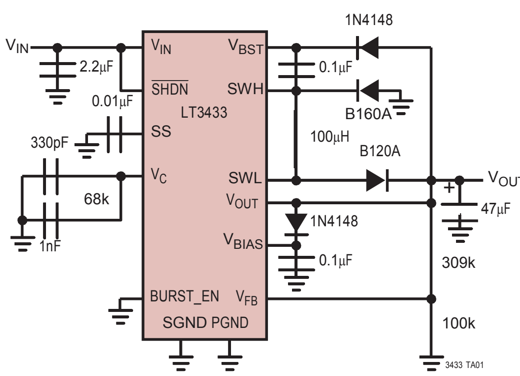


**Maximum Output Current vs $V_{IN}$**

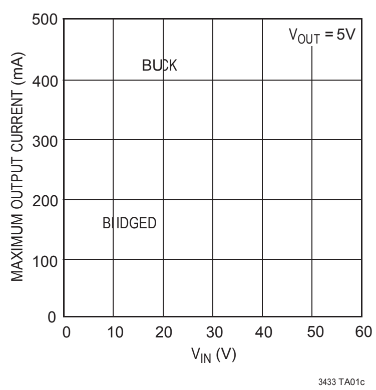


**Efficiency**

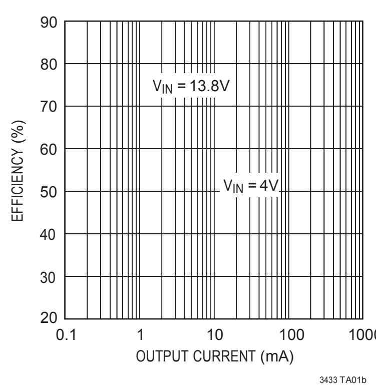

## ABSOLUTE MAXIMUM RATINGS

**(Note 1)**

Input Supply ($V_{IN}$) .................................. –0.3V to 60V
Boosted Supply ($V_{BST}$) ............. –0.3V to $V_{SW\_H}$ + 30V
($V_{BST(MAX)}$ = 80V)
Internal Supply ($V_{BIAS}$) ............................ –0.3V to 30V
SW_H Switch Voltage ................................ –2V to 60V
SW_L Switch Voltage .............................. –0.3V to 30V
Feedback Voltage ($V_{FB}$) .............................. –0.3V to 5V
Burst Enable Pin ($V_{BURST\_EN}$) .................. –0.3V to 30V
Shutdown Pin ($V_{\overline{SHDN}}$) ............................ –0.3V to 60V
Operating Junction Temperature Range (Note 5)
LT3433E (Note 6) ........................... –40°C to 125°C
LT3433I ......................................... –40°C to 125°C
Storage Temperature Range ............... –65°C to 150°C
Lead Temperature (Soldering, 10 sec)................ 300°C

## PACKAGE/ORDER INFORMATION

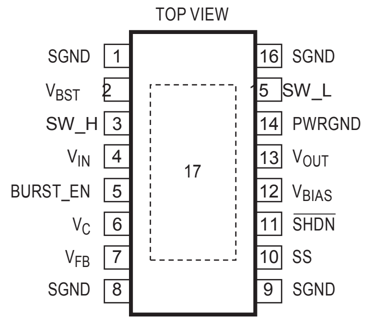


FE PACKAGE
16-LEAD PLASTIC TSSOP
$T_{JMAX}$ = 125°C, $\theta_{JA}$ = 40°C/W, $\theta_{JC}$ = 10°C/W
EXPOSED PAD (PIN 17)
MUST BE SOLDERED TO SGND

| ORDER PART NUMBER | FE PART MARKING |
|---|---|
| LT3433EFE | 3433EFE |
| LT3433IFE | 3433IFE |

Consult LTC Marketing for parts specified with wider operating temperature ranges.

## ELECTRICAL CHARACTERISTICS

**The ● denotes specifications that apply over the full operating temperature range, otherwise specifications are at $T_A$ = 25°C. $V_{IN}$ = 13.8V, $V_{FB}$ = 1.25V, $V_{OUT}$ = 5V, $V_{BURST\_EN}$ = 0V, $V_{BST}$ – $V_{IN}$ = 5V, unless otherwise noted.**

| SYMBOL | PARAMETER | CONDITIONS | | MIN | TYP | MAX | UNITS |
|---|---|---|---|---|---|---|---|
| $V_{IN}$ | Operating Voltage Range | | ● | 4 | | 60 | V |
| $V_{IN(UVLO)}$ | Undervoltage Lockout | Enable Threshold | ● | | 3.4 | 3.95 | V |
| | Undervoltage Lockout Hysteresis | | | | 160 | | mV |
| $V_{OUT}$ | Operating Voltage Range | | ● | 3.3 | | 20 | V |
| $V_{BST}$ | Operating Voltage Range | $V_{BST}$ < $V_{SW\_H}$ + 20V<br>$V_{BST}$ – $V_{SW\_H}$ | ●<br>● | <br>3.3 | | 75<br>20 | V<br>V |
| $I_{VIN}$ | Normal Operation<br>Burst Mode Operation<br>Shutdown | (Notes 2, 3)<br>$V_{VC}$ < 0.6V<br>$V_{\overline{SHDN}}$ < 0.4V | ●<br>●<br>● | | 580<br>100<br>10 | 940<br>190<br>25 | µA<br>µA<br>µA |
| $V_{BIAS}$ | Internal Supply Output Voltage | | ● | | 2.6 | 2.9 | V |
| | Operating Voltage Range | | ● | | | 20 | V |
| $I_{VBIAS}$ | Normal Operation<br>Burst Mode Operation<br>Shutdown<br>Short-Circuit Current Limit | <br>$V_{VC}$ < 0.6V<br>$V_{\overline{SHDN}}$ < 0.4V | ● | | 660<br>0.1<br>0.1<br>4.5 | 990 | µA<br>µA<br>µA<br>mA |
| $R_{SWH(ON)}$ | Boost Supply Switch On-Resistance | $I_{SW}$ = 500mA | ● | | 0.8 | 1.2 | Ω |
| $R_{SWL(ON)}$ | Output Supply Switch On-Resistance | $I_{SW}$ = 500mA | ● | | 0.6 | 1 | Ω |
| $V_{\overline{SHDN}}$ | Shutdown Pin Thresholds | Disable<br>Enable | ●<br>● | 0.4 | | <br>1 | V<br>V |
| $I_{VBST}/I_{SW}$ | Boost Supply Switch Drive Current | High Side Switch On, $I_{SW}$ = 500mA | ● | | 30 | 50 | mA/A |
| $I_{VOUT}/I_{SW}$ | Output Supply Switch Drive Current | Low Side Switch On, $I_{SW}$ = 500mA | ● | | 30 | 50 | mA/A |
| $I_{LIM}$ | Switch Current Limit | | ● | 0.5 | 0.7 | 0.9 | A |
| | Foldback Current Limit | $V_{FB}$ = 0V | | | 0.35 | | A |
| $I_{SS}$ | Soft-Start Output Current | | ● | 3 | 5 | 9 | µA |

# ELECTRICAL CHARACTERISTICS

**The ● denotes specifications that apply over the full operating temperature range, otherwise specifications are at $T_A$ = 25°C. $V_{IN}$ = 13.8V, $V_{FB}$ = 1.25V, $V_{OUT}$ = 5V, $V_{BURST\_EN}$ = 0V, $V_{BST} - V_{IN}$ = 5V, unless otherwise noted.**

| SYMBOL | PARAMETER | CONDITIONS | | MIN | TYP | MAX | UNITS |
|---|---|---|---|---|---|---|---|
| $V_{FB}$ | Feedback Reference Voltage | | <br>● | 1.224<br>1.215 | 1.231 | 1.238<br>1.245 | V<br>V |
| $\Delta V_{FB}$ | Feedback Reference Line Regulation | 5.5V ≤ $V_{IN}$ ≤ 60V | ● | | 0.002 | 0.01 | %/V |
| $I_{FB}$ | $V_{FB}$ Pin Input Bias Current | | ● | | 35 | 100 | nA |
| $g_m$ | Error Amplifier Transconductance | | ● | 200 | 270 | 330 | umhos |
| $A_V$ | Error Amplifier Voltage Gain | | | | 66 | | dB |
| $I_{SW}/V_{VC}$ | Control Voltage to Switch Transconductance | | | | 0.6 | | A/V |
| $f_O$ | Operating Frequency | $V_{FB}$ > 1V | <br>● | 185<br>170 | 200 | 215<br>230 | kHz<br>kHz |
| | Foldback Frequency | $V_{FB}$ = 0V | | | 50 | | kHz |
| $V_{BURST\_EN}$ | Burst Enable Threshold | | | | 0.8 | | V |
| $I_{BURST\_EN}$ | Input Bias Current | $V_{BURST\_EN}$ ≥ 2V | | | 35 | | μA |
| $t_{ON(MIN)}$ | Minimum Switch On Time | $R_L$ = 35Ω (Note 4) | ● | | 250 | 450 | ns |
| $t_{OFF(MIN)}$ | Minimum Switch Off Time | $R_L$ = 35Ω (Note 4) | ● | | 500 | 800 | ns |

**Note 1:** Absolute Maximum Ratings are those values beyond which the life of a device may be impaired.

**Note 2:** Supply current specification does not include switch drive currents. Actual supply currents will be higher.

**Note 3:** "Normal Operation" supply current specification does not include $I_{BIAS}$ currents. Powering the $V_{BIAS}$ pin externally reduces $I_{CC}$ supply current.

**Note 4:** Minimum times are tested using the high side switch with a 35Ω load to ground.

**Note 5:** This IC includes overtemperature protection that is intended to protect the device during momentary overload conditions. Junction temperature will exceed 125°C when overtemperature protection is active. Continuous operation above the specified maximum operating junction temperature may impair device reliability.

**Note 6:** The LT3433E is guaranteed to meet performance specifications from 0°C to 125°C junction temperature. Specifications over the –40°C to 125°C operating junction temperature range are assured by design, characterization and correlation with statistical process controls. The LT3433I is guaranteed over the full –40°C to 125°C operating junction temperature range.

# TYPICAL PERFORMANCE CHARACTERISTICS

**Maximum Output Current vs $V_{IN}$**

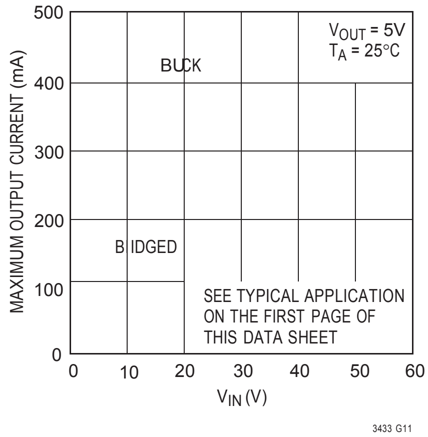


**$V_{BIAS}$ Output Voltage vs Temperature**

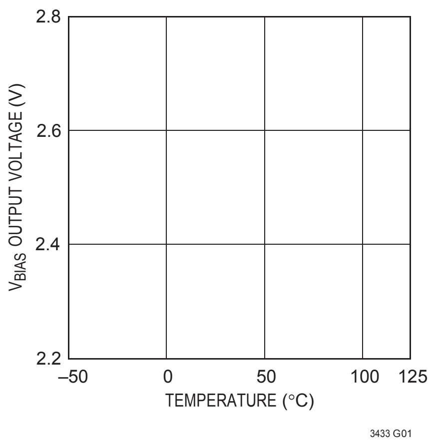


**$V_{IN}$ Supply Current vs $V_{IN}$ Supply Voltage**

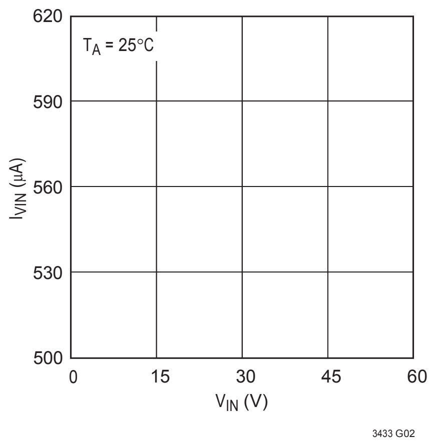

# TYPICAL PERFORMANCE CHARACTERISTICS

### Soft-Start Current vs Temperature

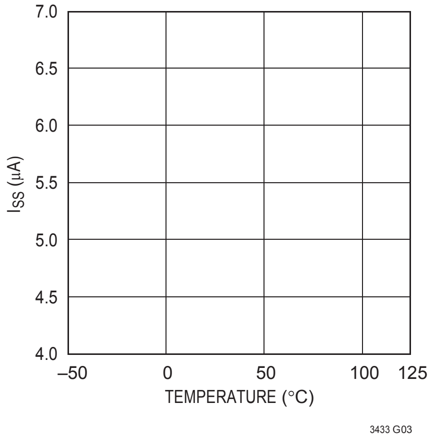


### Error Amp Reference vs Temperature

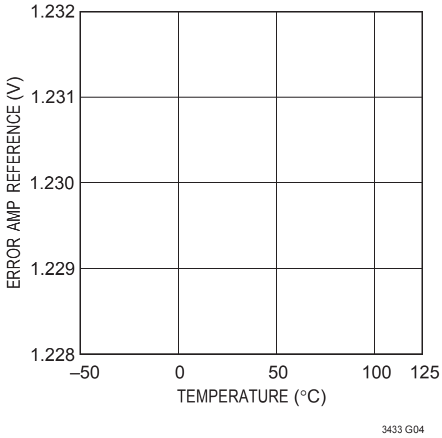


### Switch Current Limit vs $V_{FB}$

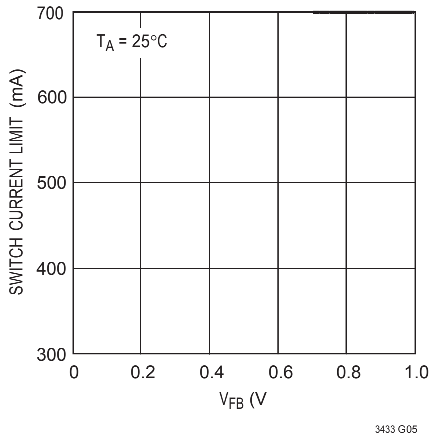


### Oscillator Frequency vs Temperature

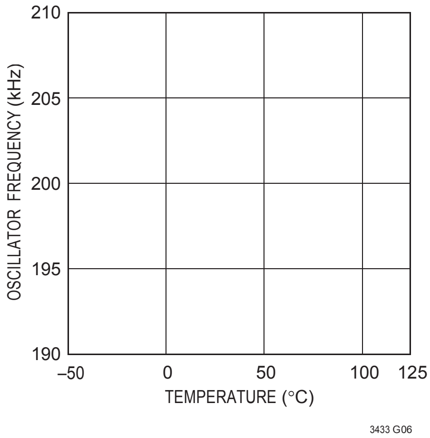


### Oscillator Frequency vs $V_{FB}$

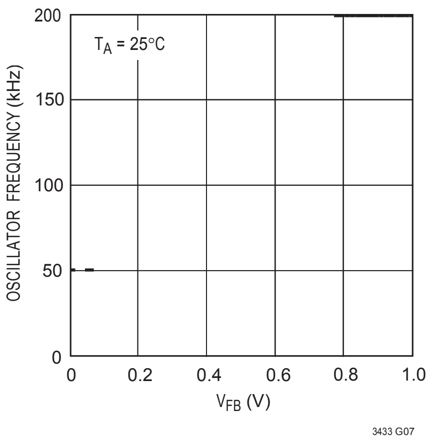


### Current Limit vs Temperature

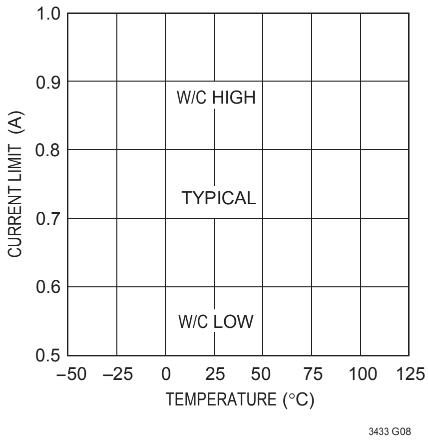


### Maximum Boost Supply Switch Drive Current vs Boost Supply Voltage

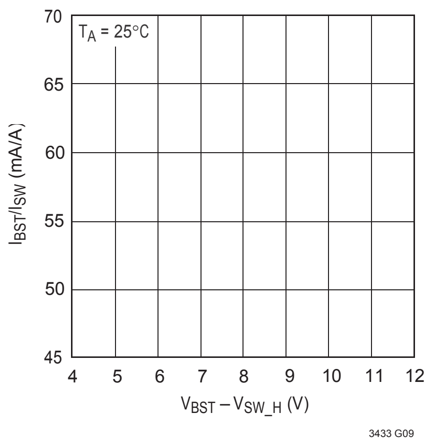


### Maximum Output Supply Switch Drive Current vs Output Supply Voltage

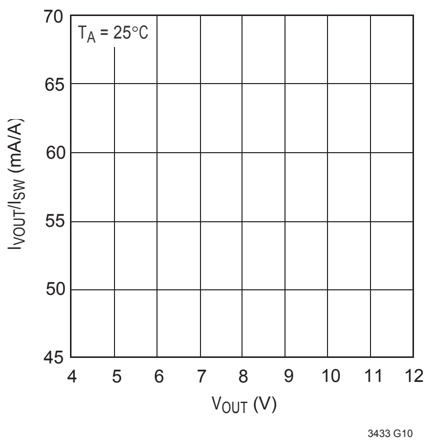

## TYPICAL PERFORMANCE CHARACTERISTICS

Switch Resistance vs Temperature ($I_{SW}$ = 500mA)

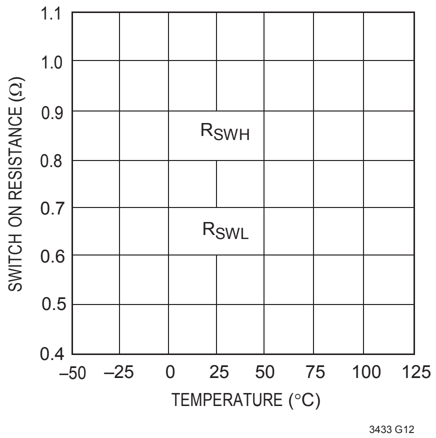


$V_{BST}$ Supply Switch Drive Current vs Temperature ($I_{SW}$ = 500mA)

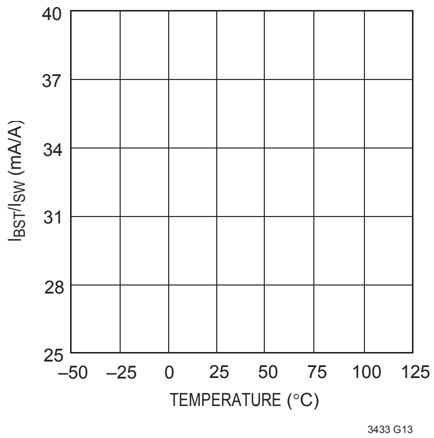


$V_{OUT}$ Supply Switch Drive Current vs Temperature ($I_{SW}$ = 500mA)

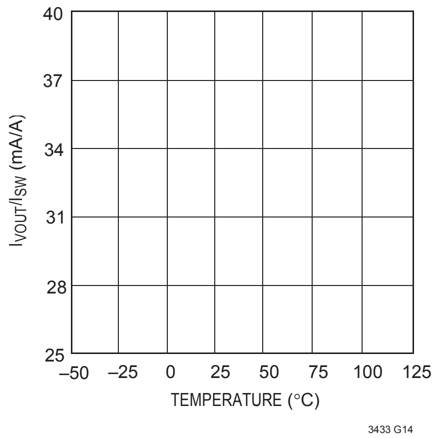


## PIN FUNCTIONS

**SGND (Pins 1, 8, 9, 16):** Low Noise Ground Reference.

**$V_{BST}$ (Pin 2):** Boosted Switch Supply. This “boosted” supply rail is referenced to the SW_H pin. Supply voltage is maintained by a bootstrap capacitor tied from the $V_{BST}$ pin to the SW_H pin. A 1μF capacitor is generally adequate for most applications.

The charge on the bootstrap capacitor is refreshed through a diode, typically connected from the converter output ($V_{OUT}$), during the switch-off period. Minimum off-time operation assures that the boost capacitor is refreshed each switch cycle. The LT3433 supports operational $V_{BST}$ sup- ply voltages up to 75V (absolute maximum) as referenced to ground.

**SW_H (Pin 3):** Boosted Switch Output. This is the current return for the boosted switch and corresponds to the emitter of the switch transistor. The boosted switch shorts the SW_H pin to the $V_{IN}$ supply when enabled. The drive circuitry for this switch is boosted above the $V_{IN}$ supply through the $V_{BST}$ pin, allowing saturation of the switch for maximum efficiency. The “ON” resistance of the boosted switch is 0.8Ω.

**$V_{IN}$ (Pin 4):** Input Power Supply. This pin supplies power to the boosted switch and corresponds to the collector of the switch transistor. This pin also supplies power to most of the IC’s internal circuitry if the $V_{BIAS}$ pin is not driven externally. This supply will be subject to high switching transient currents so this pin requires a high quality bypass capacitor that meets whatever application-specific input ripple current requirements exist.

**BURST_EN (Pin 5):** Burst Mode Enable/Disable. When this pin is below 0.3V, Burst Mode operation is enabled. Pin input bias current < 1μA when Burst Mode operation is enabled. If Burst Mode operation is not desired, pulling this pin above 2V will disable the burst function. When Burst Mode operation is disabled, typical pin input current = 35μA. BURST_EN should not be pulled above 20V. This pin is typically shorted to SGND for Burst Mode function, or connected to either $V_{BIAS}$ or $V_{OUT}$ to disable Burst Mode operation.

**$V_C$ (Pin 6):** Error Amplifier Output. The voltage on the $V_C$ pin corresponds to the maximum switch current per oscillator cycle. The error amplifier is typically configured as an integrator circuit by connecting an RC network from this pin to ground. This circuit typically creates the dominant pole for the converter regulation feedback loop. Specific integrator characteristics can be configured to optimize transient response. See Applications Information.

## PIN FUNCTIONS

**$V_{FB}$ (Pin 7):** Error Amplifier Inverting Input. The noninverting input of the error amplifier is connected to an internal 1.231V reference. The $V_{FB}$ pin is connected to a resistor divider from the converter output. Values for the resistor connected from $V_{OUT}$ to $V_{FB}$ ($R_{FB1}$) and the resistor connected from $V_{FB}$ to ground ($R_{FB2}$) can be calculated to program converter output voltage ($V_{OUT}$) via the following relation:

$$V_{OUT} = 1.231 \bullet (R_{FB1} + R_{FB2})/R_{FB2}$$

The $V_{FB}$ pin input bias current is 35nA, so use of extremely high value feedback resistors could cause a converter output that is slightly higher than expected. Bias current error at the output can be estimated as:

$$\Delta V_{OUT(BIAS)} = 35nA \bullet R_{FB1}$$

The voltage on $V_{FB}$ also controls the LT3433 oscillator frequency through a "frequency-foldback" function. When the $V_{FB}$ pin voltage is below 0.8V, the oscillator runs slower than the 200kHz typical operating frequency. The oscillator frequency slows with reduced voltage on the pin, down to 50kHz when $V_{FB}$ = 0V.

The $V_{FB}$ pin voltage also controls switch current limit through a "current-limit foldback" function. At $V_{FB}$ = 0V, the maximum switch current is reduced to half of the normal value. The current limit value increases linearly until $V_{FB}$ reaches 0.6V when the normal maximum switch current level is restored. The frequency and current-limit foldback functions add robustness to short-circuit protection and help prevent inductor current runaway during start-up.

**SS (Pin 10):** Soft Start. Connect a capacitor ($C_{SS}$) from this pin to ground. The output voltage of the LT3433 error amplifier corresponds to the peak current sense amplifier output detected before resetting the switch output(s). The soft-start circuit forces the error amplifier output to a zero peak current for start-up. A 5µA current is forced from the SS pin onto an external capacitor. As the SS pin voltage ramps up, so does the LT3433 internally sensed peak current limit. This forces the converter output current to ramp from zero until normal output regulation is achieved. This function reduces output overshoot on converter start-up.

The time from $V_{SS}$ = 0V to maximum available current can be calculated given a capacitor $C_{SS}$ as:

$$t_{SS} = (2.7 \bullet 10^5)C_{SS} \text{ or } 0.27s/\mu F$$

**$\overline{SHDN}$ (Pin 11):** Shutdown. If the $\overline{SHDN}$ pin is externally pulled below 0.5V, low current shutdown mode is initiated. During shutdown mode, all internal functions are disabled, and $I_{CC}$ is reduced to 10µA. This pin is intended to receive a digital input, however, there is a small amount of input hysteresis built into the SHDN circuit to help assure glitch-free mode switching. If shutdown is not desired, connect the SHDN pin to $V_{IN}$.

**$V_{BIAS}$ (Pin 12):** Internal Local Supply. Much of the LT3433 circuitry is powered from this supply, which is internally regulated to 2.5V through an on-board linear regulator. Current drive for this regulator is sourced from the $V_{IN}$ pin. The $V_{BIAS}$ supply is short-circuit protected to 5mA.

The $V_{BIAS}$ supply only sources current, so forcing this pin above the regulated voltage allows the use of external power for much of the LT3433 circuitry. When using external drive, this pin should be driven above 3V to assure the internal supply is completely disabled. This pin is typically diode-connected to the converter output to maximize conversion efficiency. This pin must be bypassed with at least a 0.1µF ceramic capacitor to SGND.

**$V_{OUT}$ (Pin 13):** Converter Output Pin. This pin voltage is compared with the voltage on $V_{IN}$ internally to control operation in single or 2-switch mode. When the ratios of the two voltages are such that a >75% duty cycle is required for regulation, the low side switch is enabled. Drive bias for the low side switch is also derived directly from this pin.

**PWRGND (Pin 14):** High Current Ground Reference. This is the current return for the low side switch and corresponds to the emitter of the low side switch transistor.

**SW_L (Pin 15):** Ground Referenced Switch Output. This pin is the collector of the low side switch transistor. The low side switch shorts the SW_L pin to PWRGND when enabled. The series impedance of the ground-referenced switch is 0.6Ω.

**Exposed Pad (Pin 17):** Exposed Pad must be soldered to PCB ground for optimal thermal performance.

## BLOCK DIAGRAM

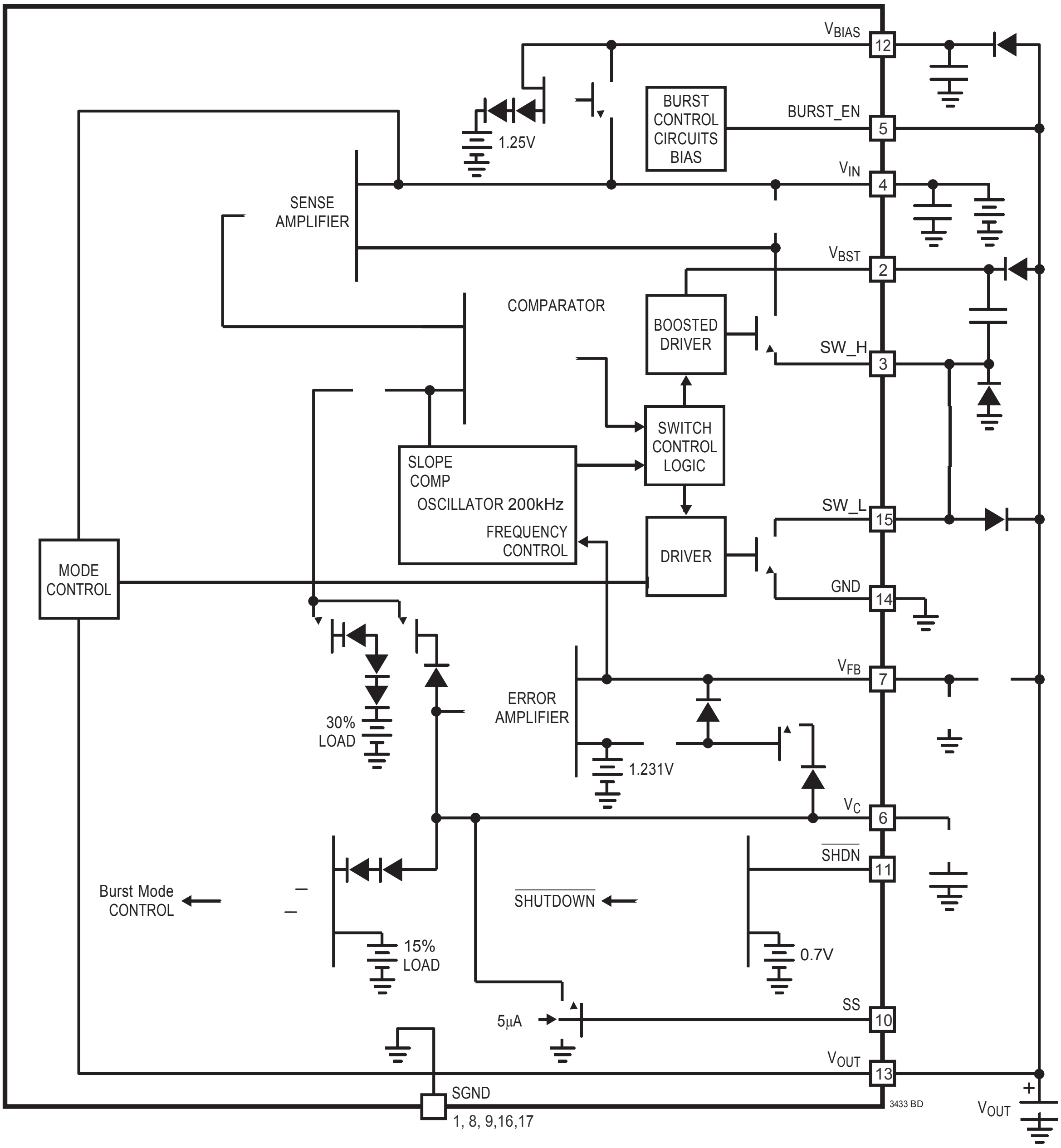

## APPLICATIONS INFORMATION

**Overview**

The LT3433 is a high input voltage range, step-up/step-down DC/DC converter IC using a 200kHz constant frequency, current mode architecture. Dual internal switches allow the full input voltage to be imposed across the switched inductor, such that both step-up and step-down modes of operation can be realized using the same single inductor topology.

The LT3433 has provisions for high efficiency, low load operation for battery-powered applications. Burst Mode operation reduces average quiescent current to 100µA in no load conditions. A low current shutdown mode can also be activated, reducing total quiescent current to 10µA.

Much of the LT3433's internal circuitry is biased from an internal low voltage linear regulator. The output of this regulator is brought out to the $V_{BIAS}$ pin, allowing bypassing of the internal regulator. The associated internal circuitry can be powered directly from the output of the converter, increasing overall converter efficiency. Using externally derived power also eliminates the IC's power dissipation associated with the internal $V_{IN}$ to $V_{BIAS}$ regulator.

**Theory of Operation (See Block Diagram)**

The LT3433 senses converter output voltage via the $V_{FB}$ pin. The difference between the voltage on this pin and an internal 1.231V reference is amplified to generate an error voltage on the $V_C$ pin which is, in turn, used as a threshold for the current sense comparator.

During normal operation, the LT3433 internal oscillator runs at 200kHz. At the beginning of each oscillator cycle, the switch drive is enabled. The switch drive stays enabled until the sensed switch current exceeds the $V_C$-derived threshold for the current sense comparator and, in turn, disables the switch driver. If the current comparator threshold is not obtained for the entire oscillator cycle, the switch driver is disabled at the end of the cycle for 250ns. This minimum off-time mode of operation assures regeneration of the $V_{BST}$ bootstrapped supply.

If the converter input and output voltages are close together, proper operation in normal buck configuration would require high duty cycles. The LT3433 senses this condition as requiring a duty cycle greater than 75%. If such a condition exists, a second switch is enabled during the switch on time, which acts to pull the output side of the inductor to ground. This "bridged" operation allows voltage conversion to continue when $V_{OUT}$ approaches or exceeds $V_{IN}$.

**Shutdown**

The LT3433 incorporates a low current shutdown mode where all IC functions are disabled and the $V_{IN}$ current is reduced to 10µA. Pulling the $\overline{SHDN}$ pin down to 0.4V or less activates shutdown mode.

**Burst Mode Operation**

The LT3433 employs low current Burst Mode functionality to maximize efficiency during no load and low load conditions. Burst Mode function is disabled by shorting the BURST_EN pin to either $V_{BIAS}$ or $V_{OUT}$. Burst Mode function is enabled by shorting BURST_EN to SGND.

In certain wide current range applications, the IC could enter burst operation during normal load conditions. If the additional output ripple and noise generated by Burst Mode operation is not desired for normal operation, BURST_EN can be biased using an external supply that is disabled during a no-load condition. This enables Burst Mode operation only when it is required. The BURST_EN pin typically draws 35µA when Burst Mode operation is disabled ($V_{BURST\_EN} \geq 2V$) and will draw no more than 75µA with $V_{BURST\_EN} = 2V$.

When the required switch current, sensed via the $V_C$ pin voltage, is below 30% of maximum, the Burst Mode function is employed. When the voltage on $V_C$ drops below the 30% load level, that level of sense current is latched into the IC. If the output load requires less than this latched current level, the converter will overdrive the output slightly during each switch cycle. This overdrive condition forces the voltage on the $V_C$ pin to continue to drop. When the voltage on $V_C$ drops below the 15% load level, switching is disabled, and the LT3433 shuts down most of its internal circuitry, reducing quiescent current to 100µA. When the voltage on the $V_C$ pin climbs back to 20% load level, the IC returns to normal operation and switching resumes.

## APPLICATIONS INFORMATION

### Antislope Compensation

Most current mode switching controllers use slope compensation to prevent current mode instability. The LT3433 is no exception. A slope compensation circuit imposes an artificial ramp on the sensed current to increase the rising slope as duty cycle increases. Unfortunately, this additional ramp corrupts the sensed current value, reducing the achievable current limit value by the same amount as the added ramp represents. As such, current limit is typically reduced as duty cycles increase.

The LT3433 contains circuitry to eliminate the current limit reduction associated with slope-compensation, or antislope compensation. As the slope compensation ramp is added to the sensed current, a similar ramp is added to the current limit threshold reference. The end result is that current limit is not compromised so the LT3433 can provide full power regardless of required duty cycle.

### Mode Switching

The LT3433 switches between buck and buck/boost modes of operation automatically. While in buck mode, if the converter input voltage becomes close enough to the output voltage to require a duty cycle greater than 75%, the LT3433 enables a second switch which pulls the output side of the inductor to ground during the switch-on time. This "bridged" switching configuration allows voltage conversion to continue when $V_{IN}$ approaches or is less than $V_{OUT}$.

When the converter input voltage falls to where the duty cycle required for continuous buck operation is greater than 75%, the LT3433 enables its ground-referred switch, changing the converter operation to a dual-switch bridged configuration. Because the voltage available across the switched inductor is greater while bridged, operational duty cycle will decrease. Voltage drops associated with external diodes and loss terms are estimated internally so that required operating duty cycle can be calculated regardless of specific operating voltages.

In the simplest terms, a buck DC/DC converter switches the $V_{IN}$ side of the inductor, while a boost converter switches the $V_{OUT}$ side of the inductor. The LT3433 bridged topology merges the elements of buck and boost topologies, providing switches on both sides of the inductor. Operating both switches simultaneously achieves both step-up and step-down functionality.

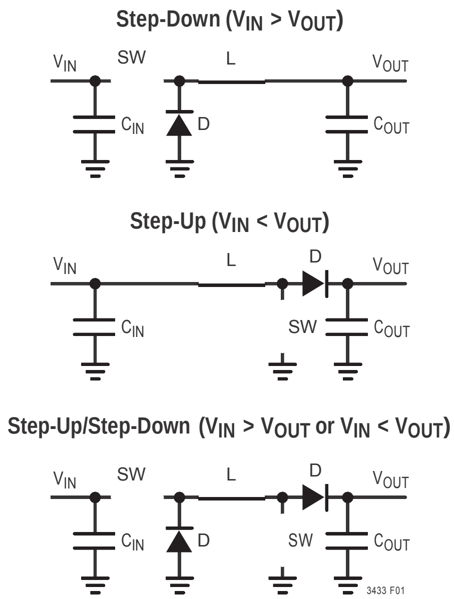


Maximum duty cycle capability ($DC_{MAX}$) gates the dropout capabilities of a buck converter. As $V_{IN} – V_{OUT}$ is reduced, the required duty cycle increases until $DC_{MAX}$ is reached, beyond which the converter loses regulation. With a second switch bridging the switched inductor between $V_{IN}$ and ground, the entire input voltage is imposed across the inductor during the switch-on time, which subsequently reduces the duty cycle required to maintain regulation. Using this topology, regulation is maintained as $V_{IN}$ approaches or drops below $V_{OUT}$.

### Inductor Selection

The primary criterion for inductor value selection in LT3433 applications is the ripple current created in that inductor. Design considerations for ripple current are converter output capabilities in bridged mode, output voltage ripple and the ability of the internal slope compensation waveform to prevent current mode instability.

## APPLICATIONS INFORMATION

The requirement for avoiding current mode instability is that the rising slope of sensed inductor ripple current (S1) is greater than the falling slope (S2). At duty cycles greater than 50% this is not true. To avoid the instability condition, a false signal is added to the sensed current with a slope ($S_X$) that is sufficient to prevent current mode instability, or $S1 + S_X \geq S2$. This leads to the following relations:

$$S_X \geq S2(2DC - 1)/DC$$

If the forward voltages of a converter's catch and pass diodes are defined as $V_{F1}$ and $V_{F2}$, then:

$$S2 = (V_{OUT} + V_{F1} + V_{F2})/L$$

Solving for L yields a relation for the minimum inductance that will satisfy slope compensation requirements:

$$L_{MIN} = (V_{OUT} + V_{F1} + V_{F2})(2DC - 1)/(DC \bullet S_X)$$

The LT3433 maximizes available dynamic range using a slope compensation generator that generates a continuously increasing slope as duty cycle increases. The slope compensation waveform is calibrated at 80% duty cycle to generate an equivalent slope of at least 0.05A/µs. The equation for minimum inductance then reduces to:

$$L_{MIN} = (V_{OUT} + V_{F1} + V_{F2})(15e\text{-}6)$$

For example, with $V_{OUT}$ = 5V and using $V_{F1} + V_{F2}$ = 1.1V (cold):

$$L_{MIN} = (5 + 1.1)(15e\text{-}6) = 91.5\mu H$$

**Slope Compensation Requirements Typical Minimum Inductor Values vs $V_{OUT}$**

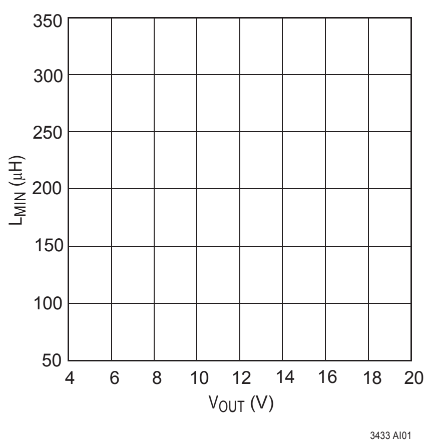


### Converter Capabilities

The output current capability of an LT3433 converter is affected by a myriad of variables. The current in the switches is limited by the LT3433. Switch current is measured coming from the $V_{IN}$ supply, and does not directly translate to a limitation in load current. This is especially true during bridged mode operation when the converter output current is discontinuous.

During bridged mode operation, the converter output current is discontinuous, or only flowing to the output while the switches are off (not to be confused with discontinuous switcher operation). As a result, the maximum output current capability of the converter is reduced from that during buck mode operation by a factor of roughly 1 – DC, not including additional losses. Most converter losses are also a function of DC, so operational duty cycle must be accurately determined to predict converter load capabilities.

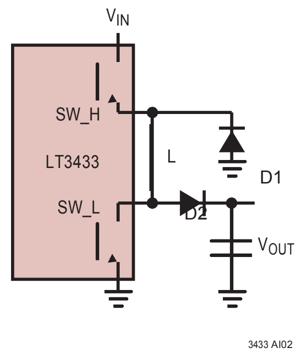


Application variables:

- $V_{IN}$ = Converter input supply voltage
- $V_{OUT}$ = Converter programmed output voltage
- $V_{BST}$ = Boosted supply voltage ($V_{BST} - V_{SWH}$)
- DC = Operational duty cycle
- $f_O$ = Switching frequency
- $I_{MAX}$ = Peak switch current limit
- $\Delta I_L$ = Inductor ripple current
- $I_{SW}$ = Average switch current or peak switch current less half the ripple current ($I_{MAX} - \Delta I_L/2$)
- $R_{SWH}$ = Boosted switch "on" resistance
- $R_{SWL}$ = Grounded switch "on" resistance
- L = Inductor value

## APPLICATIONS INFORMATION

$R_L$ = Inductor series resistance

$\Delta_{BST}$ = Boosted switch drive currents $I_{VBST}/I_{SW}$ (in A/A)

$\Delta_{OUT}$ = Grounded switch drive currents $I_{VOUT}/I_{SW}$ (in A/A)

$V_{F1}$ = Switch node catch diode forward voltage

$V_{F2}$ = Pass diode forward voltage

$I_{VIN}$ = $V_{IN}$ quiescent input current

$I_{IN}$ = $V_{IN}$ switched current

$I_{BIAS}$ = $V_{BIAS}$ quiescent input current

$R_{CESR}$ = Output capacitor ESR

Operational duty cycle is a function of voltage imposed across the switched inductance and switch on/off times. Using the relation for change in current in an inductor:

$$\delta I = V \bullet \delta t/L$$

and putting the application variables into the above relation yields:

$$\delta I_{ON(BRIDGED)} = (DC/f_O \bullet L)[V_{IN} - I_{SW} \bullet (R_{SWH} + R_{SWL} + R_L)]$$

$$\delta I_{ON(BUCK)} = (DC/f_O \bullet L)[V_{IN} - V_{OUT} - V_{F2} - I_{SW} \bullet (R_{SWH} + R_L + R_{ESR})]$$

$$\delta I_{OFF} = [(1 - DC)/f_O \bullet L][V_{OUT} + V_{F1} + V_{F2} - I_{SW} \bullet (R_L + R_{ESR})]$$

Current conservation in an inductor dictates $\delta I_{ON} = \delta I_{OFF}$, so plugging in the above relations and solving for DC yields:

$$DC_{(BRIDGED)} = [V_{OUT} + V_{F1} + V_{F2} - I_{SW} \bullet (R_L + R_{ESR})]/[V_{IN} - I_{SW} \bullet (R_{SWH} + R_{SWL} + 2R_L + R_{ESR}) + V_{OUT} + V_{F1} + V_{F2}]$$

$$DC_{(BUCK)} = [V_{OUT} + V_{F1} + V_{F2} - I_{SW} \bullet (R_L + R_{ESR})]/[V_{IN} - I_{SW} \bullet (R_{SWH} + 2R_L + 2R_{ESR}) + V_{F1}]$$

In order to solve the above equations, inductor ripple current ($\Delta I$) must be determined so $I_{SW}$ can be calculated. $\Delta I$ follows the relation:

$$\Delta I = (V_{OUT} + V_{F1} + V_{F2} - I_{SW} \bullet R_L)(1 - DC)/(L \bullet f_O)$$

As $\Delta I$ is a function of DC and vice-versa, the solution is iterative. Seed $\Delta I$ and solve for DC. Using the resulting value for DC, solve for $\Delta I$. Use the resulting $\Delta I$ as the new seed value and repeat. The calculated value for DC can be used once the resulting $\Delta I$ is close (<1%) to the seed value.

Once DC is determined, maximum output current can be determined using current conservation on the converter output:

Bridged Operation: $I_{OUT(MAX)} = I_{SW} \bullet [1 - DC \bullet (1 + \Delta_{BST} + \Delta_{OUT})] - I_{BIAS}$

Buck Operation: $I_{OUT(MAX)} = I_{SW} \bullet (1 - DC \bullet \Delta_{BST}) - I_{BIAS}$

$P_{IN} = P_{OUT} + P_{LOSS}$, where $P_{LOSS} = P_{SWON} + P_{SWOFF} + P_{IC}$, corresponding to the power loss in the converter. $P_{IC}$ is the quiescent power dissipated by the LT3433. $P_{SWON}$ is the loss associated with the power path during the switch on interval, and $P_{SWOFF}$ is the PowerPath™ loss associated with the switch off interval.

$P_{LOSS}$ equals the sum of the power loss terms:

$$P_{VIN} = V_{IN} \bullet I_{VIN}$$

$$P_{BIAS} = V_{OUT} \bullet I_{BIAS}$$

$$P_{SWON(BRIDGED)} = DC \bullet [I_{SW}{}^2 \bullet (R_{SWH} + R_{SWL} + R_L) + I_{SW} \bullet V_{OUT} \bullet (\Delta_{BST} + \Delta_{OUT}) + R_{CESR} \bullet I_{OUT}{}^2]$$

$$P_{SWON(BUCK)} = DC \bullet [I_{SW}{}^2 \bullet (R_{SWH} + R_L) + I_{SW} \bullet V_{OUT} \bullet \Delta_{BST} + R_{CESR} \bullet (I_{SW} \bullet (1 - \Delta_{BST}) - I_{BIAS} - I_{OUT})^2]$$

$$P_{SWOFF} = (1 - DC) \bullet [I_{SW} \bullet (V_{F1} + V_{F2}) + I_{SW}{}^2 \bullet R_L + R_{CESR} \bullet (I_{SW} - I_{BIAS} - I_{OUT})^2]$$

Efficiency (E) is described as $P_{OUT}/P_{IN}$, so:

$$\text{Efficiency} = \{1 + (P_{VIN} + P_{BIAS} + P_{SWON} + P_{SWOFF})/P_{OUT}\}^{-1}$$

Empirical determination of converter capabilities is accomplished by monitoring inductor currents with a current probe under various input voltages and load currents. Decreasing input voltage or increasing load current results in an inductor current increase. When peak inductor currents reach the switch current limit value, maximum output current is achieved. Limiting the inductor currents to the LT3433 specified W/C current limit of 0.5V (cold) will allow margin for operating limit variations. These limitations should be evaluated at the operating temperature extremes required by the application to assure robust performance.

PowerPath is a trademark of Linear Technology Corporation

## APPLICATIONS INFORMATION

### Design Example

4V-60V to 5V DC/DC converter (the application on the front page of this data sheet), load capability for $T_A = 85°C$.

| Application Specific Constants: | LT3433 W/C Constants: |
|---|---|
| $V_{IN} = 4V$ | $I_{MAX} = 0.55A$ |
| $V_{OUT} = 5V$ | $R_{SWH} = 1.2\Omega$ |
| $L = 100\mu H$ | $R_{SWL} = 1\Omega$ |
| $R_L = 0.28\Omega$ | $f_O = 190kHz$ |
| $V_{F1} = 0.45V$ | $\Delta_{BST} = 0.05$ |
| $V_{F2} = 0.4V$ | $\Delta_{OUT} = 0.05$ |
| $R_{CESR} = 0.01\Omega$ | $I_{VIN} = 600\mu A$ |
| | $I_{BIAS} = 800\mu A$ |

The LT3433 operates in bridged mode with $V_{IN} = 4V$, so the relations used are:

$$DC = [V_{OUT} + V_{F1} + V_{F2} - I_{SW} \bullet (R_L + R_{ESR})]/[V_{IN} - I_{SW} \bullet (R_{SWH} + R_{SWL} + 2R_L + R_{ESR}) + V_{OUT} + V_{F1} + V_{F2}]$$

$$\Delta I = (V_{OUT} + V_{F1} + V_{F2} - I_{SW} \bullet R_L) \bullet (1 - DC)/(L \bullet f_O)$$

$$I_{OUT(MAX)} = I_{SW} \bullet [1 - DC \bullet (1 + \Delta_{BST} + \Delta_{OUT})] - I_{BIAS}$$

Iteration procedure for DC:

(1) Set initial seed value for $\Delta I$ (this example will set $\Delta I = 0$).

(2) Using seed value for $\Delta I$, determine $I_{SW}$ ($I_{SW} = 0.55 - 0 = 0.55$).

(3) Use calculated $I_{SW}$ and above design constants to solve the DC relation (DC = 0.683).

(4) Use calculated DC to solve the $\Delta I$ relation (yields $\Delta I = 0.0949$).

(5) If calculated $\Delta I$ is equal to the seed value, stop. Otherwise, use calculated $\Delta I$ as new seed value and repeat (2) through (4).

| ITERATION # | SEED ΔI | CALCULATED VALUES | | |
|---|---|---|---|---|
| | | $I_{SW}$ | DC | ΔI |
| 1 | 0 | 0.55 | 0.683 | 0.095 |
| 2 | 0.095 | 0.503 | 0.674 | 0.098 |
| 3 | 0.098 | 0.501 | 0.674 | 0.098 |

After iteration, DC = 0.674 and $\Delta I = 0.098$.

Use iteration result for DC and above design constants to solve the $I_{OUT(MAX)}$ relation:

$$I_{OUT(MAX)} = 0.501 \bullet [1 - 0.674 \bullet (1 + 0.05 + 0.05)] - 800\mu A$$

$$I_{OUT(MAX)} = 129mA$$

### Increased Output Voltages

The LT3433 can be used in converter applications with output voltages from 3.3V through 20V, but as converter output voltages increase, output current and duty cycle limitations prevent operation with $V_{IN}$ at the extreme low end of the LT3433 operational range. When a converter operates as a buck/boost, the output current becomes discontinuous, which reduces output current capability by roughly a factor of 1 – DC, where DC = duty cycle. As such, the output current requirement dictates a minimum input voltage where output regulation can be maintained.

**Typical Minimum Input Voltage as a Function of Output Voltage and Required Load Current**

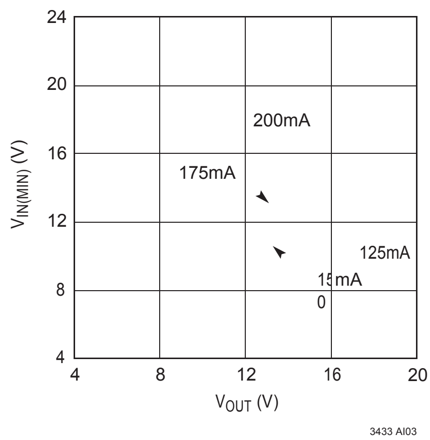

# APPLICATIONS INFORMATION

## Input Voltage Transient Suppression

Not only does a LT3433 converter operate across a large range of DC input voltages, it also maintains tight output regulation during significant input voltage transients. The LT3433 automatic transitioning between buck and buck/boost modes of operation provides seamless output regulation over these input voltage transients. In an automotive environment, input voltage transients are commonplace, such as those experienced during a cold crank condition. During the initiation of cold crank, the battery rail can be pulled down to 4V in as little as 1ms. In a 4V-60V to 5V DC/DC converter application (shown on the first page of this data sheet) a cold crank transient condition, simulated with a 1ms 13.8V to 4V input transition, yields regulation maintained to 1% with a 125mA load.

**4V-50V to 5V Converter Input Transient Response 1ms 13.8V to 4V Input Transition**

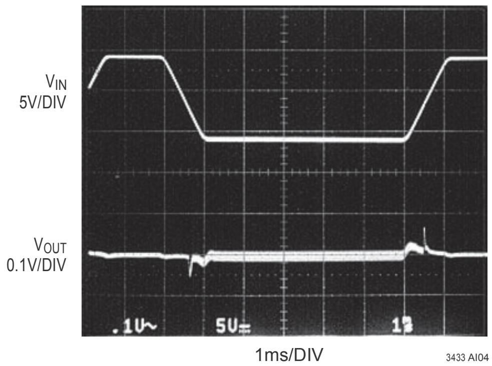


# TYPICAL APPLICATIONS

**4V-60V to 5V Converter with Switched Burst Enable and Shutdown**

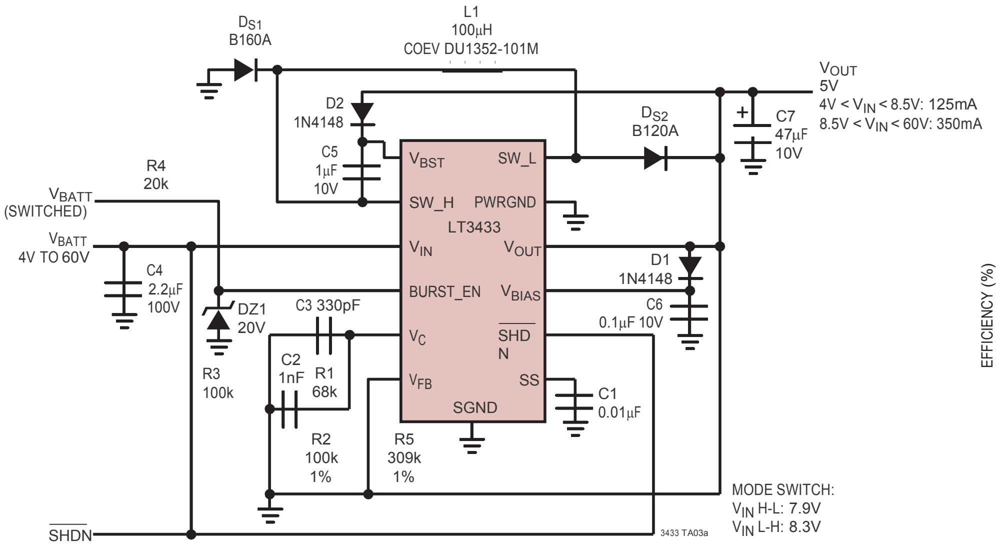


**Efficiency**

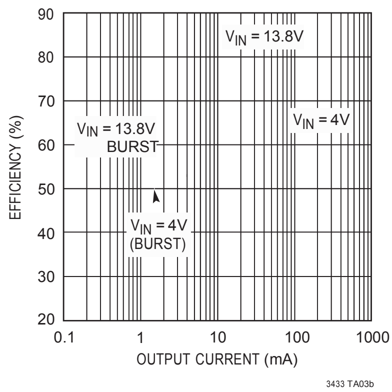

## TYPICAL APPLICATIONS

8V-60V to 12V Converter

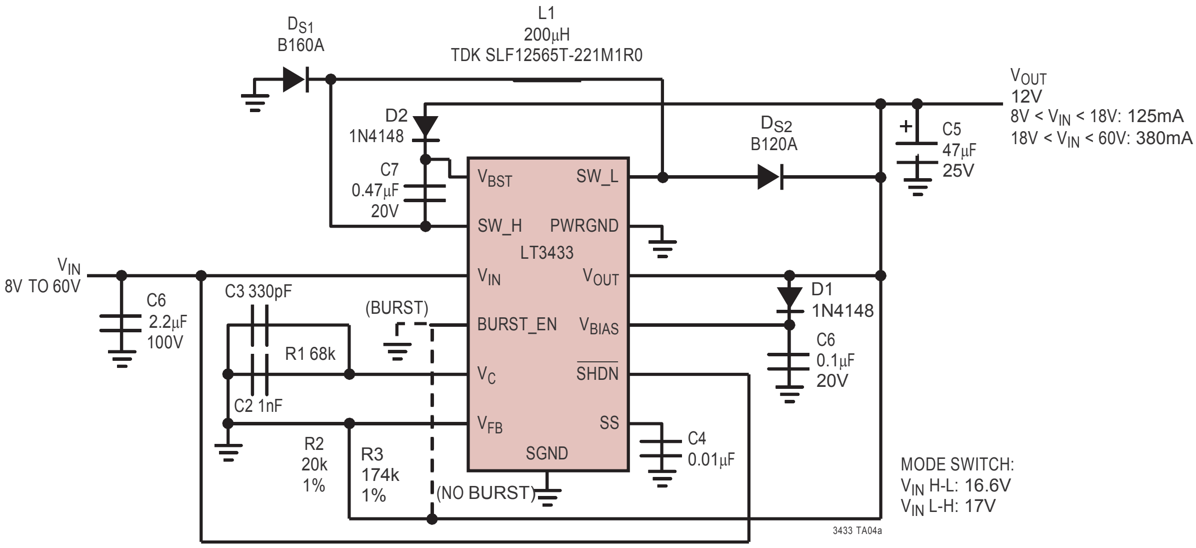


Efficiency

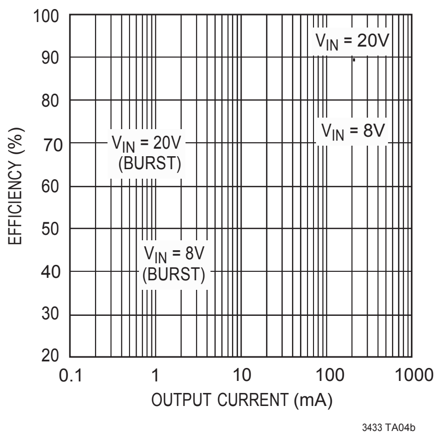


Minimum Output Current vs $V_{IN}$

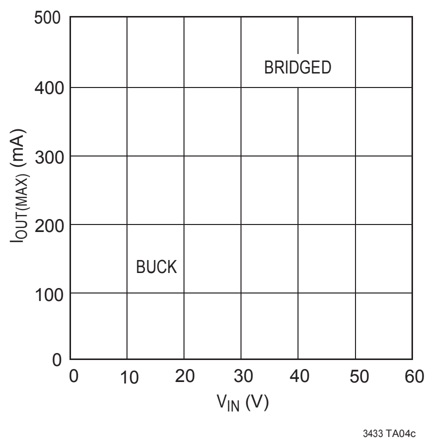

# PACKAGE DESCRIPTION

**FE Package**
**16-Lead Plastic TSSOP (4.4mm)**
(Reference LTC DWG # 05-08-1663)

**Exposed Pad Variation BB**

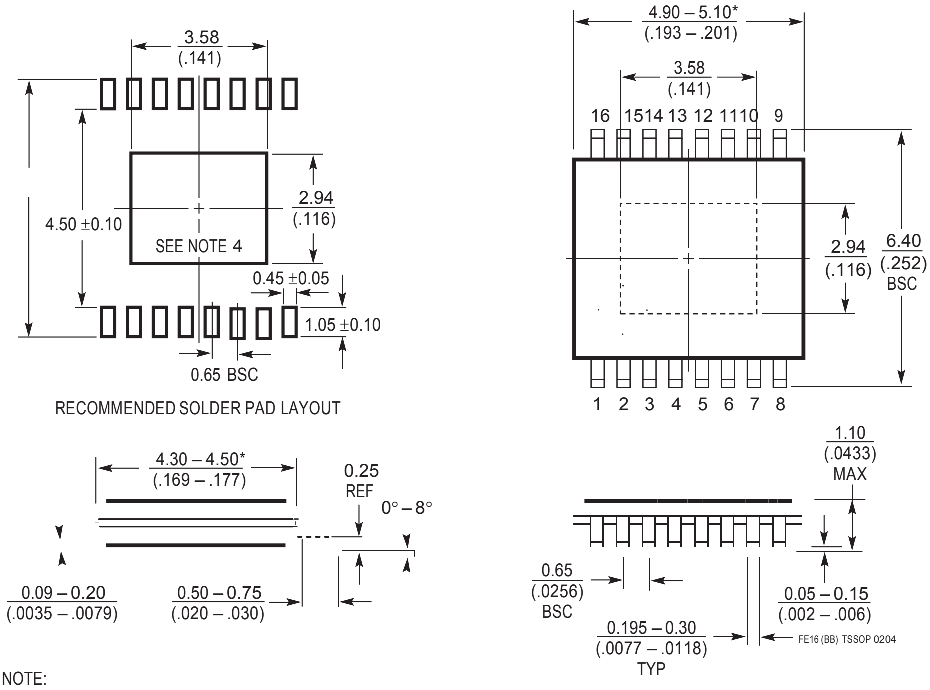


NOTE:
1. CONTROLLING DIMENSION: MILLIMETERS
2. DIMENSIONS ARE IN $\frac{\text{MILLIMETERS}}{\text{(INCHES)}}$
3. DRAWING NOT TO SCALE
4. RECOMMENDED MINIMUM PCB METAL SIZE FOR EXPOSED PAD ATTACHMENT

*DIMENSIONS DO NOT INCLUDE MOLD FLASH. MOLD FLASH SHALL NOT EXCEED 0.150mm (.006") PER SIDE

## TYPICAL APPLICATION

**Burst Only Low Noise 5V Maintenance Supply**

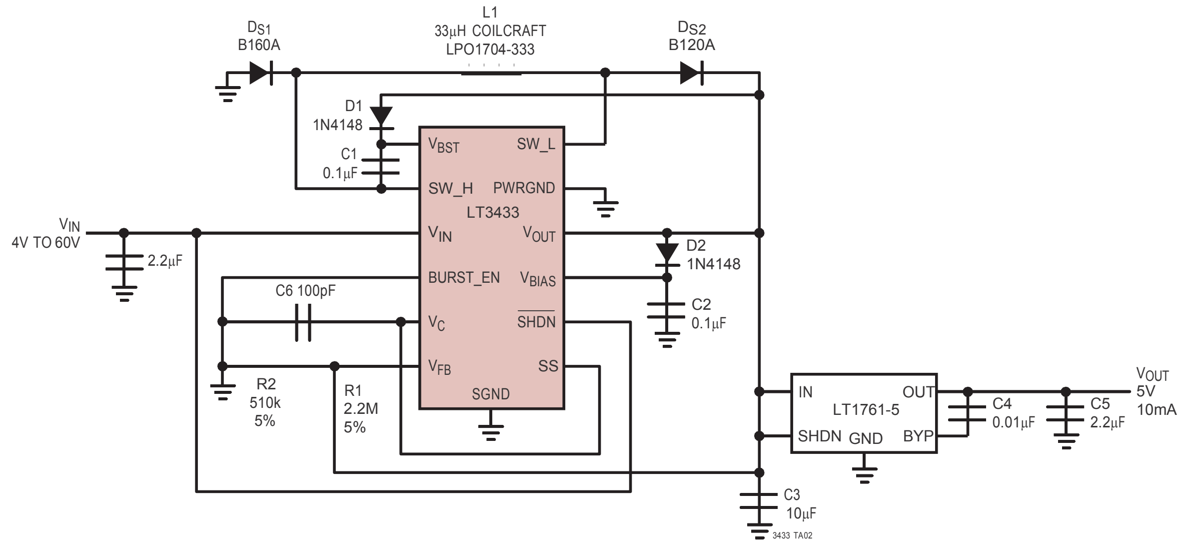


## RELATED PARTS

| PART NUMBER | DESCRIPTION | COMMENTS |
|---|---|---|
| LT1076/LT1076HV | 1.6A ($I_{OUT}$), 100kHz High Efficiency Step-Down DC/DC Converters | $V_{IN}$: 7.3V to 45V/64V, $V_{OUT(MIN)}$ = 2.21V, $I_Q$ = 8.5mA, $I_{SD}$< 10µA, DD5/DD7, TO220-5/TO220-7 |
| LT1676 | 60V, 440mA ($I_{OUT}$), 100kHz High Efficiency Step-Down DC/DC Converter | $V_{IN}$: 7.4V to 60V, $V_{OUT(MIN)}$ = 1.24V, $I_Q$ = 3.2mA, $I_{SD}$ < 2.5µA, SO-8 |
| LT1765 | 25V, 2.75A ($I_{OUT}$), 1.25MHz High Efficiency Step-Down DC/DC Converter | $V_{IN}$: 3V to 25V, $V_{OUT(MIN)}$ = 1.20V, $I_Q$ = 1mA, $I_{SD}$ < 15µA, SO-8, TSSOP16E |
| LT1766/LT1956 | 60V, 1.2A ($I_{OUT}$), 200kHz/500kHz High Efficiency Step-Down DC/DC Converters | $V_{IN}$: 5.5V to 60V, $V_{OUT(MIN)}$ = 1.20V, $I_Q$ = 2.5mA, $I_{SD}$ < 25µA, TSSOP16/TSSOP16E |
| LT1767 | 25V, 1.2A ($I_{OUT}$), 1.25MHz High Efficiency Step-Down DC/DC Converter | $V_{IN}$: 3V to 25V, $V_{OUT(MIN)}$ = 1.20V, $I_Q$ = 1mA, $I_{SD}$ < 6µA, MS8/MS8E |
| LT1776 | 40V, 550mA ($I_{OUT}$), 200kHz High Efficiency Step-Down DC/DC Converter | $V_{IN}$: 7.4V to 40V, $V_{OUT(MIN)}$ = 1.24V, $I_Q$ = 3.2mA, $I_{SD}$ < 30µA, N8, SO-8 |
| LT1976 | 60V, 1.2A ($I_{OUT}$), 200kHz High Efficiency Micropower ($I_Q$ < 100µA) Step-Down DC/DC Converter | $V_{IN}$: 3.3V to 60V, $V_{OUT(MIN)}$ = 1.20V, $I_Q$ = 100µA, $I_{SD}$ < 1µA, TSSOP16E |
| LT3010 | 80V, 50mA Low Noise Linear Regulator | $V_{IN}$: 1.5V to 80V, $V_{OUT(MIN)}$ = 1.28V, $I_Q$ = 30µA, $I_{SD}$ < 1µA, MS8E |
| LTC3412/LTC3414 | 2.5A ($I_{OUT}$), 4MHz Synchronous Step-Down DC/DC Converters | $V_{IN}$: 2.5V to 5.5V, $V_{OUT(MIN)}$ = 0.8V, $I_Q$ = 60µA, $I_{SD}$ < 1µA, TSSOP16E |
| LTC3414 | 4A ($I_{OUT}$), 4MHz Synchronous Step-Down DC/DC Converter | $V_{IN}$: 2.3V to 5.5V, $V_{OUT(MIN)}$ = 0.8V, $I_Q$ = 64µA, $I_{SD}$ < 1µA, TSSOP20E |
| LTC3727/LTC3727-1 | 36V, 500kHz High Efficiency Step-Down DC/DC Controllers | $V_{IN}$: 4V to 36V, $V_{OUT(MIN)}$ = 0.8V, $I_Q$ = 670µA, $I_{SD}$ < 20µA, QFN32, SSOP28 |
| LT3430/LT3431 | 60V, 2.75A ($I_{OUT}$), 200kHz/500kHz High Efficiency Step-Down DC/DC Converters | $V_{IN}$: 5.5V to 60V, $V_{OUT(MIN)}$ = 1.20V, $I_Q$ = 2.5mA, $I_{SD}$ < 30µA, TSSOP16E |
| LTC3440/LTC3441 | 600mA/1.2A ($I_{OUT}$), 2MHz/1MHz Synchronous Buck-Boost DC/DC Converter with 95% Efficiency | $V_{IN}$: 2.5V to 5.5V, $V_{OUT(MIN)}$ = 2.5V, $I_Q$ = 25µA, $I_{SD}$ < 1µA, MS10 |


Linear Technology Corporation
1630 McCarthy Blvd., Milpitas, CA 95035-7417
(408) 432-1900 • FAX: (408) 434-0507 • www.linear.com
LT/TP 0504 1K • PRINTED IN USA